AFRL-SN-HS-TR- 2002-001

PROCEEDINGS OF THE 2000 ANTENNA APPLICATIONS SYMPOSIUM –VOLUME II

Daniel H. Schaubert, et al
Electrical and Computer Engineering Department
University of Massachusetts
Amherst MA 01002

Electromagnetics Laboratory
University of Illinois
Urbana-Champaign

FINAL REPORT : September 20 – 22, 2000

APPROVED FOR PUBLIC RELEASE: DISTRIBUTION UNLIMITED

AIR FORCE RESEARCH LABORATORY
Sensors Directorate
Electromagnetics Technology Division
80 Scott Dr
Hanscom AFB MA 01731-2909

TITLE OF REPORT:
2000 Antenna Applications Symposium
VOLUME II

PUBLICATION REVIEW

This report has been reviewed and is approved for publication.

APPROVED:

Livio D. Poles

Livio D. Poles
Antenna Technology Branch
Electromagnetics Technology Division

FOR THE DIRECTOR

Robert V. McGahan

Robert V. McGahan,
Division Technical Advisor
Electromagnetics Technology Division

REPORT DOCUMENTATION PAGE			Form Approved OMB No. 0704-0188

The public reporting burden for this collection of information is estimated to average 1 hour per response, including the time for reviewing instructions, searching existing data sources, gathering and maintaining the data needed, and completing and reviewing the collection of information. Send comments regarding this burden estimate or any other aspect of this collection of information, including suggestions for reducing the burden, to Department of Defense, Washington Headquarters Services, Directorate for Information Operations and Reports (0704-0188), 1215 Jefferson Davis Highway, Suite 1204, Arlington, VA 22202-4302. Respondents should be aware that notwithstanding any other provision of law, no person shall be subject to any penalty for failing to comply with a collection of information if it does not display a currently valid OMB control number.

PLEASE DO NOT RETURN YOUR FORM TO THE ABOVE ADDRESS.

1. REPORT DATE *(DD-MM-YYYY)*	2. REPORT TYPE	3. DATES COVERED *(From - To)*
11 February 2002	FINAL	20-22 September 2000

4. TITLE AND SUBTITLE PROCEEDINGS OF THE 2000 ANTENNA APPLICATION SYMPOSIUM	**5a. CONTRACT NUMBER** GS01K99BKM0012
	5b. GRANT NUMBER Task Order Number R1570132D
	5c. PROGRAM ELEMENT NUMBER
6. AUTHOR(S) Daniel H. Schaubert et, al	**5d. PROJECT NUMBER**
	5e. TASK NUMBER
	5f. WORK UNIT NUMBER
7. PERFORMING ORGANIZATION NAME(S) AND ADDRESS(ES) Air Force Research Laboratory 80 Scott Rd Electromagnetics Technology Division Sensors Directorate Hanscom AFB, MA 01731	**8. PERFORMING ORGANIZATION REPORT NUMBER** Volume II
9. SPONSORING/MONITORING AGENCY NAME(S) AND ADDRESS(ES) Air Force Research Laboratory 80 Scott Rd Electromagnetics Technology Division Sensors Directorate Hanscom AFB, MA 01731	**10. SPONSOR/MONITOR'S ACRONYM(S)**
	11. SPONSOR/MONITOR'S REPORT NUMBER(S) AFRL-SN-HS-TR-2002-001

12. DISTRIBUTION/AVAILABILITY STATEMENT
Approved for Public Release; Distribution Unlimited

13. SUPPLEMENTARY NOTES
SNHA Project Engineer
Volume I contains Pages 1-245, Volume II contains Pages 246-414

14. ABSTRACT
The Proceedings of the 2000 Antenna Applications Symposium is a collection of state-of-the-art papers relating to phased array antennas, multibeam antennas, satellite antennas, microstrip antennas, reflector atnennas, HF, VHF, UHF, and various other antennas.

15. SUBJECT TERMS
Antennas, Satellite Antennas, Broadband Antennas, Microstrip Antennas, Reflectors, HF, VHF, UNF, Multibeam Antenna, Array Antennas

16. SECURITY CLASSIFICATION OF:			17. LIMITATION OF ABSTRACT	18. NUMBER OF PAGES	19a. NAME OF RESPONSIBLE PERSON
a. REPORT	b. ABSTRACT	c. THIS PAGE			Livio D. Poles AFRL/SNHA
U	U	U	SAR	168	**19b. TELEPHONE NUMBER** *(Include area code)* 781-377-4087

Standard Form 298 (Rev. 8/98)
Prescribed by ANSI Std. Z39.18

Elements

Arrays II

Identifiers for Proceedings of Symposia

The USAF Antenna Research and Development Program

Year	Symp. No.	Identifier
1951	First	____________
1952	Second	C054 520
1953	Third	AD63794
1954	Fourth	AD63139
1955	Fifth	AD90397
1956	Sixth	AD114702
1957	Seventh	AD138500
1958	Eighth	AD301151
1959	Ninth	AD314721
1960	Tenth	AD244388 (Vol. 1)
		AD319613 (Vol. 2)
1961	Eleventh	AD669109 (Vol. 1)
		AD326549 (Vol. 2)
1962	Twelfth	AD287185 (Vol. 1)
		AD334484 (Vol. 2)
1963	Thirteenth	AD421483
1964	Fourteenth	AD609104
1965	Fifteenth	AD474238L
1966	Sixteenth	AD800524L
1967	Seventeenth	AD822894L
1968	Eighteenth	AD846427L
1969	Nineteenth	AD860812L
1970	Twentieth	AD875973L
1971	Twenty-First	AD888641L
1972	Twenty-Second	AD904360L
1973	Twenty-Third	AD914238L

Antenna Applications Symposium

		TR#	ADA#
1977	First	None	955413
1978	Second	None	955416
1979	Third	____________	077167
1980	Fourth	____________	205907
1981	Fifth	____________	205816
1982	Sixth	____________	129356
1983	Seventh	____________	142003; 142754
1984	Eighth	85-14	153257; 153258
1985	Ninth	85-242	166754; 165535
1986	Tenth	87-10	181537; 181536
1987	Eleventh	88-160	206705; 206704
1988	Twelfth	89-121	213815; 211396
1989	Thirteenth	90-42	226022; 226021
1990	Fourteenth	91-156	237056; 237057
1991	Fifteenth	92-42	253681; 253682
1992	Sixteenth	93-119	268167; 266916
1993	Seventeenth	94-20	277202; 277203
1994	Eighteenth	95-47	293258; 293259
1995	Nineteenth	96-100	309715; 309723
1996	Twentieth	97-189	341737
1997	Twenty First	1998-143	
1998	Twenty Second	1999-86	
1999	Twenty Third		

USING MULTIPLE RESONANT RADIATORS FOR INCREASING THE IMPEDANCE BANDWIDTH OF ELECTRICALLY SMALL ANTENNAS

Paul E. Mayes
University of Illinois
1406 West Green Street
Urbana, IL 61801
and
Walter Gee
Walter Gee & Associates
1683 Cassiar Drive
San Jose, CA 95130

Abstract: Antennas that can be enclosed in a sphere with radius, *a*, such that *ka* < *1*, are considered to be electrically small. Such antennas are widely recognized to have input impedance that varies rapidly with frequency. This paper describes an antenna structure that combines several radiators so that, even though remaining electrically small, the band of reasonable match can be increased several fold. Each of the component radiators is a conical resonator, bounded on two sides by conducting coaxial cones with polar angles that differ by a few degrees. The tips of the cones are truncated at a small radius for insertion of a feed wire that effectively connects the resonators in series. The large ends are truncated at radii that may differ somewhat depending upon the preferred shape of the composite structure. In one view of the operation of the antenna, each pair of adjacent cones forms a resonator that radiates through the aperture at the large end. The size of each resonator at resonance can be made small with inductive elements across the aperture. The resonant frequency of each resonator can be adjusted to be slightly different by making the radius and/or the reactive termination slightly different. An equivalent circuit of series-connected resonant transmission lines is used for preliminary design. Most of the line parameters are easily determined, but the radiation resistances require a moment method solution for each resonator and for the complete antenna.

1. Introduction

The observed impedance characteristics of antennas leads to the presumption of an upper limit on a gain-bandwidth/size factor for radiating devices. Such a factor would be a generalization of the concept of the gain-bandwidth limitation for networks [1]. The bandwidth and Q of a network behave reciprocally and the Q becomes finite only with the introduction of lossy elements. Only as the size of a structure increases in comparison to the wavelength can radiation increase to be the dominant loss phenomenon. When an antenna is electrically small ($ka < 1$), the impedance is naturally reactive, but can be made real by adding a lumped reactive element. The radiation loss is likely to be smaller than or comparable to the heat loss. Thus the efficiency is low [2].

For impedance matching to connected circuitry, operation of an electrically small antenna is positioned at a resonance point. The match bandwidth is then dependant upon the device Q. The resonance condition is frequently obtained by adding a predominantly reactive lumped element at the feedpoint. However, it is shown here that improved efficiency is possible by placing the reactive element within the radiator.

2. Conical Radiating Resonators (CRR)

The basic component of the systems presented here is a radiating resonator formed by the space between two coaxial conducting cones. The cones are each described in spherical coordinates by two polar angles and two radial limits, as depicted in Figure 1. In practice, a single resonator is excited by extending the center conductor of a coaxial cable through a small aperture at the tip of the lower cone and connecting it to the tip of the upper cone. The shield of the coax feed is attached to the lower cone as shown in Figure 2. The rotational symmetry of the resulting structure ensures that the radiation pattern will be omnidirectional in azimuth and have nulls along the polar axis.

The conducting cones are truncated at distances *rmx(j)* from the origin. Although these distances are arbitrary, they are usually chosen to be equal or nearly so. The region between the cones may contain dielectric to provide support for the cones. Ordinarily, it will be desirable to limit the volume occupied by dielectric in order to minimize the losses in the resonator.

Conical antennas were introduced by Barrow, et al in 1939 [3]. Extensive measurements on conical monopoles with various flare angles were reported by Brown and Woodward in 1952 [4]. In much of the succeeding literature consideration has been focussed on medium flare angles since the input impedance for those angles converges toward the values of popular cables as frequency increases [5]. Hence, most of the conical antennas in use today are electrically large in order to use advantageously the wide impedance bandwidth of conical structures of sufficient size [6].

3. Equivalent Circuits

Maxwell's equations for TEM fields in the rotationally symmetric region between coaxial cones can be reduced to ordinary differential equations for the sole field components E_θ and H_ϕ. The fact that these equations are identical with those for a uniform transmission line leads to an equivalent circuit model for a conical resonator as shown in Figure 3. The ratio of E_θ to H_ϕ for an outgoing TEM wave in the region between the cones (defined by polar angles, $\theta(1)$ and $\theta(2)$) is given by the characteristic impedance, Z_0, where

$$Z_0 = 60 \ln\left[\frac{\tan\left(\frac{\theta(1)}{2}\right)}{\tan\left(\frac{\theta(2)}{2}\right)}\right] \tag{1}$$

The phase constant for the line is the intrinsic phase constant for the homogeneous medium between the cones. The length of the line is equal to the distance from the (virtual) apices of the cones to the aperture between them. Thus, all parameters of the model are known except the termination at the aperture end of the line. The terminating impedance is the parallel combination of a resistance that absorbs power equal to that radiated by the conical resonator and a reactive element that represents the (near-field) energy stored near the aperture. Evaluation of the terminal impedance requires a solution of the electromagnetic boundary-value problem represented by the radiating resonator of Figure 1.

Numerical solutions for the conical radiating resonator have been obtained using the method of moments as implemented in the software package FERM (Finite Element Radiation Model) originally developed at the Lincoln Laboratory of Massachusetts Institute of Technology [7]. Figure 4 shows the geometry of a typical set of patch subsections used in the analysis of a low-profile CRR. Single resonators with cones having polar angles near ninety degrees satisfy the requirement of some applications for reduced height. Resonators with small angles between the cones can be packaged in multi-resonator systems, as will be shown later. The rotational symmetry produces dipole-like radiation patterns; vertically polarized, omnidirectional in azimuth with nulls at the poles.

The computed input impedance shown on the Smith chart of Figure 5 is typical of the frequency behavior of conical antennas. At extremely low frequencies the input impedance is primarily reactive. As frequency increases, the impedance goes through successive conditions of zero reactance (resonance) and the distance from the edge of the chart increases because of increasing radiation. Only when the structure becomes large compared to the wavelength does the impedance approach the (real) value given by Equation (1).

Since the first resonance does not occur until the radius of the CRR is about one-quarter wavelength, the input impedance of a smaller resonator will ordinarily be reactive. A conventional method of achieving match to a real impedance is to add a series reactance of the same value but opposite in sign. Canceling the capacitive reactance of an electrically small CRR may thus be accomplished by adding a series inductor appropriate for the frequency of operation. The small tuned antenna can be represented by an equivalent series circuit as shown in Figure 6.

Since the radiation resistance of an electrically small antenna may be comparable or smaller than the resistance of the tuning inductor, the efficiency is an important performance parameter. For the circuit of Figure 6 the efficiency, e, is given by

$$e = \frac{R_A}{R_A + R_L} \tag{2}$$

For the data of Figure 5, $R_A = 0.03$ ohms at 100 MHz. Resonance at 100 MHz requires a series inductive reactance of 23.9 ohms. If the Q of the inductor is 50, $R_L = 0.48$ ohms and the efficiency is 5.8%. If $Q = 100$, the efficiency becomes 11.2%. Since the losses in the cones were not included in these calculations, the results actually represent upper bounds on the efficiency of a physical antenna.

4. A Size-Reduced Conical Radiating Resonator

An electrically small CRR can be made resonant (real input impedance), with negligible disturbance of the radiation pattern, by placing inductors across the aperture. The equivalent circuit of Figure 3 is then modified as shown in Figure 7. The net terminating inductive reactance is thus near the boundary in the upper half of the Smith chart as shown in Figure 8. Moving less than one-quarter wavelength toward the generator produces a real-axis crossing on the high-impedance side of the chart.

According to the equivalent circuit of Figure 7, resonance can be produced at 100 MHz for the CRR of Figure 4 by terminating the line with a normalized inductive reactance of 2.41. To minimize the effects of an asymmetric termination, four inductors were simulated across the aperture of the CRR. Since the characteristic impedance is 10.5 ohms, the reactance at each of the four loads is equal to

$$X_L = (10.5)(2.41)(4) = 101.2 \text{ ohms}$$

and the net terminal reactance shown in Figure 7 is 25.3 ohms.

The patch geometry used in the computer simulation for this terminated CRR is shown in Figure 9 and a Smith chart plot of the computed input impedance is presented in Figure 10. If all materials used to construct the antenna are assumed to be lossless, the non-zero result for the real part of the input impedance must be caused by radiation. Using a lossless model permits the determination of the resistive termination in the equivalent circuit. For this purpose the inverted line equations are used to solve for the terminal resistance when the input impedance, Z_0, phase constant and length of the line are known. From the data of Figure 10. the terminal resistance at 100 MHz (resonance) is found to be about 9,000 ohms.

If, as before, the loss in the walls of the resonator is ignored, the efficiency is given by

$$e = \frac{1}{1 + \frac{\frac{R_A}{R_L}}{1+Q^2}} \tag{3}$$

where Q is the quality factor for the terminating inductor in Figure 7.

For tuning coils with $Q = 50$, the efficiency is 12.3%. If the Q of the coils can be increased to 100, the efficiency goes up to 21.9%. These values are comparable to the results of measurements using the Wheeler Cap Method [8]. This shows that size reduction by inductive loading of the aperture gives higher efficiency than input inductive tuning for the same size CRR. It also demonstrates once again the importance of using low-loss components in an electrically small antenna.

5. Increasing the Impedance Bandwidth

Using aperture tuning rather than input tuning gives a significant increase in the bandwidth as well as the efficiency. However, much greater bandwidths can be obtained by combining several resonators tuned to slightly different frequencies. Figure 11 shows two cross-sectional views of a set of six CRR elements. The top view shows the outer extremities of the seven conducting cones, 50a-g, each terminated in one of the lumped elements, 51a-f, and 52a-f that are visible in the cross-section shown. The lower, enlarged view of region 60 shows how the center conductor,17, of the feed cable, 15, passes through apertures in the other cones and is attached to the apex of cone 50g. The shield, 16, of the feed cable is connected around the aperture of the lowest cone, 50a.

The input impedance of a series connection of several parallel RLC circuits is dominated by the large values obtained at the resonances. The deviation of the impedance between resonances depends upon the separation of the resonant frequencies. The input impedance of a series connection of six equivalent lines, as shown in Figure 12, can be shown to display similar behavior. Figure 13 shows the input impedance computed for a circuit like Figure 12 but containing ten resonators. The ten resonant frequencies serve to define the limits of nine loops on the Smith chart. The sizes of the loops are governed by the separation between resonant frequencies. Proper choice of the resonant frequencies produces loops of nearly the same size.

The loops tend to rotate around the chart. This rotation can be practically eliminated by putting series LC elements at the input. The collection of near coincident loops can then be centered on the chart by adding a transformer with the correct transformation ratio. These elements are shown in the circuit of Figure 12.

6. Practical Realization

A ten-resonator antenna was constructed to cover the frequencies around 100 MHz. The defining properties of the cones are listed in Table 1. The cones were spun from copper sheet and assembled using machined dielectric spacers. Thin dielectric washers were also inserted between the cones at the feed apertures to prevent short circuits. The aperture inductors were wound using copper wire (0.052 in dia) on a coil form of 0.37-in diameter in an effort to maintain high values of Q. Figure 14 is a photograph of the completed antenna.

The values for the inductors were originally determined using a computer analysis (Eagleware SuperStar) of the circuit shown in Figure 12. Since the values of the terminal resistances were determined from measurements and a computer simulation for a single resonator, the original inductor values did not yield optimum results. Starting with the computed values, cut-and-try experiments were performed on the antenna to improve the performance. The aperture inductors were varied with the goal of making the impedance loops have the desired diameter (thereby determining the SWR) and to be nearly coincident. Figures 15a-c show Smith charts with frequency spans that encompass no more than two loops. Markers at the real-axis crossings define the effective resonant frequencies of each resonator in the presence of the others. At this writing, a few resonators at the low-frequency end of the band are still not optimally tuned. This can be seen in Figure 15c wherein the two loops are not nearly coincident. Figure 16 shows the measured input impedance over the band of best impedance. Although most of the circles are nearly coincident, they cover an area on the high-impedance side of the chart. The best impedance match would be obtained by using a feed cable with characteristic impedance equal to the mean of the measured values. Matching to a standard value (such as 50 ohms) could be accomplished by inserting a transformer with the proper ratio. Figure 16 shows the impedance measured from 80 to 135 MHz at the input of a 3:1 transformer. Although eight loops can be observed in this band, it is clear that three of them are significantly larger than the others. It is also clear that the addition of the transformer has greatly reduced the variation in the impedance.

Table 1. Dimensions of cones for ten-resonator CRR

Cone	Radius*(cm)	Angle**(deg)
0	29.56	310
1	24.80	320
2	21.94	330
3	20.22	340
4	19.29	350
5	19.00	0
6	19.00	10
7	19.00	20
8	19.00	30
9	19.00	40
10	19.00	50

*Measured from origin of coordinates.

**Measured counter-clockwise from horizontal line to the right.

Figure 17 gives a comparison of the SWR measured with and without the transformer. The half-power bandwidth, between frequencies at which the SWR equals 5.8, is about 133 – 86 = 47 MHz. (44%). Lower SWR could be obtained by moving the resonances closer together with a resulting decrease in bandwidth.

7. Plans for the Future

The FERM software, like some other moment method codes, cannot accurately treat patches that are very small compared to the wavelength. Hence, the patch geometries used in this work have not accurately modeled the details of the feed region of CRR elements. This problem is currently under investigation at the Center for Numerical Electromagnetics at the University of Illinois in Urbana-Champaign.

The efficiency of electrically small antennas, particularly systems of CRR elements, is critically dependent upon the availability of low-loss components. Decreasing the losses in inductors and transformers is especially important for enhancing the efficiency of CRR antennas.

The design of electrically small systems of CRR elements would benefit from additional data, both computed and measured. Achieving near constant match and directivity does not guarantee constant gain. Efficiency versus frequency should be studied.

References

[1] R. M. Fano, "Theoretical Limitations on the Broadband Matching of Arbitrary Impedances," Technical Report No. 41, Massachusetts Institute of Technology, 1948.

[2] W. L. Stutzman and G. A.Thiele, Antenna Theory and Design, pp. 49-50, New York, Wiley, 1983.

[3] W. L. Barrow, L. J.Chu and J. J. Jansen, "Biconical Electromagnetic Horns," Proceedings of IRE, vol. 27, pp.769-779, December 1939.

[4] G. H. Brown and O. M. Woodward. Sr., "Experimentally Determined Radiation Characteristics of Conical and Triangular Antennas,' RCA Review, vol. 13, No. 4, pp. 425-452, December 1952.

[5] C. H. Papas and R. King, "Input Impedance of a Wide-Angle Conical Antenna Fed by a Coaxial Line", Proc. IRE, vol. 37, pp.1269-1271, 1949.

[6] Y. T.Lo and S. W. Lee (eds), Antenna Handbook, p. 3-29, New York, Van Nostrand Reinhold, 1988.

[7] S. Lee, D. A. Shnidman and F. A. Lichauco, "Numerical Modeling of RCS and Antenna Problems", Technical Report No.785, Lincoln Laboratory, Massachusetts Institute of Technology, December 1987.

[8] Harold A. Wheeler, "Small Antennas", IEEE Trans. Antennas Propagat., vol. AP-21, No.4, July 1975.

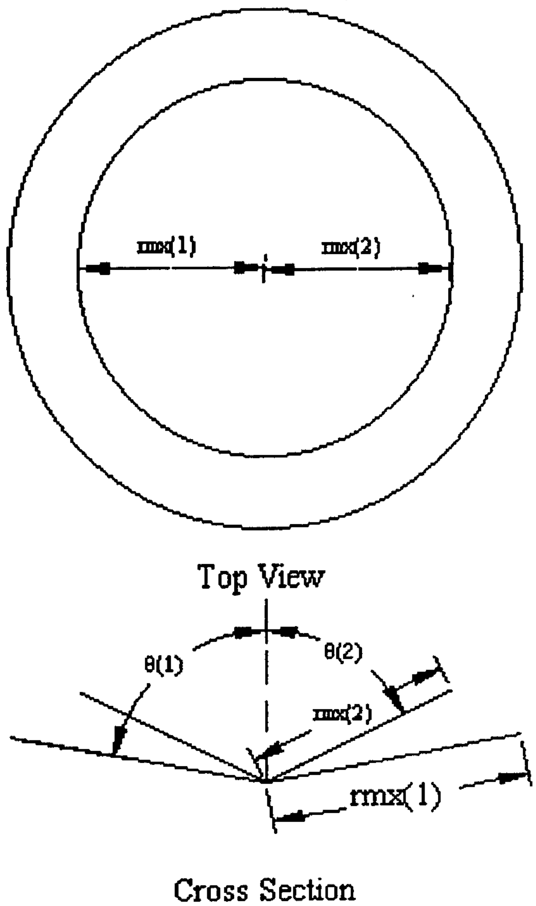

Figure 1. A conical radiating resonator (CRR) and its parameters.

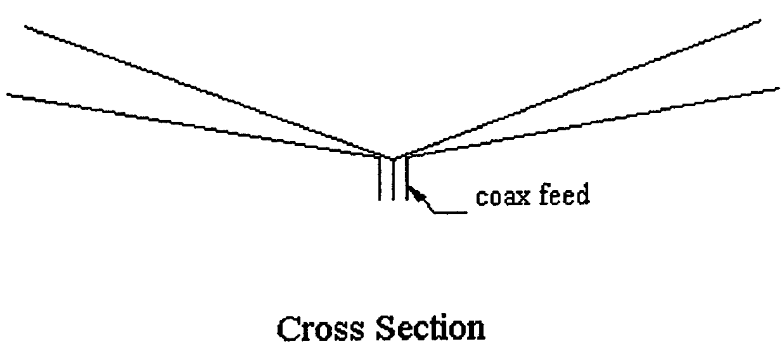

Figure 2. Rotationally symmetric excitation of a conical radiating resonator.

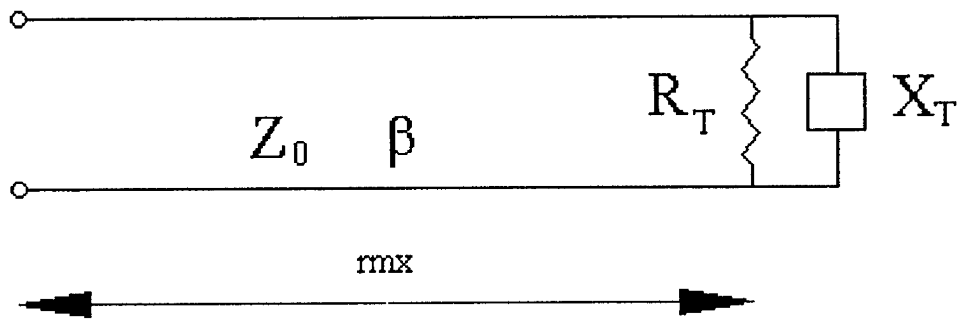

Figure 3. Equivalent circuit model for a conical radiating resonator.

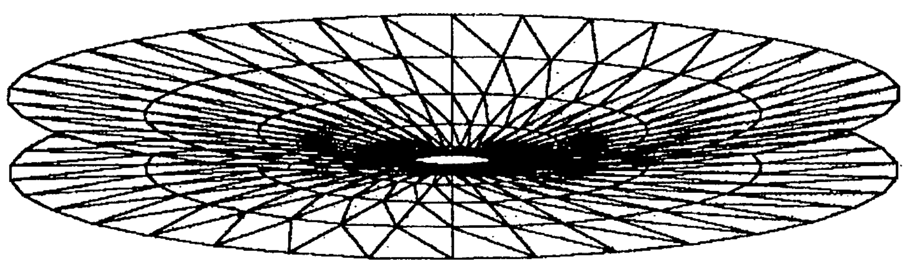

Figure 4. Geometry of subsectional patches used in the FERM analysis of a low-profile conical radiating resonator. The polar angles defining the cones are 80 and 90 degrees.

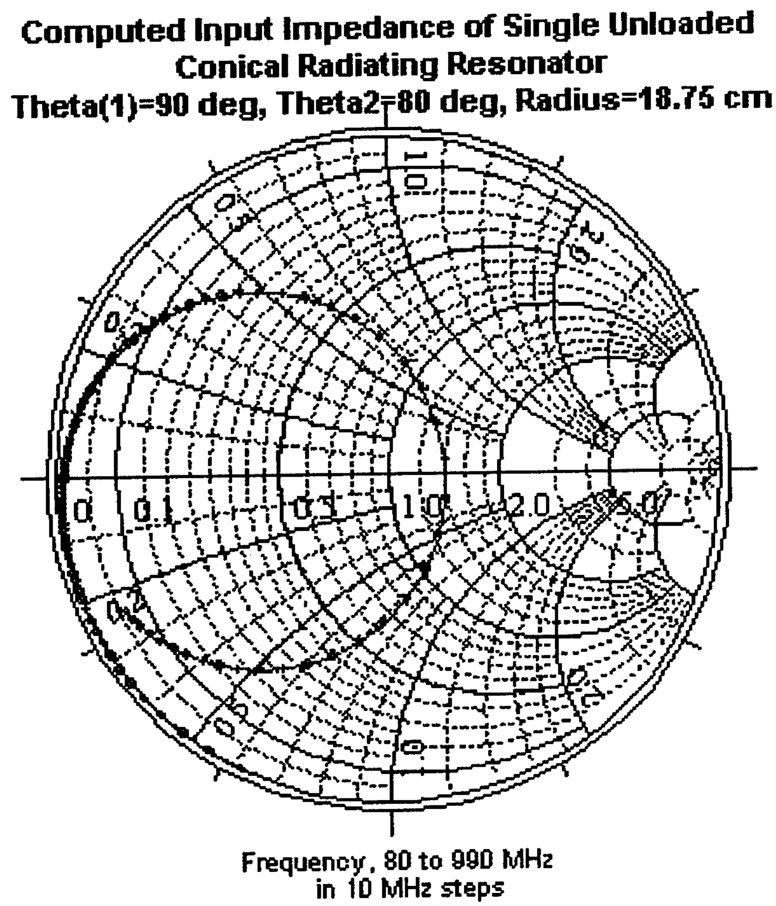

Figure 5. Input impedance for a conical radiating resonator computed over a wide range of frequency.

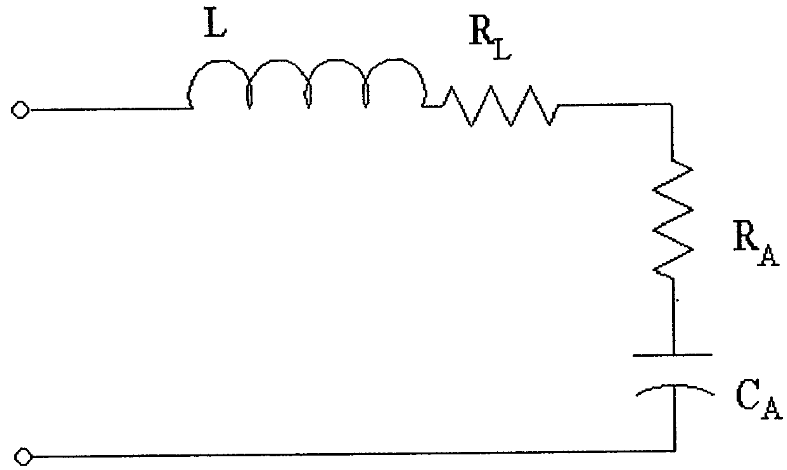

Figure 6. Equivalent circuit for an electrically small CRR.

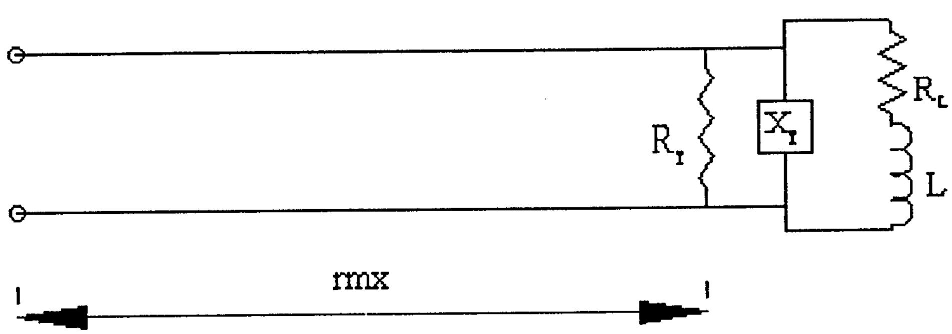

Figure 7. Equivalent circuit of a conical radiating resonator with size reduced by the addition of inductance at the aperture.

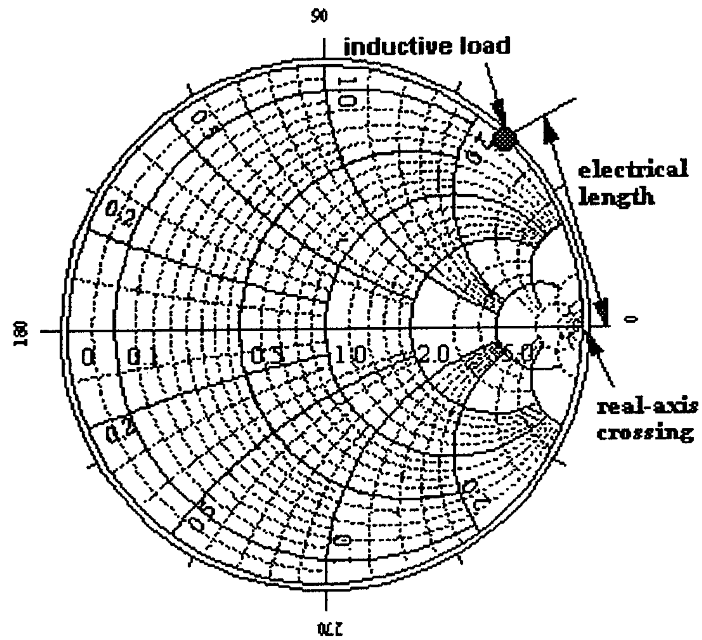

Figure 8. Smith chart illustration of size reduction of transmission line resonators by means of terminal inductive loading.

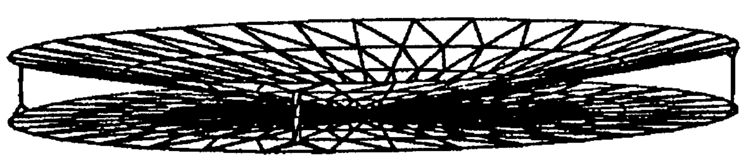

Figure 9. Patch geometry used in the FERM analysis of a CRR with inductive loading across the aperture. The polar angles defining the cones are 80 and 90 degrees.

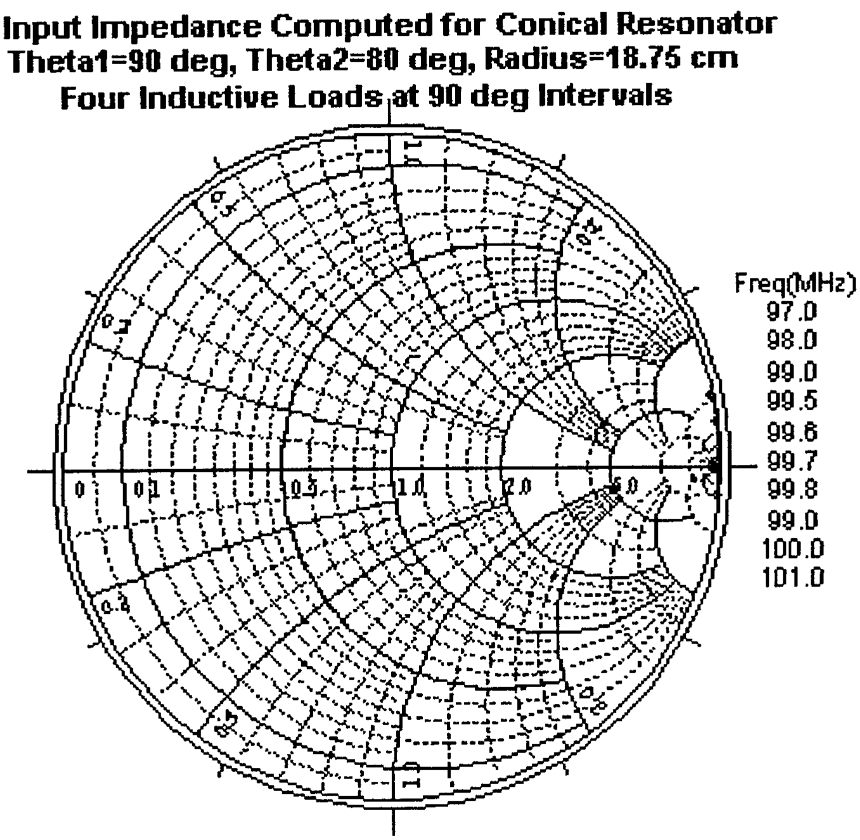

Figure 10. Input impedance computed for the CRR geometry shown in Figure 9.

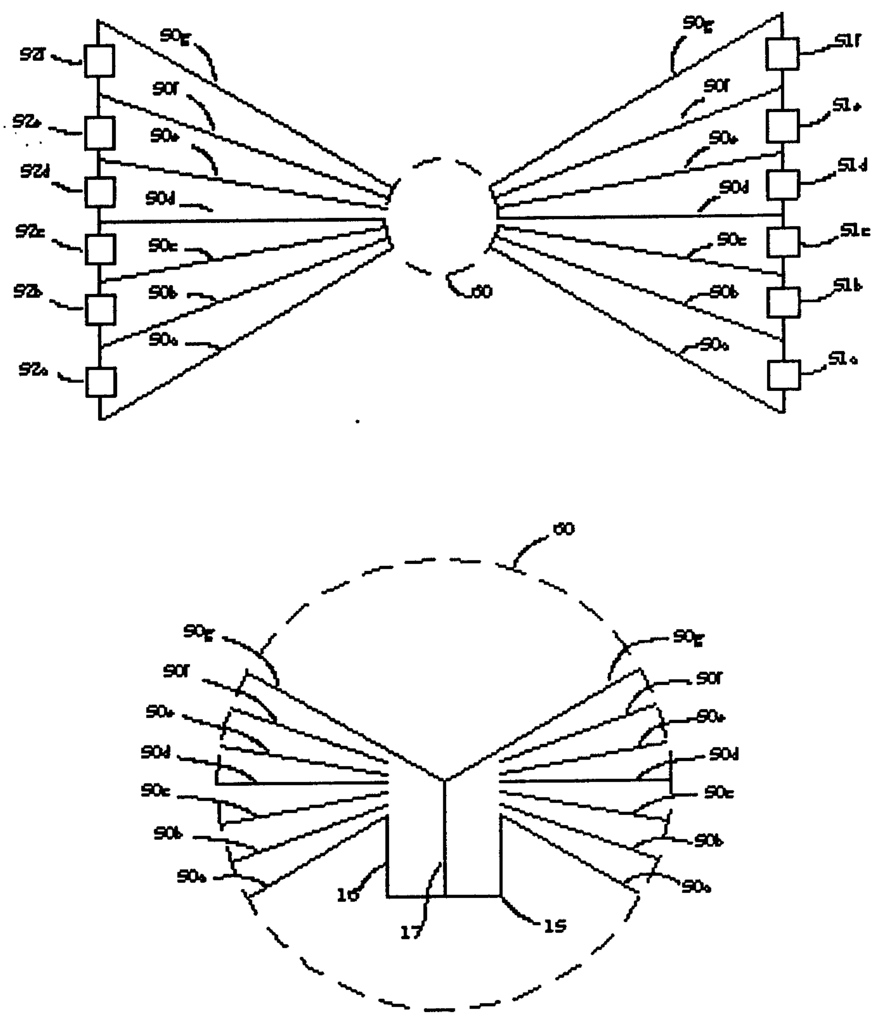

Figure 11. Two crossectional views of a system of six conical radiating resonators.

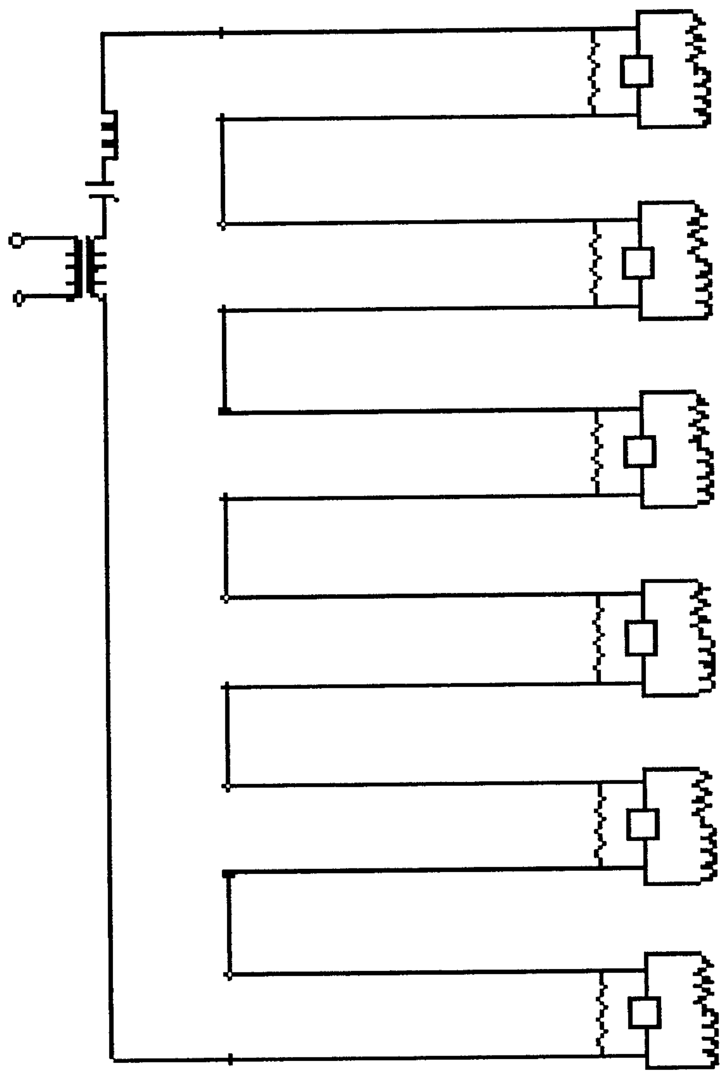

Figure 12. Approximate equivalent circuit for a system of six series-connected conical radiating resonators with aperture inductance loading.

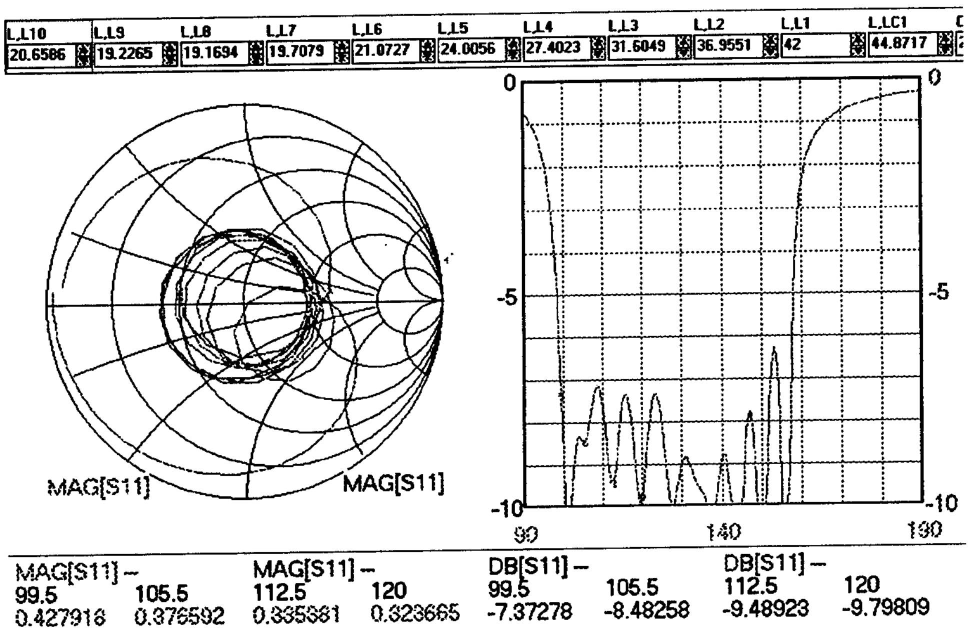

Figure 13. Input impedance (left) and return loss (right) for the transmission line model of a set of ten CRR elements.

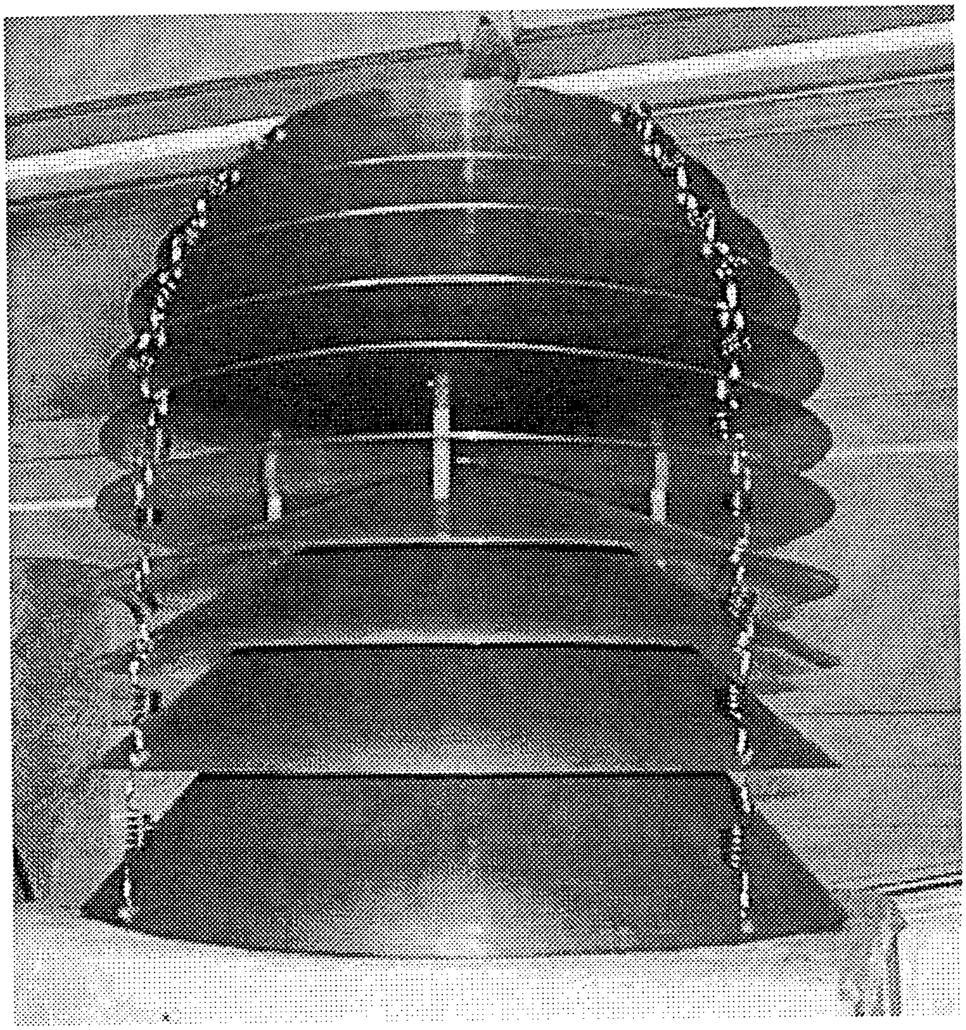

Figure 14. Photo of a set of ten conical radiating resonators.

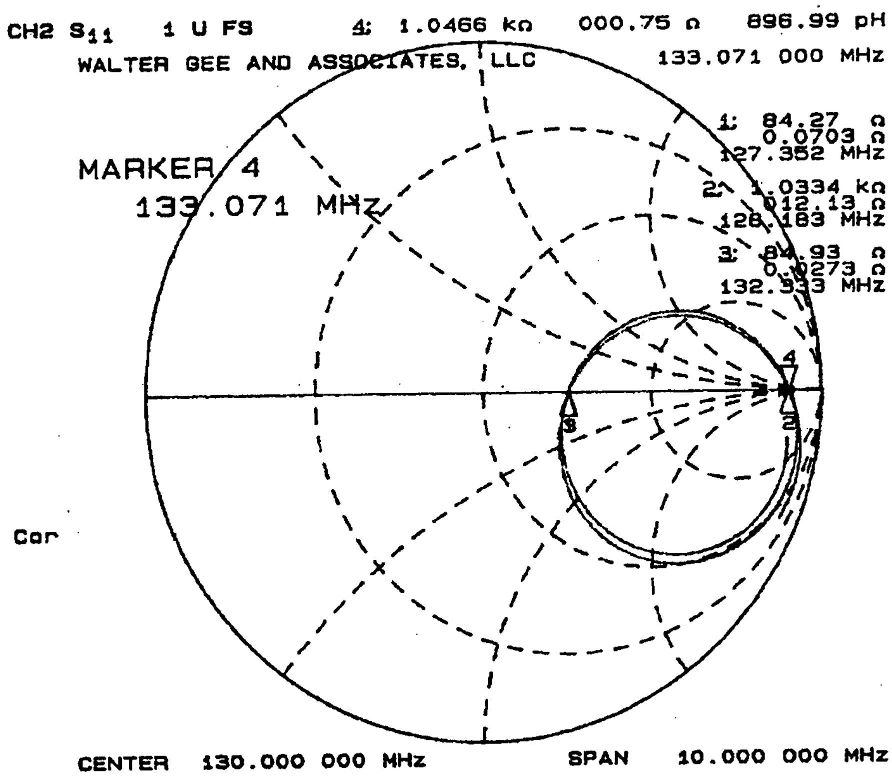

Figure 15a. Measured data for the two impedance loops (Loops 8 and 9) at the upper end of the operating band of the ten-resonator system.

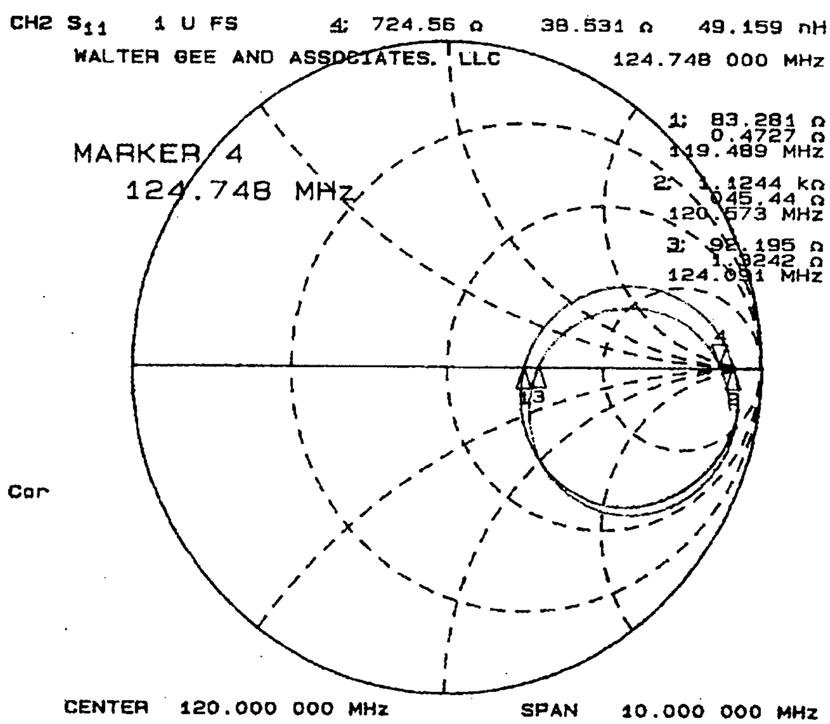

Figure 15b. . Measured data for the next two impedance loops (Loops 6 and 7) of the ten-resonator system.

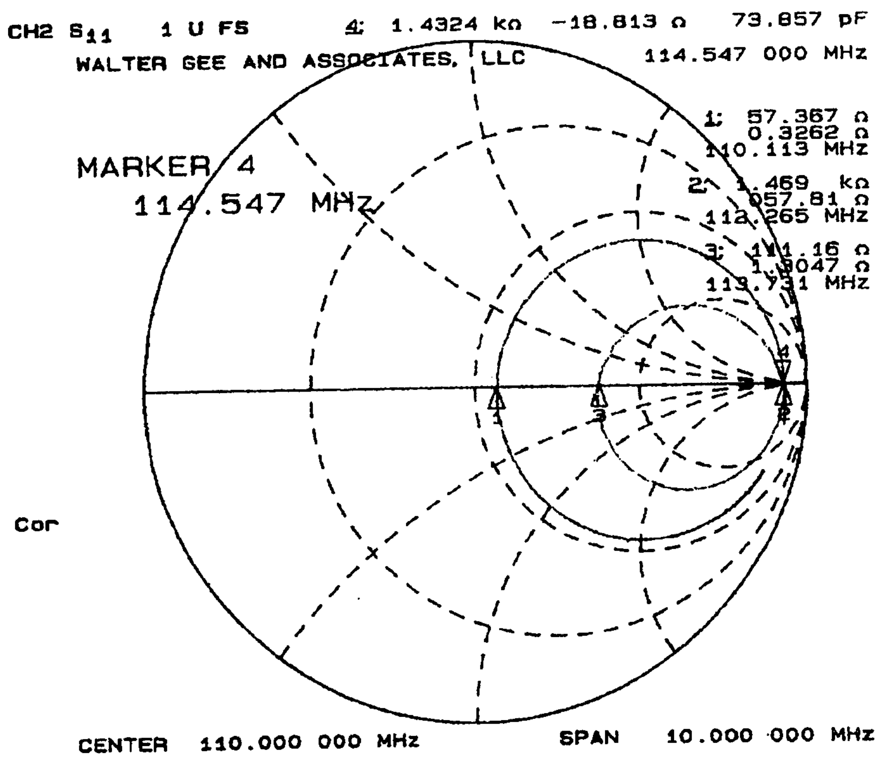

Figure 15c.. Measured data for the next two impedance loops (Loops 4 and 5) of the ten-resonator system.

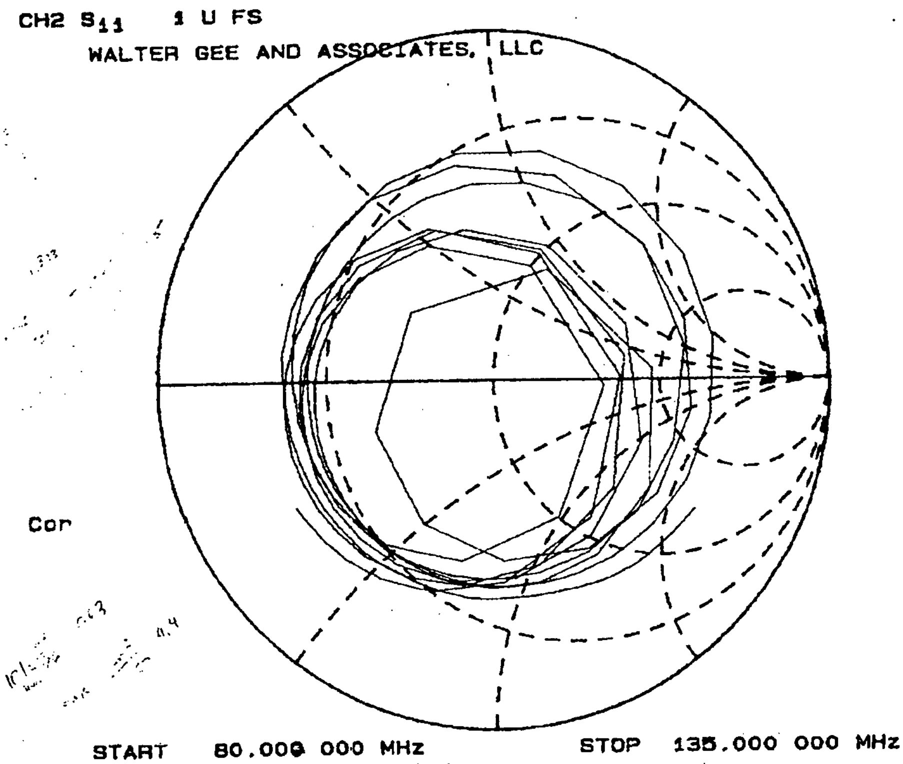

Figure 16. Impedance measured at the input of a 3:1 transformer terminated with the ten-resonator CRR.

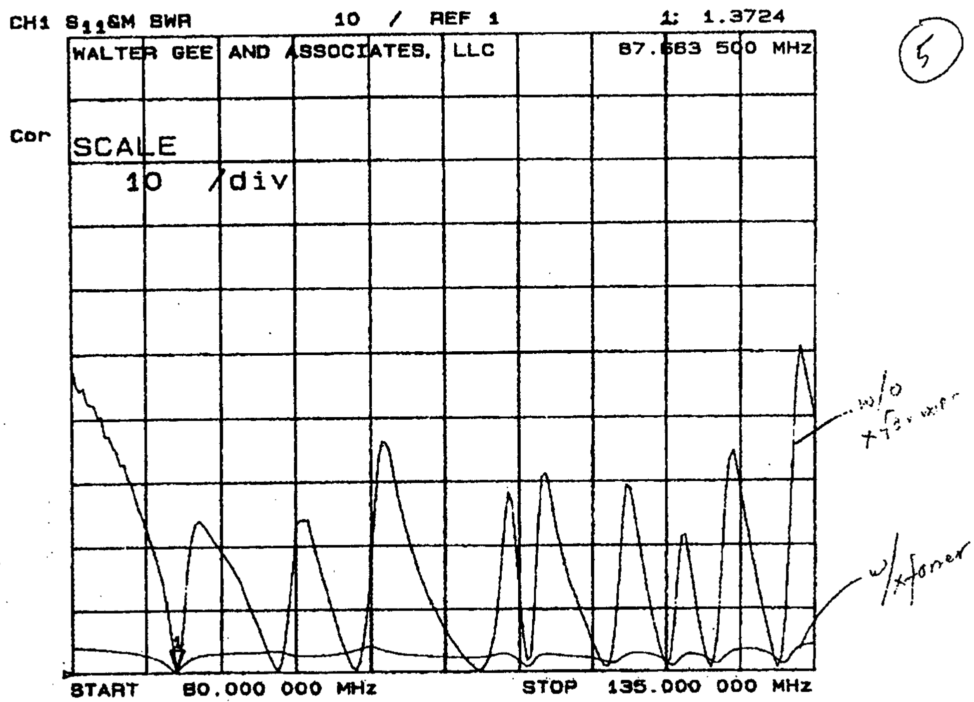

Figure 17. Comparison of SWR of ten-resonator CRR measured with transformer (lower curve) and without transformer (upper curve).

Miniaturized shorting post microstrip antenna for mobile handsets

Dave Mc Neil**, Tayeb A. Denidni* and Gilles Y. Delisle**

*Department of Mathematics, Computer and Engineering, University of Quebec at Rimouski, Quebec, Canada G5L 3A1

**Electrical Engineering Dept., Laval University, Quebec, Canada, G1K 7P4

Tayeb_denidni@uqar.uquebec.ca

Abstract—Many studies show that there are considerable interests in the subject of microstrip antenna. With the aim of miniaturization of antenna element for handsets applications, we present a new small antenna. This paper investigates the design of a miniaturized shorting post microstrip antenna. A lossless foam material is sandwiched between the two patches for providing the impedance bandwidth of the antenna. A bandwidth of 13 percent is measured around a center frequency of 1.91 GHz. Measurement, gain and polar pattern are also presented. This type of antenna could find useful application in mobile application handset.

1 Introduction

One of the components that seem to have been given less consideration at the mobile level by phone manufacturer is the antenna. In fact little change have been done at the antenna. PCS antenna required being compact, light, low profile and sensitive to two perpendicular polarizations. It operates beside the human body, so that the effect of electromagnetic radiation on the human body should be as small as possible. With the possibility to have smart antenna at the mobile and the urge to reduce the spatial peak specific absorption rate (SAR), interest of the antenna at the mobile is growing. One candidate that can fulfil this is the microstrip antenna. This type of antenna is lightweight and low profile, two qualities very important in mobile communication. Further more, they can be placed into the handset by integrated it to the Printed Circuit Board (PCB) or the plastic case of the phone.

In the past years, several new ways of designing small microstrip antennas were developed. Using microstrip antenna for the handset will be more possible that ever. Certain techniques such as using high dielectric have been investigated in several papers, but this technique has the disadvantage of reducing the bandwidth and the efficiency [1].

Another technique is to take advantage of the fact that the electric field component beneath the patch and the ground plane has approximately a cosinusoidal distribution variation with length. The maximum value of the field is at the edge and it goes to zero at the center and returns to a maximum at the other edge. Since the E-field is zero at the center, a short circuit can be placed at the center, and basic operation will not be affected. Shorting the circuit to his zero potential plane, reduce the antenna to haft of its original length. Instead ofshorting the whole plane only a partially shorted antenna can be used. This can be done by simply using shorting pins. These appear as an inductive reactance rather than a pure short. The patch length must be adjusted to account for this added inductance. This technique was shown to be the more promising. According to the new studies [3] for probe feed microscrip antenna, good impedance matching, is obtain when the shorting pin is close to the probe feed. However this characteristic makes them more difficult to manufacture. To overcome this situation, the probe feed can be replaced by aperture coupling. The interest of using aperture coupled feed structure is the elimination of the probe penetrating trough the subtract layer.

In this paper, small aperture microstrip patch antenna is investigated. In the first section, we presented the concept. Numerical results developed with Ensemble package software and design consideration are presented in the second section. In the third section, we present experimental results. The last section summarised the paper and suggestions for future improvement are given.

2 Antenna design

The main objective is to design a small aperture microstrip antenna for personnel communication system band (1.85 GHz to 1.99 GHz). During the design, to accurately analyse the shorted patch, the full-wave software package Ensemble 5.1 [4] was utilised. This software is capable of handling arbitrary shaped patches, coupling apertures, and feed networks.

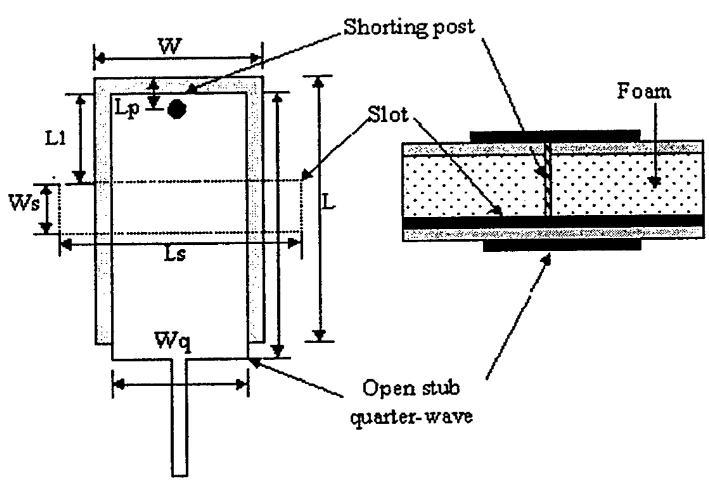

Fig. 1. Schematic of a shorted aperture coupled microstrip antenna.

The small microstrip antenna geometry is shown in Fig. 1. This antenna is constituted by a 12.7 mm foam layer Rochacell 31 with $\varepsilon_r = 1.07$, between two subtract layer. The rectangular patch is etched on a 0.787 mm RT/Duroïd 5880 which have a dielectric constant of $\varepsilon r = 2.2$. The radius of the shorting pin is 0.81 mm. The last layer is a 1.27mm RT/Duroïd 6006 with $\varepsilon_r = 6.15$, on which is etched the feeding network.

Since the various parts of the antenna interact, determining the best design is a long and tedious process, even when carried out systematically. To understand the choices made for the selection of the parameters leading to the final result, some elements will be mentioned. First, adjusting the size of the aperture can control the coupling level, which in turn controlled the size of the locus on the Smith chart. Increasing the slot length and width, give a higher coupling, and so increase the diameter of the circular portion of the locus. Dimension of the slot also influences the back radiation level, one parameter important if the SAR is considered. The slot itself must not resonate over the operating frequency band of the antenna because this would produce radiation toward the back of the antenna. For these considerations, we placed the slot in the middle of the patch. We took this parameter as a fix one, but different position along the resonance direction could have been used. The size and the position of the shorting pin also have an influence on the impedance. The microstrip length determines de resonance frequency while the width effect the resonance resistance of the antenna. Even thought we did not mention it, all the above parameter influence de resonance frequency when fine tuning the antenna, but the principal parameter to influence the resonance frequency is the length. Antenna subtract affects the bandwidth and the radiation efficiency of the antenna. Low permittivity gives wider impedance bandwidth and reduced surface wave, as a thicker subtract results in wider bandwidth, but less coupling for an aperture size. For good design, the feed dielectric subtract would range from 2 to 10 and the thickness between 0.01 λ and 0.02 λ. Higher dielectric constant and thinner subtract result in less spurious radiation from the feed line, but higher loss.

If broad bandwidth is required several ways to improve bandwidth can be used. We can increase its thickness, or to use either planar or non-planar stacked parasitic elements. All these methods will increase the size of the antenna. For example, parasitic elements usually range from a half-wavelength to a quarter-wavelength at least. Impedance-matching technique can be used for increasing the bandwidth of antenna [8]. Where the maximum VSWR = S realisable bandwidth is inversely proportional to both the element quality factor and the specified return loss (expressed in dB). Using Fano's theory, the resultis given by

$$B_m = \frac{1}{Q}\frac{\pi}{\ln\{(S+1)/(S-1)\}} \tag{1}$$

Into design of aperture small antenna, matching network in the feed line is used to enhance the bandwidth without enlarging the size of the antenna structure. Impedance matching using stub for this type of antenna was described in [9]. In some cases even matching network is too large for this kind of antenna. For example, if the impedance matching only needs to be real, quarter-wave transformer can be used. The quarter-wave transformer is being about the same length that the antenna. It actually double the space taken by the antenna on the subtract , which make it unsuitable for small antenna. In this paper we use an open stub quarter-wave directly fitted under the aperture. This avoids the antenna to become too large. Open stub quarter-wave does not react only with the real part of the impedance, but also with the imaginary part as well. In our case, the position of the quarter-wave open stub with respect to the aperture has influence on the imaginary part. Using transmission line theory for lossless line [7], the equation at the end of open stub quarter-wave can be found as

$$Z_{in} = \frac{ZZ_c}{Z_c + jZ\cot(\beta l_1) + Z_c(\cot(\beta l_1))^2} \tag{2}$$

Where Z_c is the characteristic impedance of the microstripline, Z includes the self-admittance of the slot, the admittance of the slot looking at the patch antenna, the characteristic impedance and a discontinuity voltage vector. Since, most of the parameters are interdependent, the last equation does not give useful insight, and simple rule of design can be found to help our comprehension.

Because the quarter-wave open stub is directly beneath the slot is width not only controlled the feeding impedance, but the width affects the coupling to the slot as well. This means that the quarter-wave open stub can be used not only to match the real part but also match the imaginary part as well, giving an extra degree of freedom. As the quarter-wave open stub move down along the resonance dimension, the center of the resonance loops move toward the edge of a Smith chart just in the inductive side of the short position. This is du probablyto the fact tat the structure looks like a stub with a slightly capacitive input impedance in series with a small aperture in a ground plane, which is inductive.

If impedance is not high enough during matching, it might be tempting to use the slot size to get the higher coupling, and in some case the slot size can get longer than the antenna width. Since the biggest dimension of the antenna defines his total dimension. Enlarging the slot is not always the best solution. Another solution is to adjust the width of the quarter-wave. Wider quarter-wave will result in higher impedance and a keeping the slot to a reasonable size.

Fig. 2 shows the effect of the shorting pin and the quarter-wave to the real impedance response of the antenna. The first curve shows the first resonance at 2.6 GHz of the antenna, without the shorting pin. The second curve shows the effect of the shorting pin that creates a parallel resonance occurring at 1.9 GHz with an impedance of $12 + j16\ \Omega$. Working with this new frequency, the quarter-wave descriptive above for impedance matching was used. The result is given by the third curve. The two peaks in the third curve create the locus that is illustrated on in the Smith chart in Fig. 3.

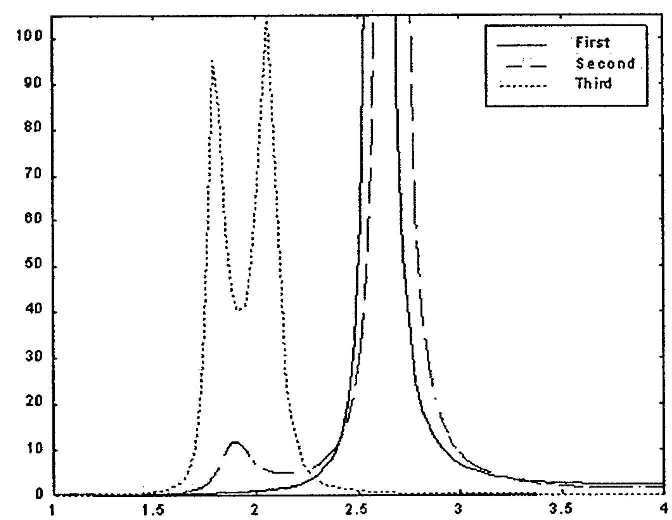

Fig. 2. Real part of impedance.

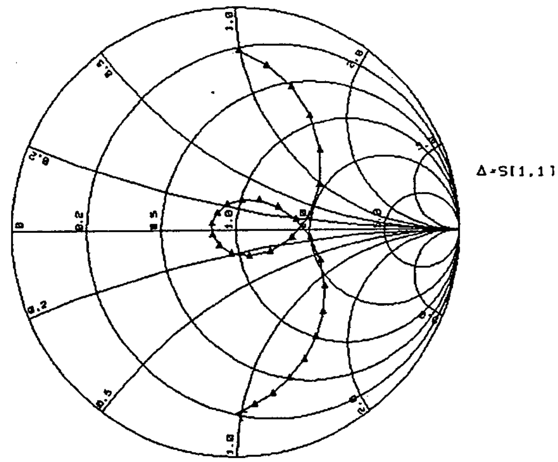

Fig. 3. Smith chart plot of the impedance.

The shorted aperture coupled microstrip antenna has a several dimensional parameters and material that we can adjust during the optimization process. Several solutions can be found with the same material that fit the desired characteristic. With one shorting pin, a bandwidth of 10 % (VSWR 2:1) was achieved. The length is L = 17.35 mm which represents a 69 % reduction over the conventional λ/2 microstrip antenna. Dimension values can be found in Table 1.

One other method to improve the bandwidth is to place multiples shorting pin, as in general bandwidth increase with the number of shorting pin. Of course this is truth to a certain extended and a limit of shorting pin can be used. Changing the number of shorting pins will also affect the frequency. It is mentioned in [9] that the resonant frequency and the bandwidth reach their maximum values when the sum of the diameter of shorting pins is approximately one-half the width of the rectangular patch. A model was derived in [6] assuming the pins are across a parallel plate transmission line backed by an open circuit. The equivalent circuit elements for this model are then used to determine end correction for the patch length. The change in the patch length is given by

$$\frac{\Delta l}{a} = \frac{1}{2\pi}\left\{\ln\left(\frac{a}{2\pi r}\right) - 4\pi^2\frac{r^2}{a^2} + 0.601\frac{a^2}{\lambda^2}\right\} \quad (3)$$

Where a is the separation between pins, r the pin radius, and λ the wavelength in the dielectric.

An other problem resulting from using multiple shorting pins is the more difficult manufacturing. Using this technique a 22 % bandwidth in the PCS frequency was achieved. In this case, we use three shorting pins. The bandwidth was also obtained at the expense of a larger antenna. As in the previous design quarter-wave was used as extra degree of freedom during the design. Dimension values can be found in Table 2.

Fig. 4 shows the antenna radiation pattern with infinite ground plane. It can be seen that the front to back ratio is pretty high. This is du of the fact that the slot is relatively large compared to the antenna. Since the antenna is on a small ground plane, the pattern should be also more isotropic. It is been discuss that SAR is an important characteristic especially when designing antenna at the mobile. The solution to get the front to back ration lower is presented in [5] It consists to put an other layer on top of the feeding layer. This stops the slot to radiate to the back of the antenna du to the new ground plane.

3 Experimental results

Following the analyses of the simulated model, prototypes were built. The measurements were taken using a HP8719C network analyser and are showed in Fig.5 and Fig. 6 show the measured and the predicted VSWR for the antenna

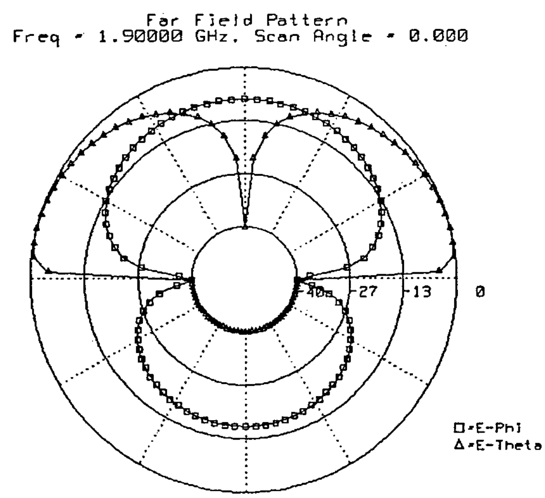

Fig. 4. Radiation pattern of the antenna on a infinite ground plane.

using only one shorting post. The prototype gives a bandwidth of 13 % with a center frequency of 1.91 GHz.

Fig. 6 shows the measured and the predicted VSWR for the second antenna using three shorting posts. The second prototypes give a bandwidth of 21 % with a center frequency of 1.99 GHz.

One important parameter that was not considered so far is the size of the ground plane. Truncating the ground plane, reduces the size and cost of the antenna. It changes the radiation pattern to a more isotropic form and improves its sensitivity to the two perpendicular polarizations. For all these reasons, we built two prototypes on small ground plane of about 7 cm x 7 cm. Fig. 7 represents the radiation pattern of the prototype with one shorting post at 1.9 GHz. Fig8 shows a picture of the first prototype with one shorting pin. It can be seen from the picture that the radiating element is pretty small compare to a conventional microstrip antenna.

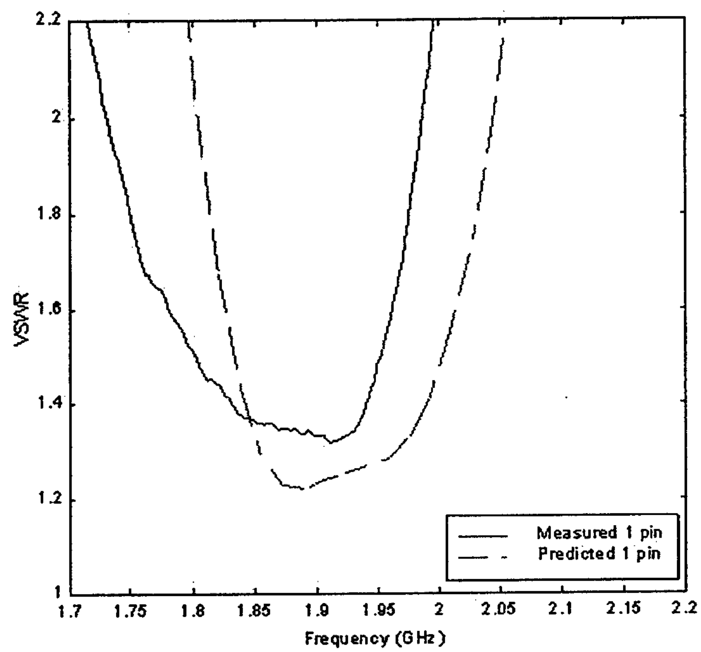

Fig. 5. Measured and predicted VSWR

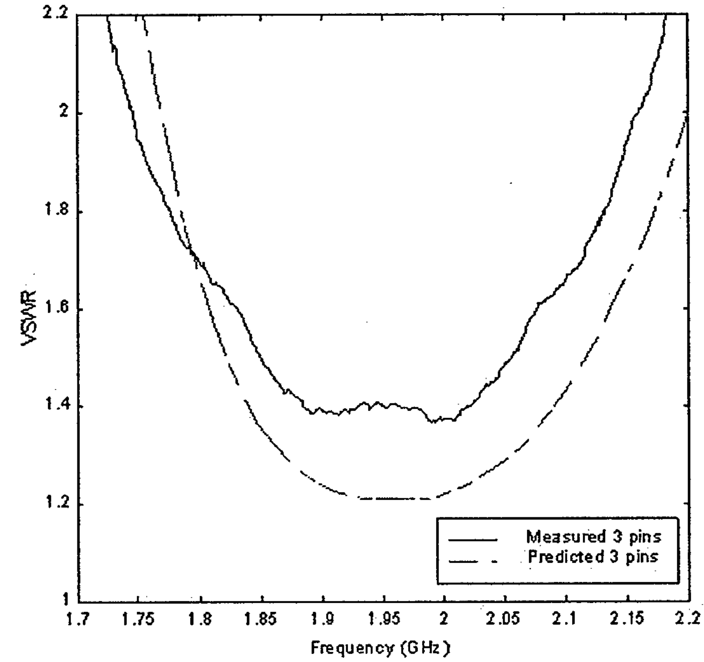

Fig. 6. Measured and predicted VSWR

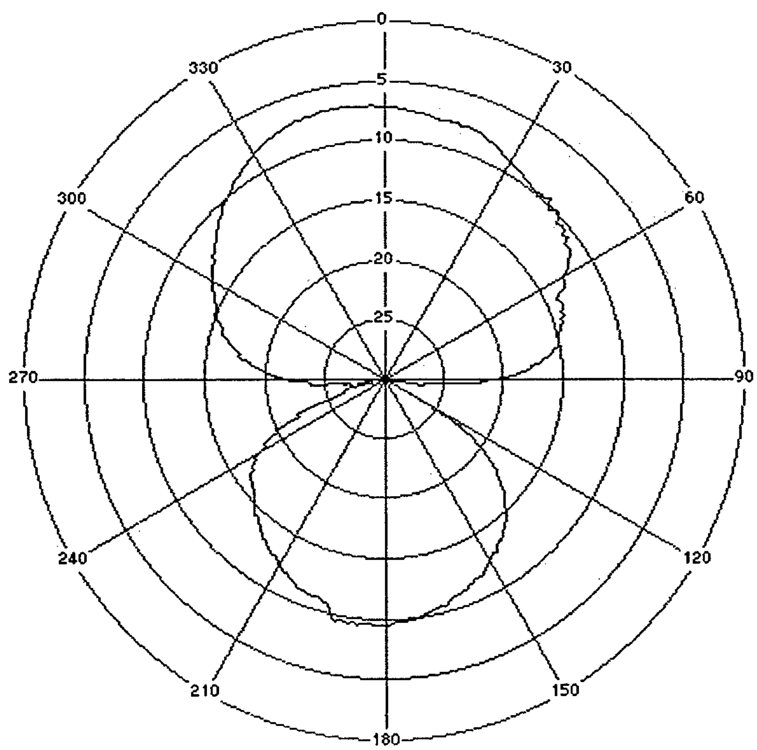

Fig. 7. H plane radiation pattern at 1.90GHz.

4 Conclusion

Using Ensemble 5.1, a small aperture antenna was designed. Open quarter-wave stub was shown to give an extra degree of freedom during the design of the antenna. Insight for the design of such an antenna was given. Prototypes were build and measurements were shown to be in good agreements with the numerical result. Future work can be carried out by using this type of antenna in a smart antenna for applications in mobile communication systems.

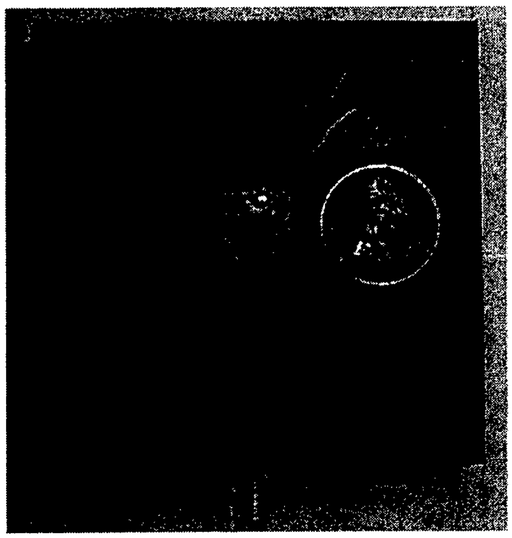

Fig. 8. Picture of the first prototype

5 Reference

[1]T.K. Lo, C.-O. Ho, Y. Hwang, E. K. W. Lam, and B. Lee, "Miniature aperture coupled microstrip antenna of very high permittivity," Electron. Lett., vol. 33, pp. 9-10, Jan. 1997.

[2]I. Park and R. Mittra, "Aperture-coupled small microstrip antenna," Electron. Lett., vol. 32, no. 19, pp. 1741-1742, Sept 1996.

[3]R. B. Waterhouse, S. D. Targonski, D. M. Kokotoff, "Design and Performance of Small Printed Antennas," IEEE Trans. Antennas and Propagat., vol. 46, pp. 1629-1633, Feb. 1998.

[4]Boulder Microwave Technologies, Inc., ENSEMBLE, Design, Review and 1D Array Synthesis User's Guide, Version 5.1, Ansoft, USA, 1998

[5]T. A. Denidni, M. Hotton, "Experimental investigations of a broadband microstrip antenna for PCS application," IEEE symposium on Veh. Tech. Com. (VTC '99), Houston, USA, pp. 1764-1767, May 1999.

[6]James, J. R., P. S. Hall, and C. Wood, Microstrip Antennas, Theory and Design, London, UK: Peter Peregrinus, 1980.

[7]D.M. Pozar, "A reciprocity method of analysis for printed slot and slot-coupled microstrip antennas," IEEE Trans. Antennas & Prop., vol. AP-34, pp. 1439-1446, Dec. 1986.

[8]H.F. Pues and A. R. Van de Capelle, "An impedance-matching technique for increasing the bandwidth of microstrip antennas," IEEE Trans. Antennas & Prop., vol. 37, pp. 1345-1354, Nov. 1989.

[9]I. Park, B. J. Cho and R. Mittra, "Aperture-coupled small microstrip antenna with enhanced bandwidth" APS Society, International symposium, vol. 2, pp. 1212-1215, 1999.

Table 1: Design parameters for small aperture antenna (mm)

Design	# pins	a	Lp	L	W	Ls	Ws	Wq	Lq	L1	r
1	1	-	0.95	17.35	10.2	19.2	3	9.2	17.38	6.175	1.63
2	3	5	9.95	27	17	22.8	3	4,87	17.38	12	1.63

A Coaxial Cavity Antenna Exhibiting Low Dispersion Over a Wide Field of View

Dr. Tim Holzheimer, P.E.
Raytheon
Aircraft Integration Systems
Majors Field and FM-1570
Greenville, Texas 75403

Abstract:

A coaxial cavity antenna, patent pending, has been developed, by Raytheon, that exhibits low dispersion over wide field-of-view (FOV). This antenna has essentially a flat phase and amplitude response over a +/- 60 degree FOV. The antenna design is scaleable over multiple frequency ranges and antennas have been built covering frequency ranges from 400 MHz to as high as 44 GHz with bandwidths on the order of four and one-half octaves. This antenna is a four point feed design where the natural base polarizations are dual linear. Both senses of circular polarization can be obtained, and have been demonstrated with the addition of a hybrid. Designs have been built where any linear or circular polarization can be switched as an output of these antennas.

These antennas have been used in interferometers and polarimeters. The flat phase and amplitude response have proven this antenna to be an excellent choice for polarimetry. The same is true in direction finding (DF) systems where these elements are presently being implemented in a 360 degree FOV circular DF array. These elements are also being implemented in linear interferometers where the FOV is relaxed.

Introduction:

Wide band or wide bandwidth antennas, that operate over multiple octaves, have been investigated by many researchers. [1-4] These types include horns, spirals, combinations of these with polarizers, various cavity designs and others. The sub-system perspective, desires an antenna that covers multiple octaves, has multiple polarization capability, flat amplitude and phase response over field of view and among similar elements, low cross-polarization and high efficiency. The coupling among arrayed elements should be small and when installed should have high isolation.

Figure 1, illustrates how the, patent pending, concentric cavity or coaxial cavity antenna, the subject of this paper, was determined.[5] The antennas that are first investigated are the spiral and the horn antenna. The spiral antenna is broadband, a single polarization although it can receive energy from all polarizations except for the opposite circular polarization, and is a low efficiency, low gain element. The horn antenna is a high gain element, typically a single or dual polarization depending on the use of multiple feed points, and can exhibit poor phase tracking. The horn antenna is typically larger in depth at lower frequencies such as 2 GHz as compared to an equivalently designed spiral antenna.

Ideally, the requirement usually presents itself for dual polarization, which is met in the natural polarization states of these elements. The spiral antenna is naturally circularly polarized and investigators, including Raytheon, have designed, developed and fabricated dual polarization spirals using switching techniques changing the arm rotations and feeding from the ends of the arms as opposed to feeding at the center of the arms. The problems that occur are low efficiency, limited bandwidth, and low reliability in the polarizations, due to switching, and the low cross-polarization isolation.

The dual polarized horns exhibit good bandwidth when fed with two probes for each natural polarization. When the horns are designed correctly, excellent phase and amplitude tracking over the desired field of view are obtained. The horns exhibit high cross-polarization isolation, 30 dB, and high polarization isolation, 25 dB, between the two feeds. The issue of size still exists, as compared to the spiral, but higher gain is obtained on the order of 10 to 14 dBli. Circular polarization can be obtained from the horn by adding rotation in the feed area or by using polarizers, which complicate the antenna construction.

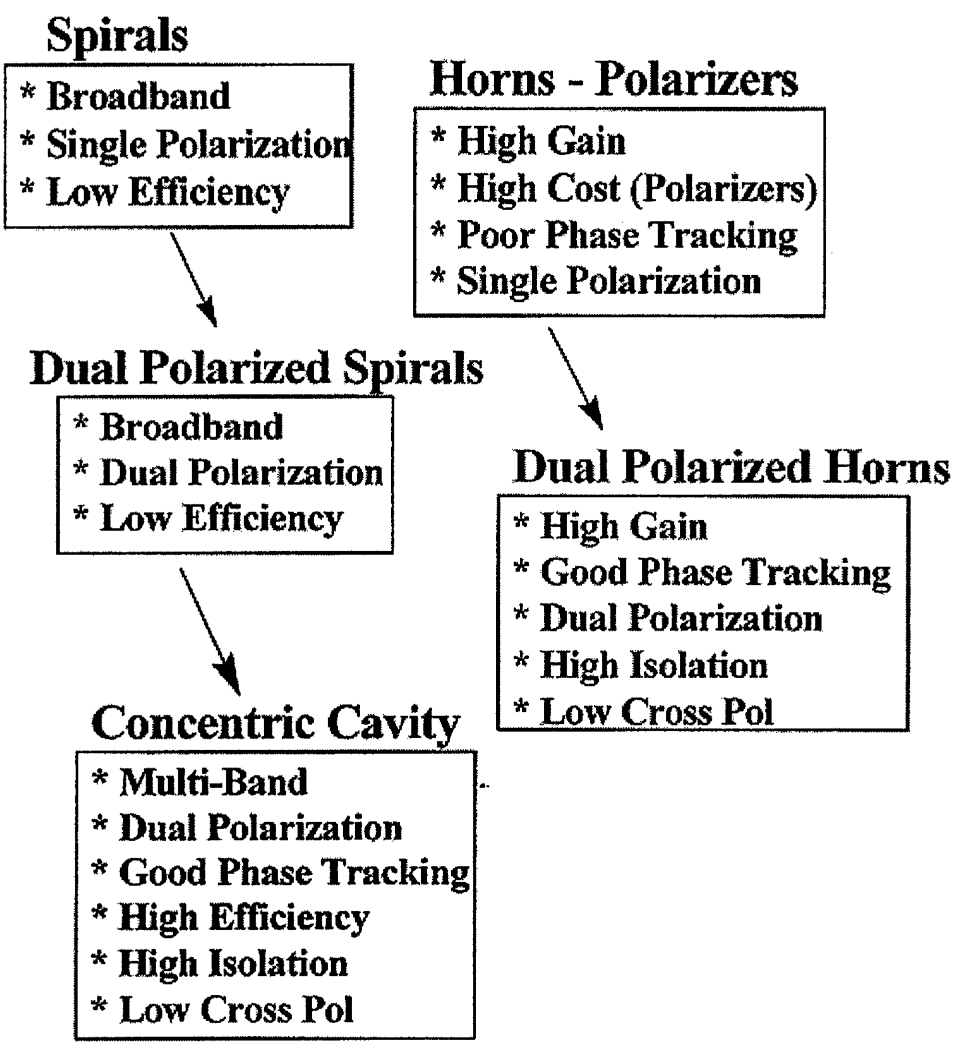

Figure 1. Roadmap of Existing Wide Band Antennas to the Coaxial or Concentric Cavity Antenna.

The concentric or coaxial cavity antenna presents itself as a moderate gain element with excellent phase and amplitude tracking over the desired field of view. These antennas are easily scaled for use in multiple bands, Raytheon demonstrated from 400 MHz to 44 GHz. The coaxial cavity antenna can be used for any polarization, by rotation of the cavity or by appropriate networking for linear or circular polarization. Figure 2 illustrates the method for obtaining the linear polarizations, which can then be combined via 90-degree hybrids to obtain dual circular polarizations. The same cross-polarization isolation and polarization isolation occur as for the horns with the added benefit of excellent phase tracking over the field of view.

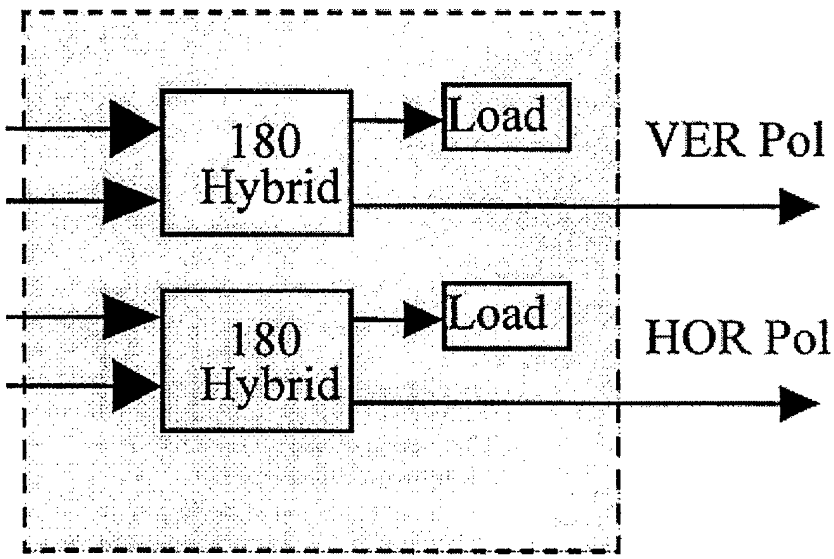

Figure 2. Networking Required Behind the Coaxial Cavity Antenna in Order to Provide Dual Linear Polarization.

Applications:

The applications for these types of antennas, regardless of whether they are spirals, horns or coaxial cavity antennas, are in use as interferometer elements, direction finders, radar warning receiver (RWR) antennas, phased array elements, polarimeters and others. The interferometer and the polarimeter place the most stringent requirements on the antennas that are used in these systems. They require flat amplitude and phase over both field of view and frequency of operation. Stated another way, if the antenna can radiate an exact duplicate of an impulse then it will have the desired properties for use as an interferometer and polarimeter antenna element.

The elements that are used in these systems must be balanced against desired polarizations (usually all-polarization capable), operational frequency range, useful field of view and detection range, which translates into the amount of gain required of the antenna element. Mechanical considerations also exist, such as weight, complexity, and reliability of the design to hold together through normal and operational vibration, shock, altitude, and/or other environmentals.

The following discussions will show the performance of horns for use in these applications, which can then be compared to the coaxial cavity antenna. The coaxial cavity data will illustrate the single and the arrayed performance that can be obtained.

Low Dispersion Horns:

A complete series of dual polarized horns have been developed and fully flight qualified for use in a multitude of systems. The horns are illustrated in figures 3 and 4. These horns have been designed in all the standard octave and multi-octave bands up to 44 GHz and as low as 2 GHz. The horns are extremely lightweight and mechanically strong. Tables 1 and 2 illustrate the performance and lightweight design that results with these horn antennas.

Figure 5 shows the typical E-plane and H-plane patterns of the horns with the cross-polarized component. The data shows the greater than 25 dB cross-polarization and isolation that is obtained with these horns. These horns exhibit azimuthal 3 dB beamwidths of greater than 55 degrees and elevation 3 dB beamwidths of greater than 15 degrees. The phase tracking of these horns is less than 5 degrees. These antennas have been built incorporating high-speed switches so that the polarizations can be switched and the RF can be run down a single coax to the receiving part of the sub-system. The horns are considered high gain and exhibit gains of +10 to +17 dBli.

These horns can be used in interferometers, provide long detection ranges due to the higher elemental gain, and interference rejection due to the sidelobe structure. The horns are typically used in the dual linear polarization mode and if circular polarization was a requirement then the feed points could be modified to provide it or an easier approach is to use a polarizer over the mouth of the horn.

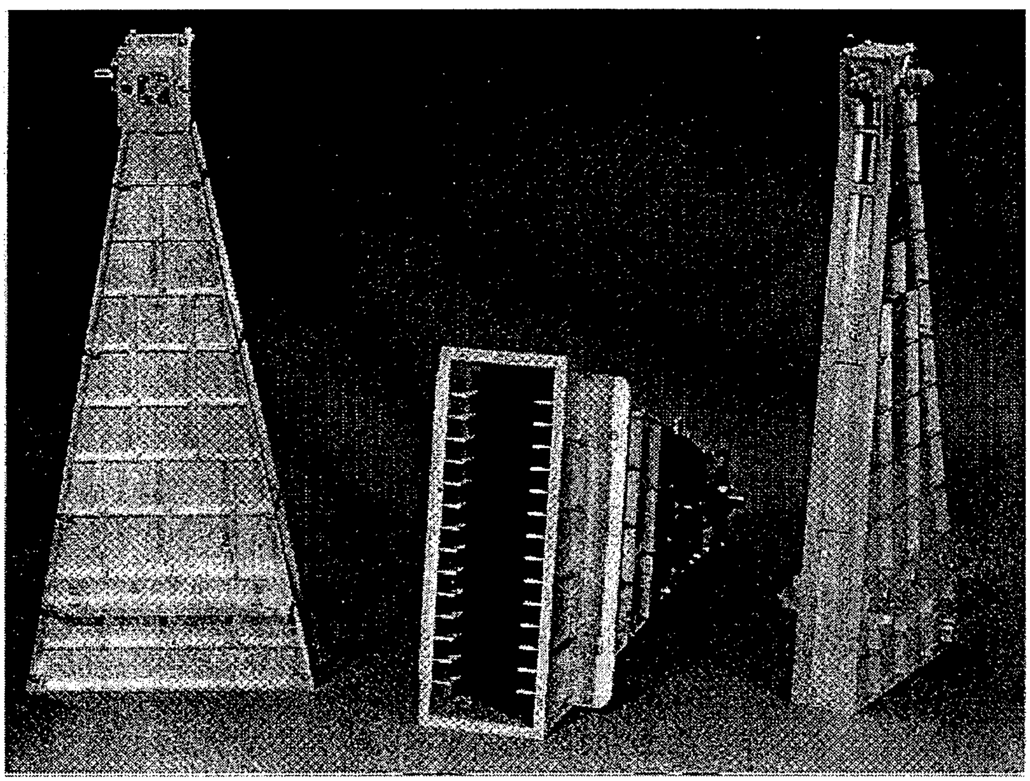

Figure 3. Extremely Lightweight Horns Exhibiting Low Dispersion and Dual Polarization.

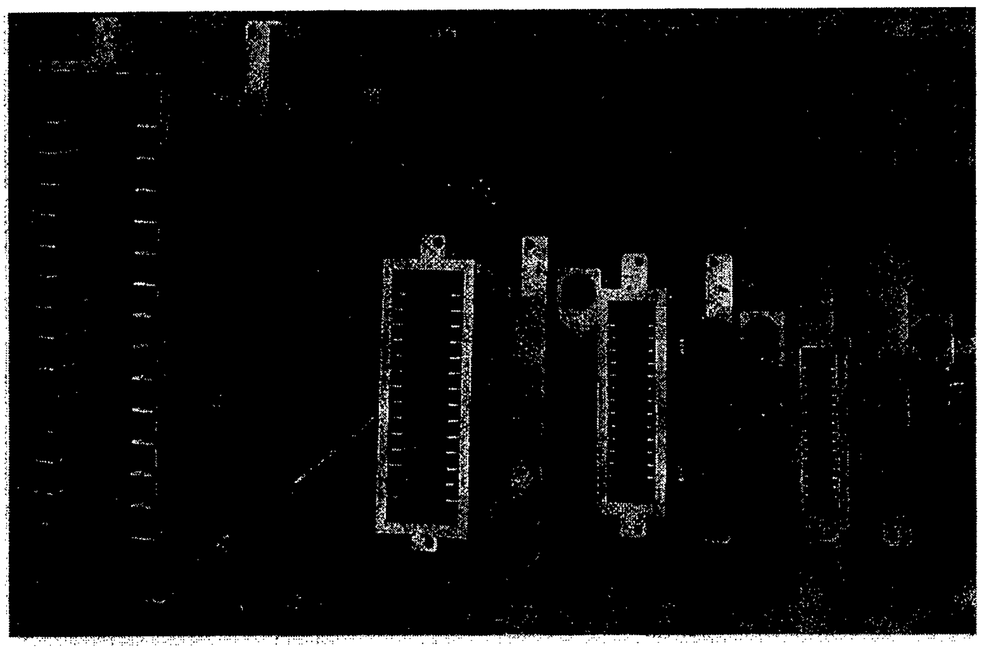

Figure 4. A Set of Lightweight, Low Dispersion Horns Covering the Four Typical Microwave Frequency Bands.

Table 1. Lightweight Horn Antenna Electrical Performance.

Electrical Performance Summary

Band	Frequency (GHz)		Gain (dBli) Measured	Az 3dB BW (deg) Measured	El 3dB BW (deg) Measured
3	F3L to F3H	E	11.0 to 16.0	75.0 to 55.0	25.0 to 15.0
		H	10.5 to 16.0	85.0 to 60.0	35.0 to 20.0
4	F4L to F4H	E	13.0 to 16.5	70.0 to 50.0	20.0 to 14.0
		H	12.5 to 16.0	70.0 to 55.0	28.0 to 15.0
5	F5L to F5H	E	14.0 to 17.0	60.0 to 55.0	20.0 to 15.0
		H	12.5 to 16.5	65.0 to 50.0	15.0 to 10.0

Table 2. Lightweight Horn Antenna Mechanical Performance.

Mechanical Summary

	Dimensions (in)			* Weight	
Band	Height	Width	Length	(grams)	(lbs)
3	5.47	1.76	9.10	352.4	0.776
4	4.32	1.30	10.30	256.4	0.565
5	3.49	0.76	10.00	182.5	0.402

*Note: Weight includes screws and connectors

E Probe Pattern

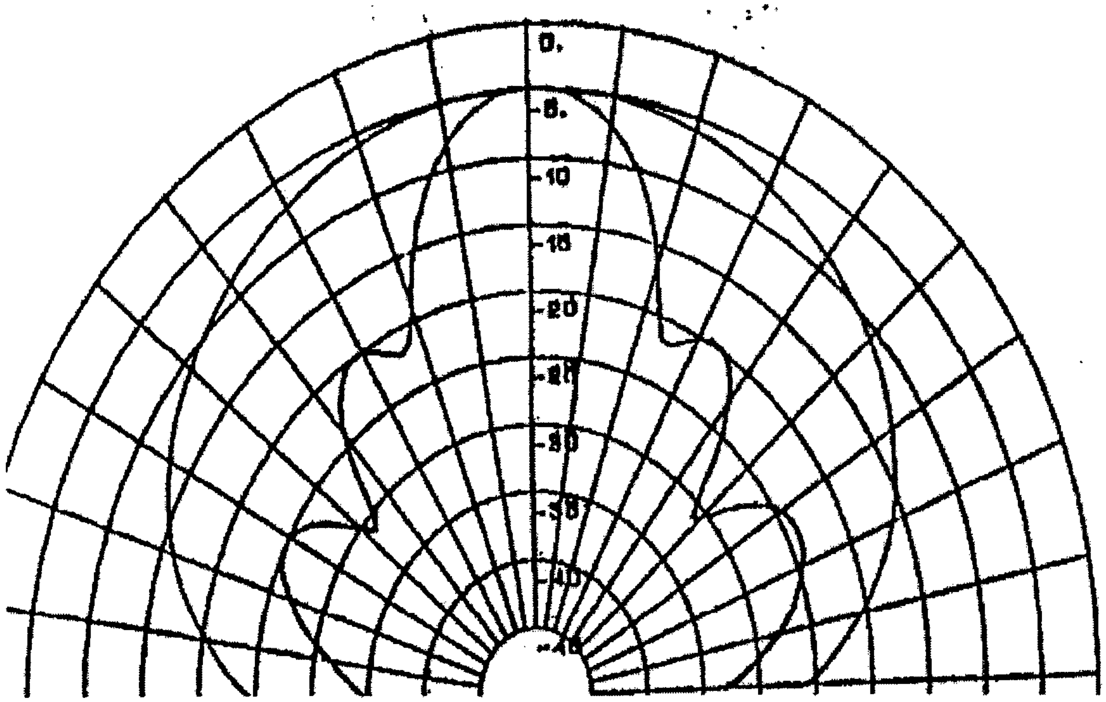

H Probe Pattern

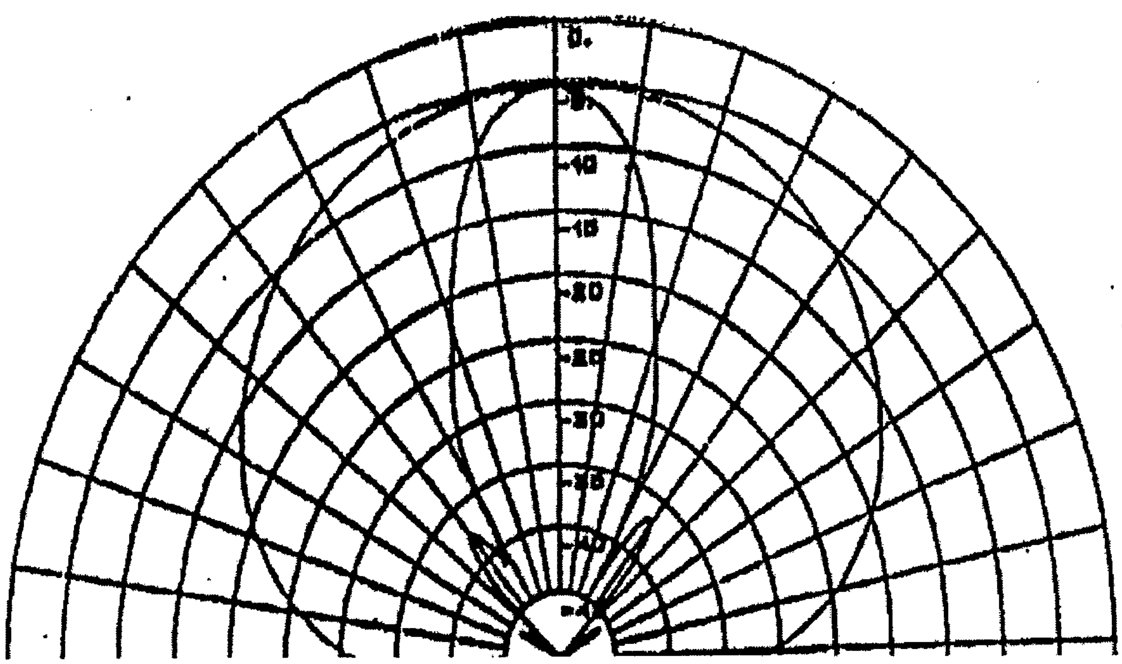

Figure 5. Typical Horn E- and H-Plane Patterns with Cross-Polarization

Coaxial Cavity Antenna:

The coaxial cavity antennas were developed over a 9-year period. A full set of design curves have been developed in order to provide proper sizing for scaling, nesting of multiple sub-bands, and for gain optimization. The design curves that have been generated also provide the key information for impedance matching to the coaxial cavity. The antenna is four point probe fed from the rear, which allows for easy assembly of any beamforming and attachment to the rear of the antenna. These antennas are also lightweight and mechanically robust in environmentals as is the horn antennas previously described. These antennas use a 180-degree hybrid to combine two of the feed probes resulting in the desired linear polarization. As stated earlier, the linear polarizations can then be combined resulting in the generation of circular polarizations.

The coaxial cavity antennas are illustrated in figures 6 and 7. The antennas are easily scaleable over any octave, multi-octave or partial octave as desired. Figure 8 illustrates three coaxial cavity antennas, which operate over different octave bandwidths without sub-banding. The sub-banding does help the overall sub-system performance by allowing filtering of each sub-band and thereby minimizing interference due to the adjacent operating bands.

The coaxial cavity antennas are approximately one third to one fourth the weight of an equivalent cavity loaded crossed dipole antenna. The phase tracking of these antennas is less than 3.0 degrees and with the all polarization capability they are excellent for polarimeters and interferometers. The gain of the coaxial cavity is better than an equivalent sized spiral. The radiation patterns are excellent as shown in figure 9. They show that the patterns in the principal planes overlay each other out at least to +/- 60 degrees, which meets the bulk of sub-system requirements.

The plots of figures 10 through 13 illustrate the applicability and performance of the coaxial cavity antenna for use as a polarimeter element. Figure 10 shows the cross-polarization isolation to be at least 35 dB, which is 10 dB better than a standard horn antenna. Figure 11 illustrates the separation of the two linear polarizations,

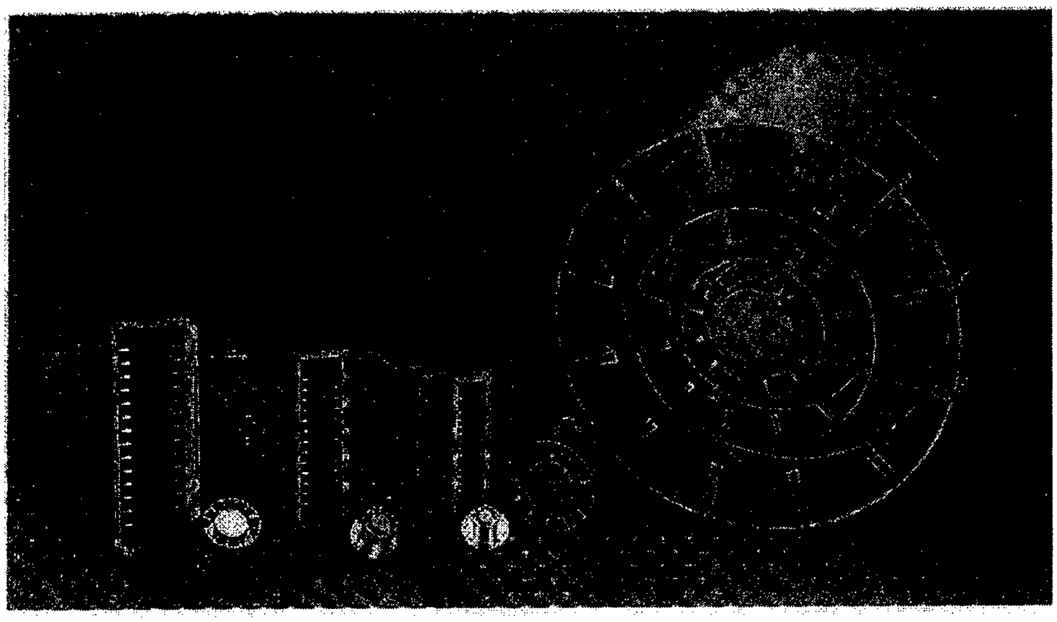

Figure 6. Size of Different Coaxial Cavity Antennas and Horns.

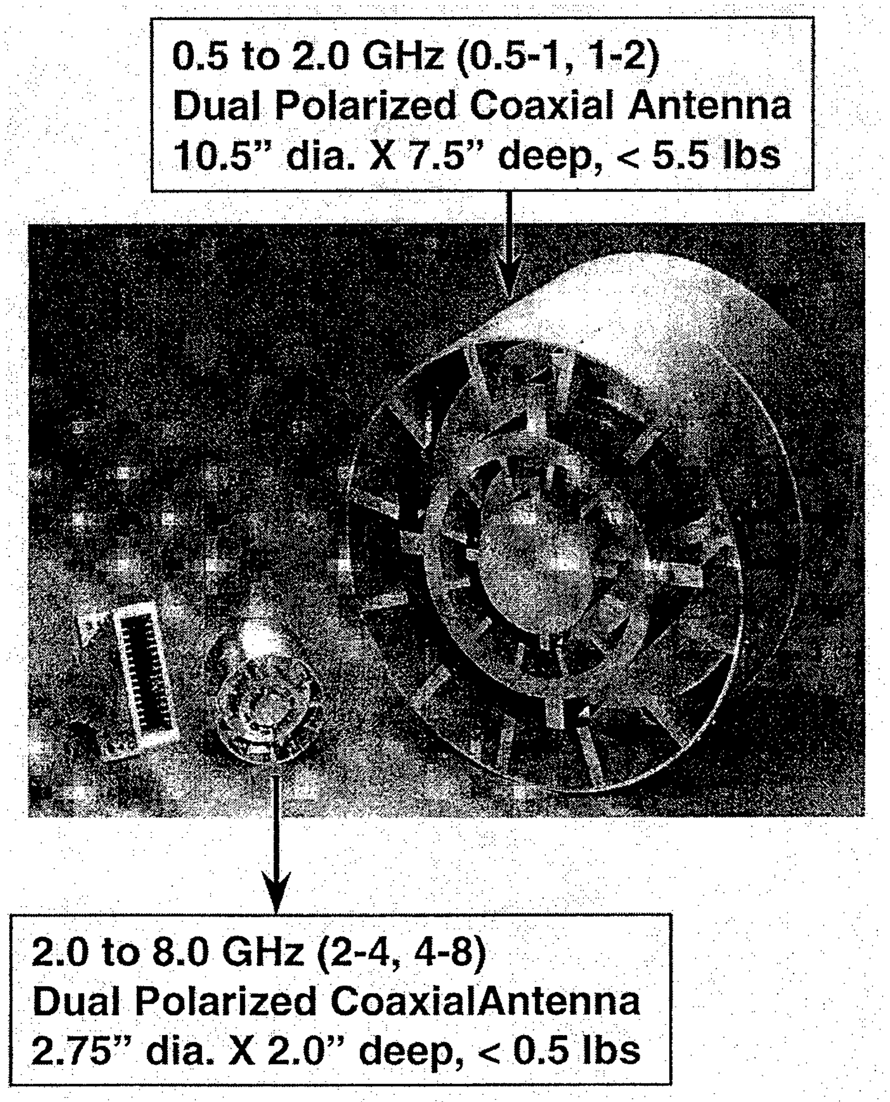

Figure 7. The Coaxial Cavity Antennas illustrating the Sub-banding, Size and Weights Achieved.

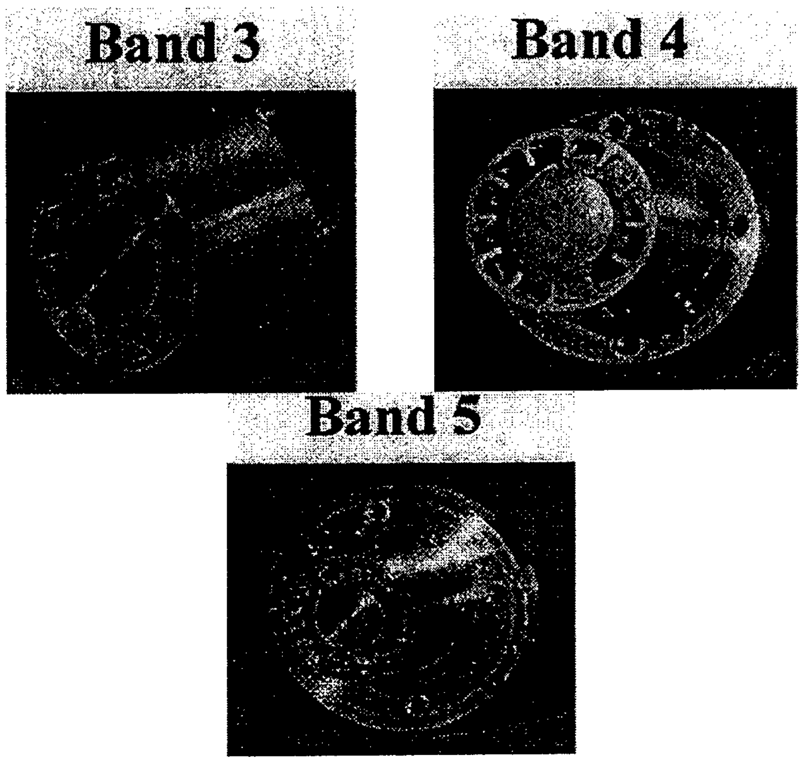

Figure 8. Three Coaxial Cavity Antennas Designed for Operation Over Single Octave Frequency Bands with No Sub-banding.

E-Plane Probe

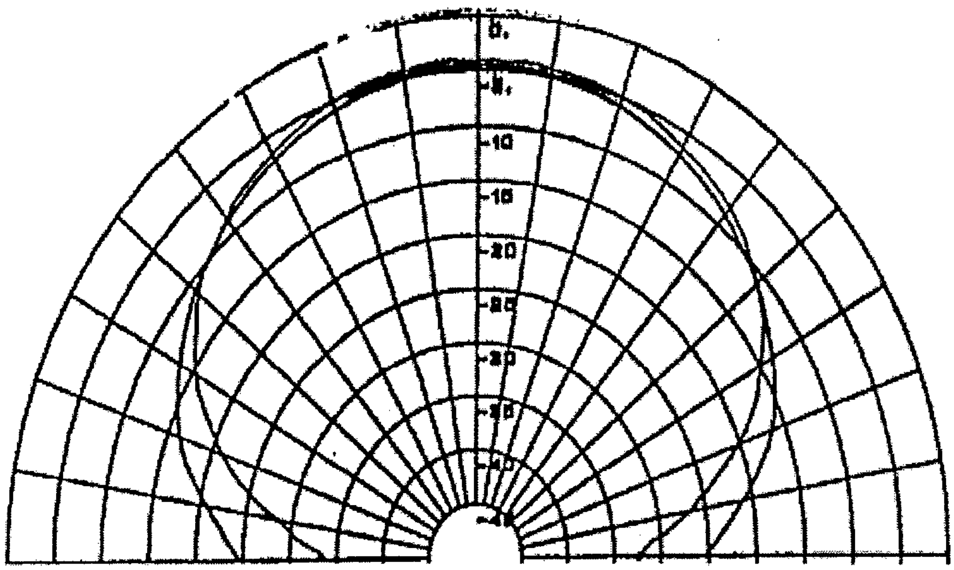

H-Plane Probe

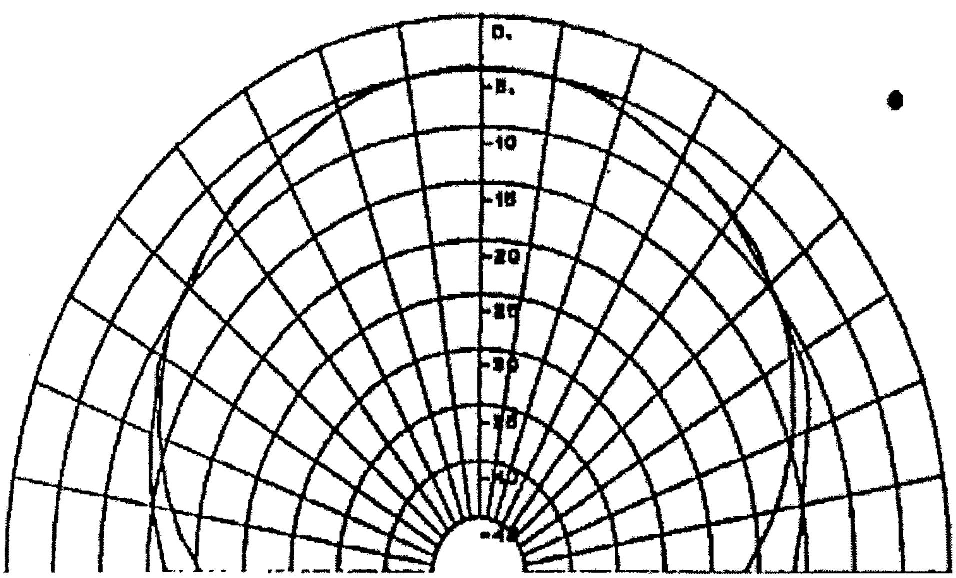

Figure 9. Radiation Patterns of the Coaxial Cavity Antenna Illustrating the Balance in the Patterns for Each Principal Plane.

vertical and horizontal, based on the amplitude response over a field of view of +/- 60 degrees. Figure 12 illustrates the problem in determining a slant-polarized signal. The response is theoretically equal into both linear polarized ports of the coaxial cavity antenna such that the amplitude responses overlay on top of each other. The only way to separate the slant linears is by looking at the phase response. Figure 13 illustrates the phase separation measured at both linear polarization ports of the coaxial cavity antenna allowing the determination of which slant linear polarization is received. The separation in phase is approximately uniform over both the field of view of +/- 60 degrees and over the operational frequency range of the antenna. This is the same response exhibited by the amplitude separation of figure 11.

An example of multi-octave frequency coverage in a coaxial cavity antenna is illustrated in figure 14. This antenna is 2.0 inches in diameter and approximately 1.5 inches in depth and covers the frequency range of 2 to 40 GHz. Pictured is the coaxial cavity antenna, which is loaded in this case, the RF feed network which slips onto the back of the cavity, and the millimeter wave downconverter, that attaches to the RF feed network assembly, all onto the back of the coaxial cavity antenna.

A flight qualified coaxial cavity antenna is shown in figure 15. This antenna covers the required octave frequency band and has the hybrids attached and integral to the back of the antenna. The hybrids are shown in figure 16. This makes for a very compact antenna, which is now in full rate production as part of a sub-system. The coaxial cavity antenna and hybrid total weight is approximately 10 ounces.

Sample Pattern & Polarimetry

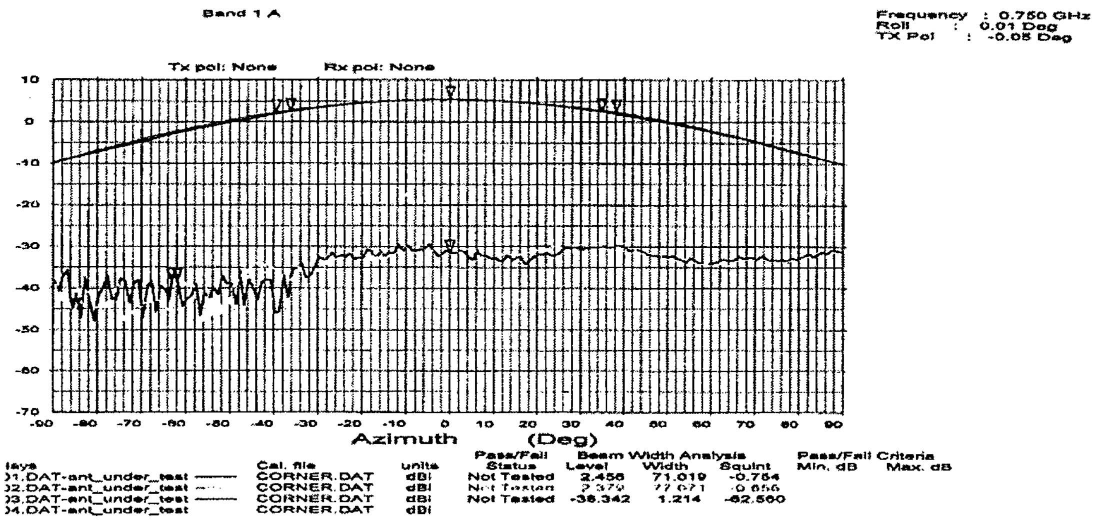

Figure 10. Co-Polarization and Cross-Polarization of the Coaxial Cavity Antenna.

Linear Emitter (Hor / Ver)
Large Amplitude Separation

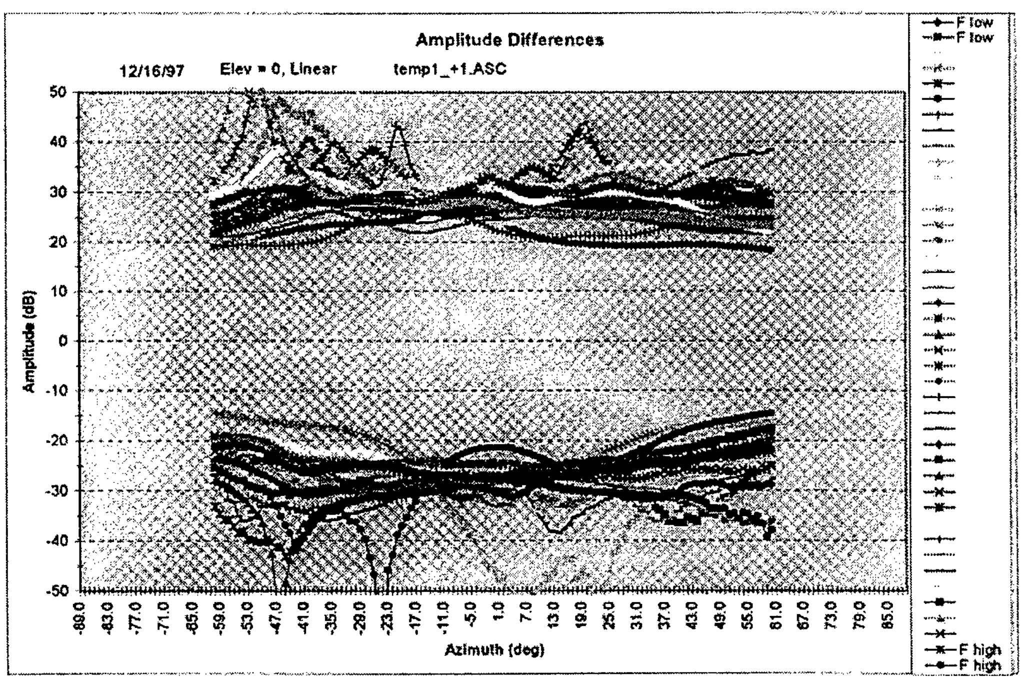

Figure 11. Large Amplitude Separation for Reception of Vertical and Horizontal Polarization with the Coaxial Cavity Antenna.

Slant Linear Emitter
Small Amplitude Separation
Use Phase to Discriminate

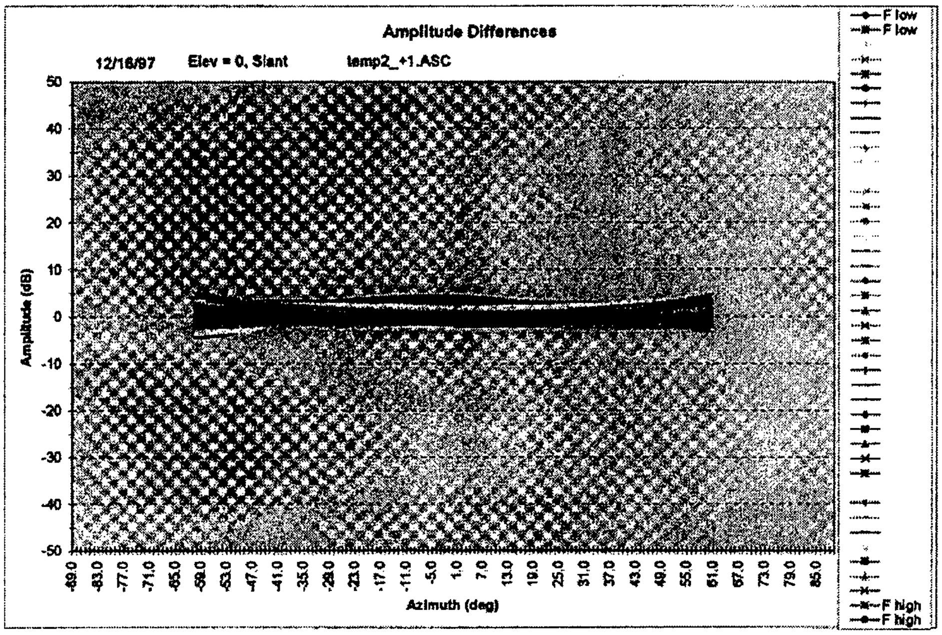

Figure 12. The Lack of Amplitude Separation as Response to Slant Linear Polarization with the Coaxial Cavity Antenna.

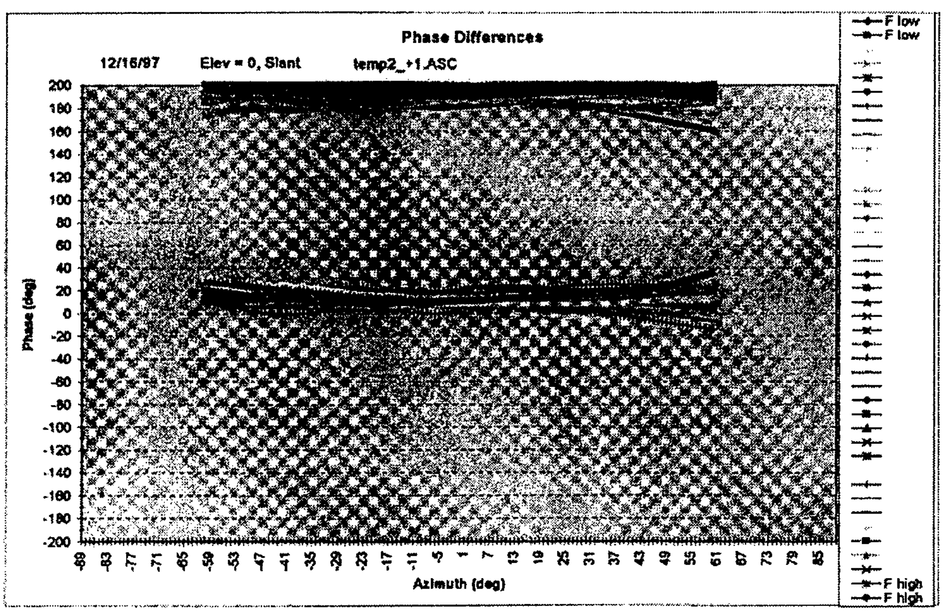

Figure 13. The Large Phase Separation Response to Slant Linear Polarization by the Coaxial Cavity Antenna.

2 to 40 GHz Coaxial Cavity

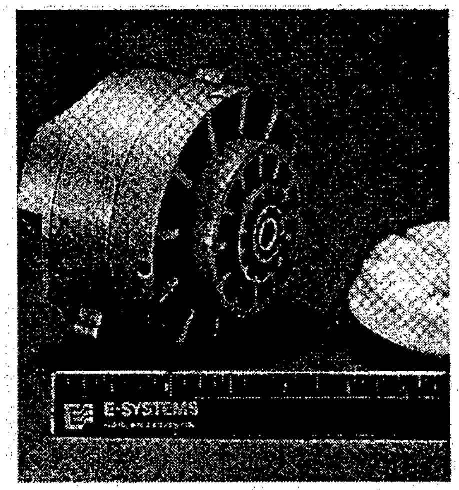

RF Feed Network

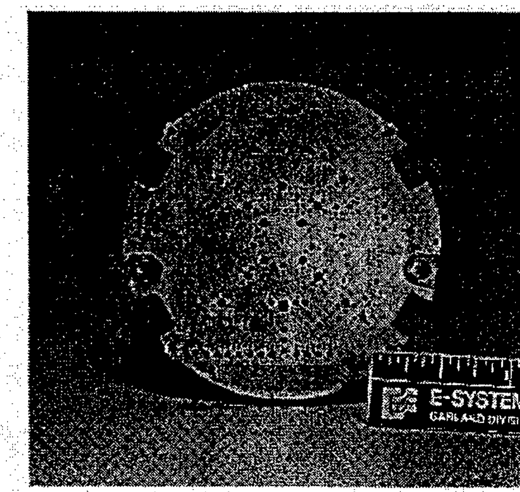

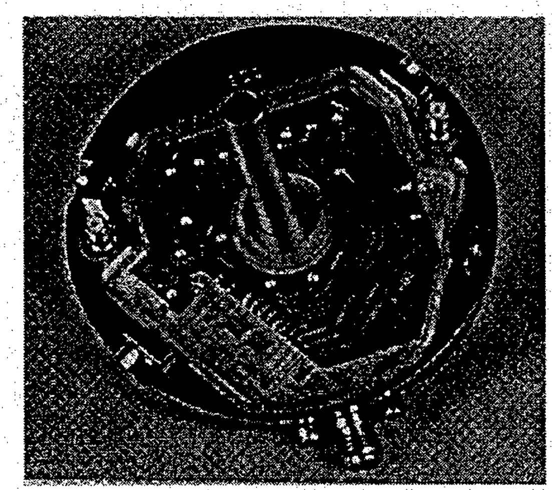

Millimeter Wave Downconverter

Figure 14. Radar Warning Receiver Using Coaxial Cavity Antenna over the 2 to 40 GHz frequency Range.

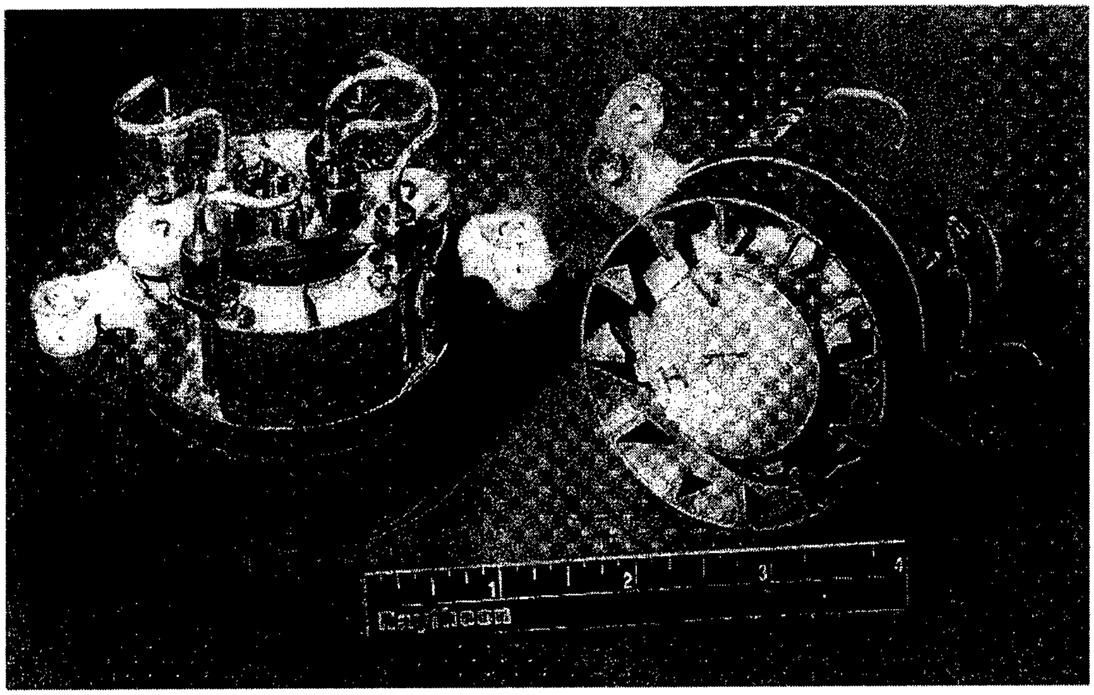

Figure 15. Flight Qualified Coaxial Cavity Antenna with Integral Hybrid Attached.

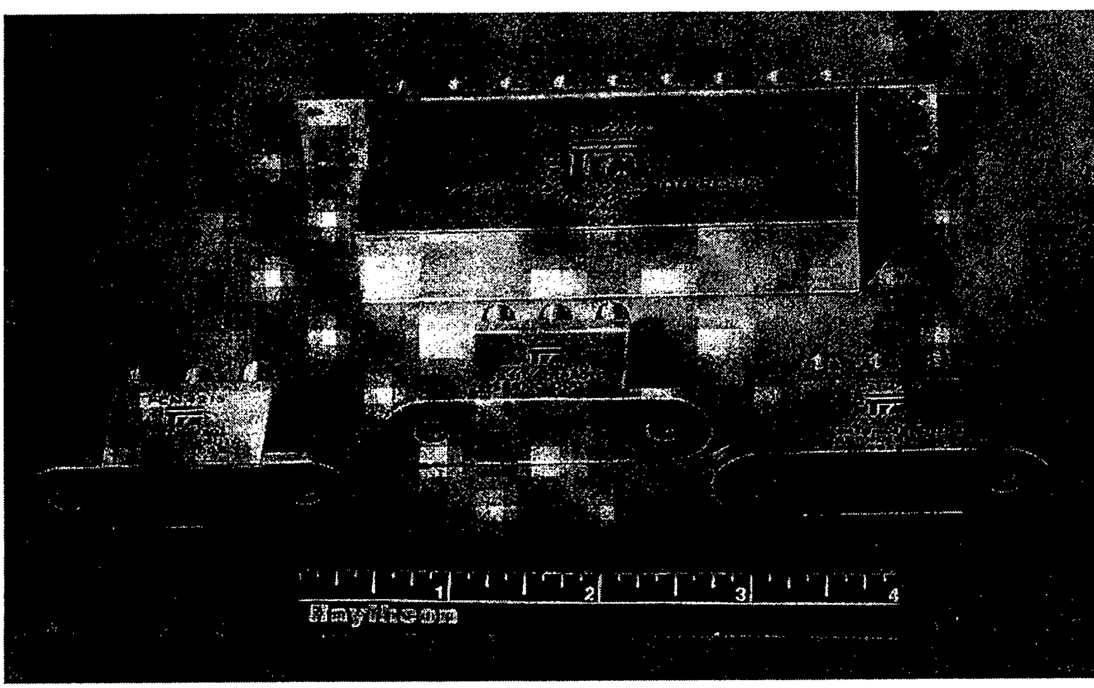

Figure 16. Flight Qualified Hybrids that are then Attached to the Coaxial Cavity Antenna.

Arrayed Coaxial Cavity Antennas:

The coaxial cavity antennas have been arrayed in two-element line array form factor with the elements butting right up to each other, i.e. the outer cavities were physically touching. The premise prior to performing this set of measurements was that the coaxial cavity antennas exhibit almost zero coupling as predicted from the measured high efficiency (approximately 75%) of the antenna. Figures 17 through 22 illustrate these points.

The gain of the array is shown in figure 17. Included on this plot is the gain of a single reference element whose patterns are shown later in this report for comparison. What stands out is the gain of the array of two coaxial cavity antennas is almost at the theoretical 3 dB over the gain of a single element. This points to almost zero coupling between the elements and the higher efficiency over other types of antennas. The other point is that the coaxial cavity elements are well balanced, illustrating and alluding to the amplitude and phase tracking of the elements. The gain for the vertical and horizontal port outputs is almost identical.

Radiation patterns are shown for the vertical probe pairs in figures 18 and 19 and for the horizontal probe pairs in figures 20 and 21. These patterns illustrate the frequency range of over an octave from 2 to 4.8 GHz. These patterns can be compared to the single coaxial cavity element patterns shown in figure 22. The arrayed azimuthal patterns overlay the single coaxial cavity element patterns and the arrayed elevation patterns are consistent with two elements versus the single element patterns of figure 22. The arrayed patterns have excellent shapes over the 2 to 4.8 GHz frequency range.

- Two High Gain, Dual Linearly Polarized Coaxial Cavity Antennas Vertically Arrayed
- Element Dimensions: 2.4” dia. X 1.6” deep
- Polarization: Dual Linear (or Dual Circular)
- Pattern: Wide Azimuth, Narrow Elevation

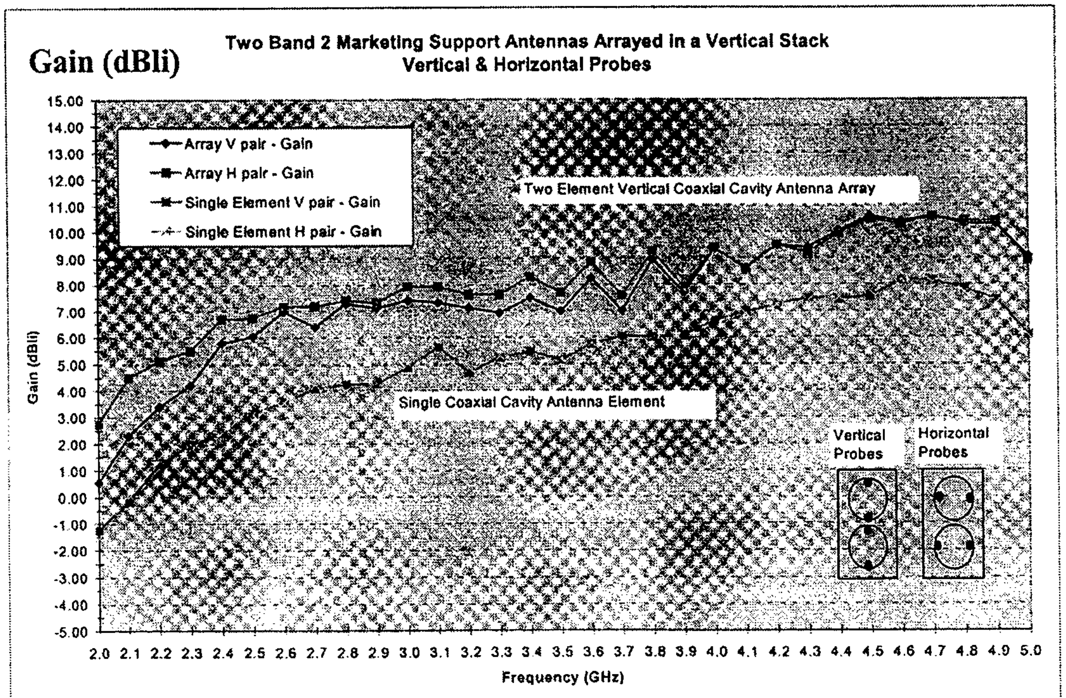

Two Element

Vertical Stack

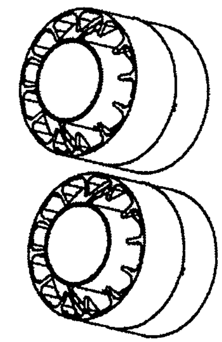

Performance:

- Near 3dB Gain Improvement Over Individual Element
- Excellent Amplitude & Phase Response
- 3dB BW:
  - Azimuth 80 to 55 deg
  - Elevation 50 to 25 deg
- Beam Squint < 2.0 deg

Figure 17. Gain of Arrayed Coaxial Cavity Antennas.

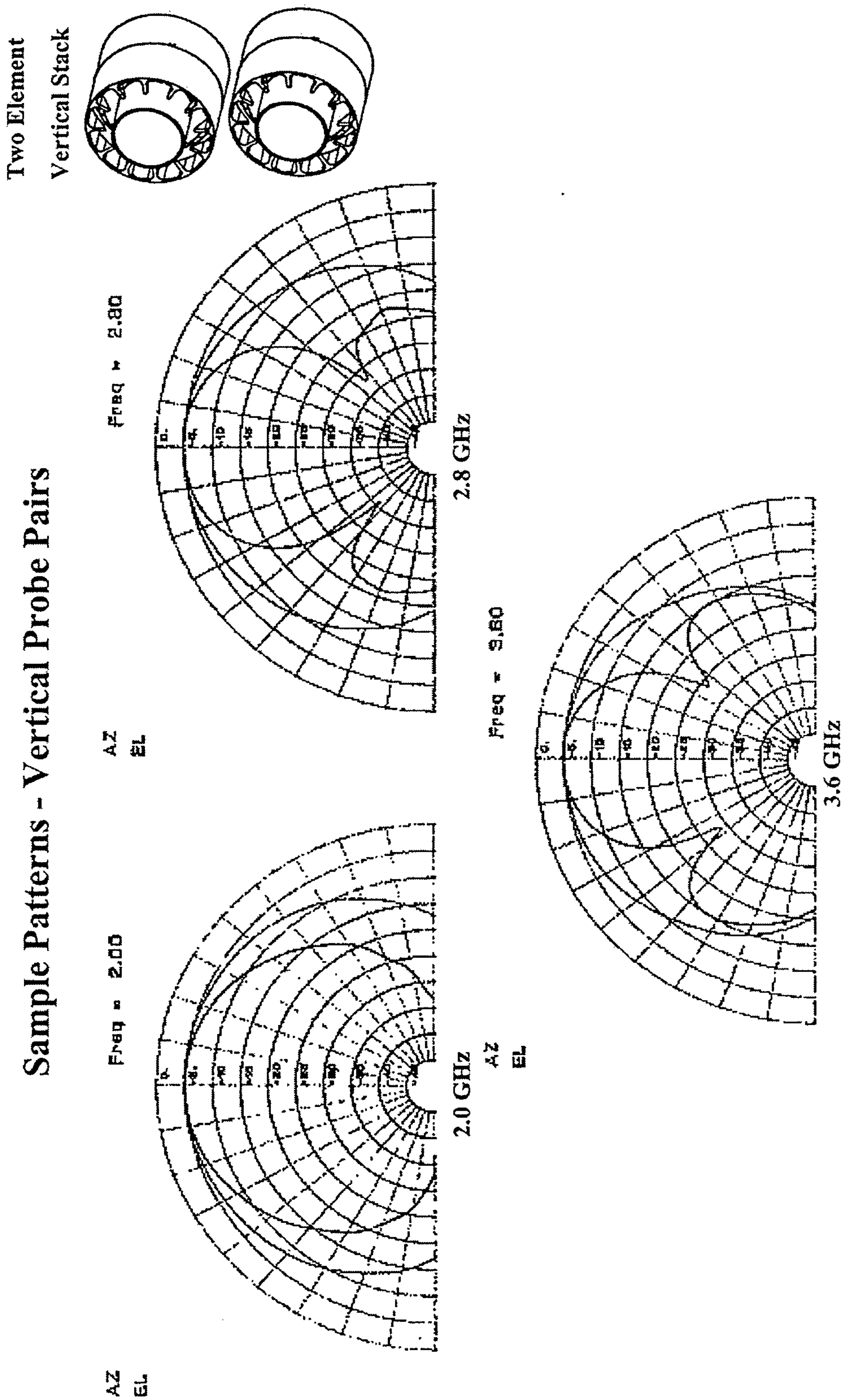

Figure 18. Arrayed Coaxial Cavity Antenna Radiation Patterns for the Vertical Probe Pairs, 2 to 3.6 GHz.

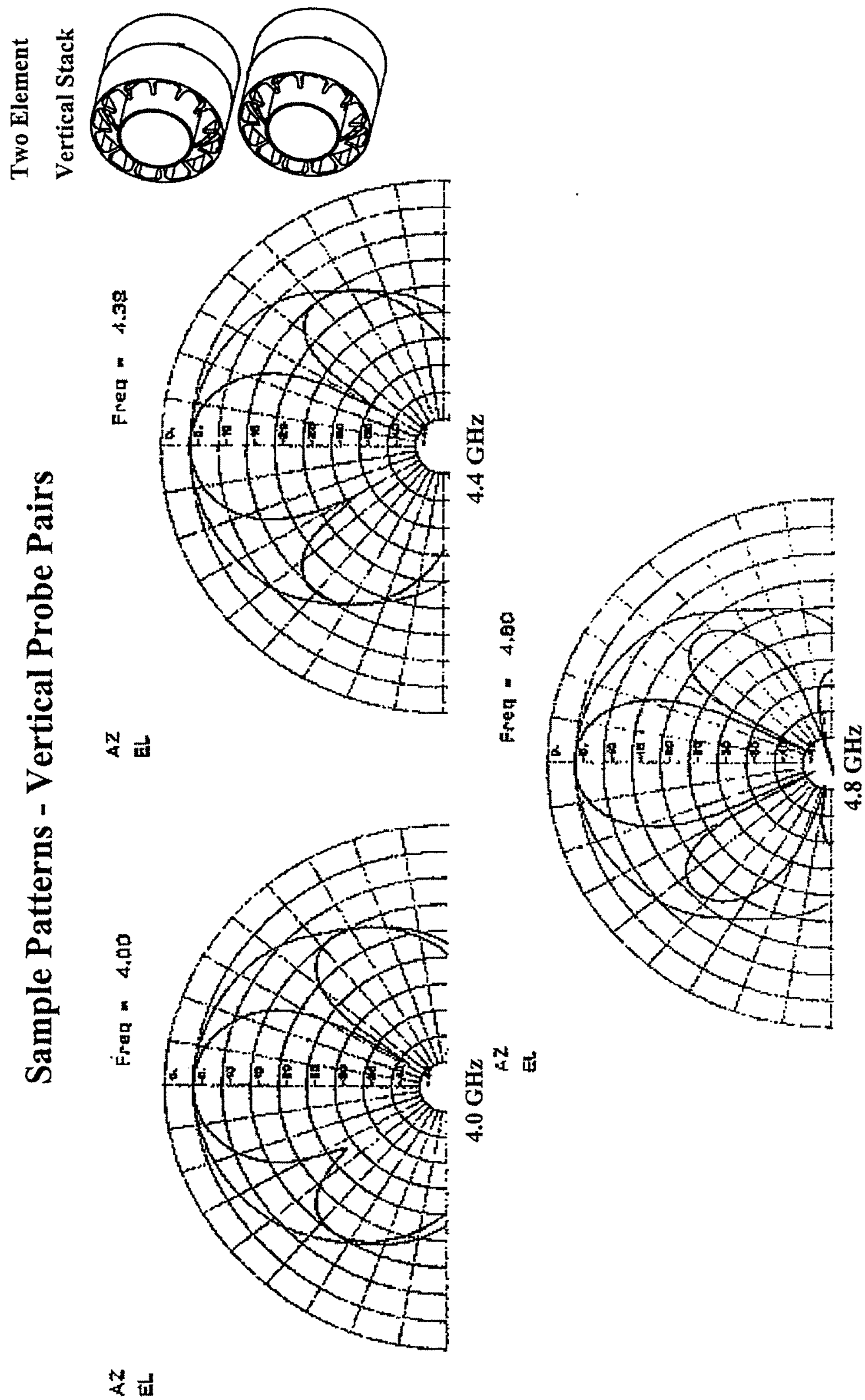

Figure 19. Arrayed Coaxial Cavity Antenna Radiation Patterns for the Vertical Probe Pairs, 4 to 4.8 GHz.

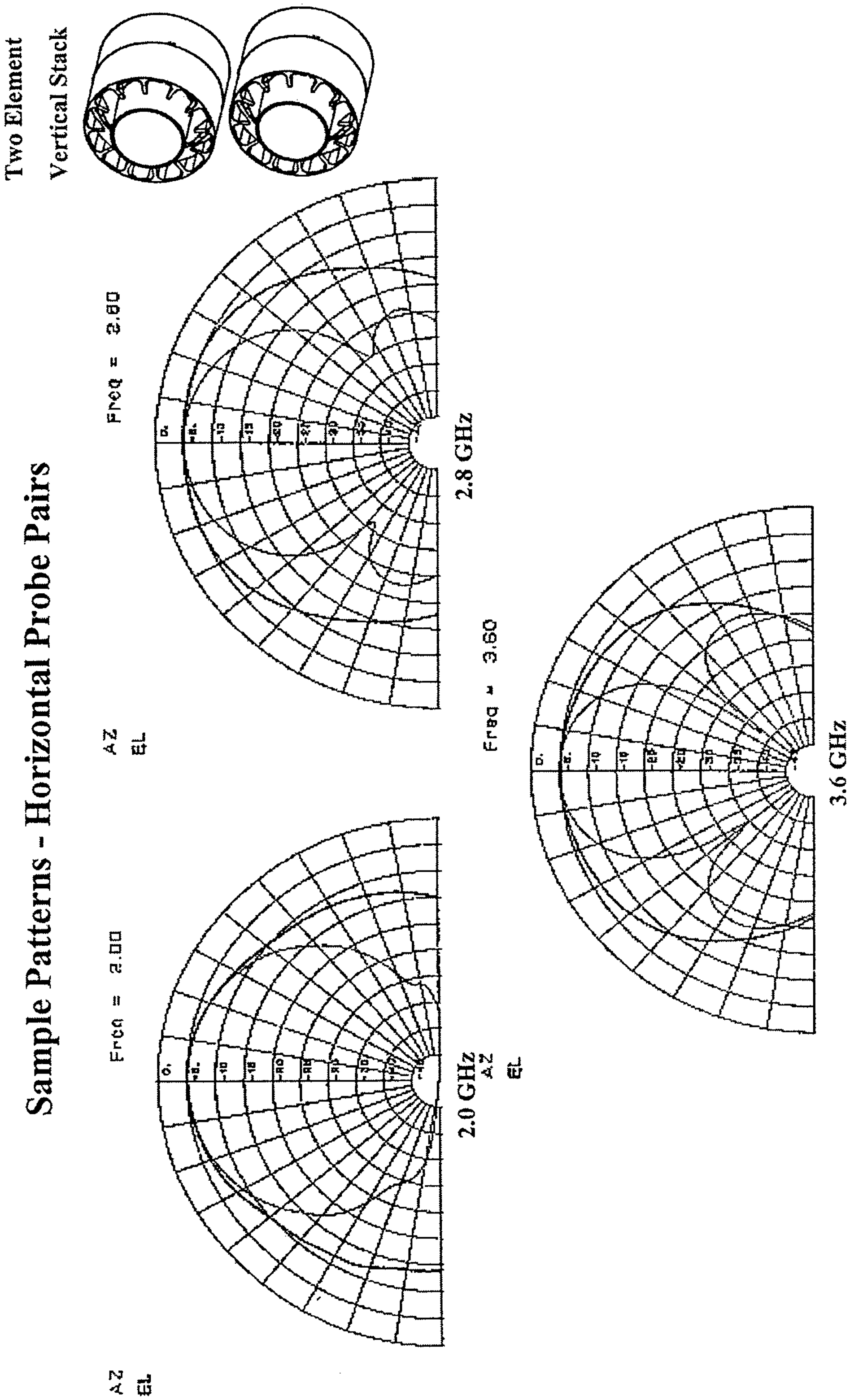

Figure 20. Arrayed Coaxial Cavity Antenna Radiation Patterns for the Horizontal Probe Pairs, 2 to 2.8 GHz.

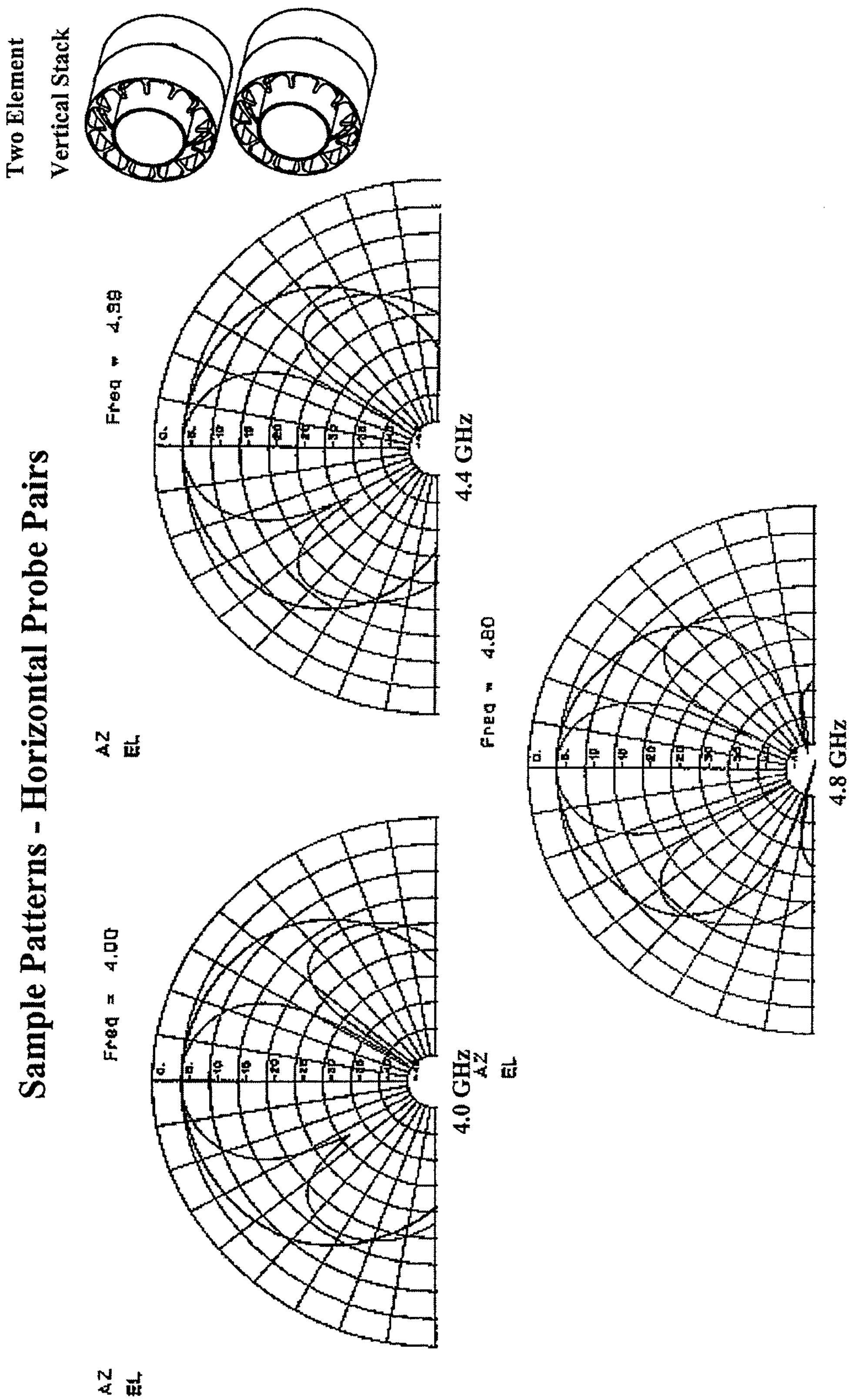

Figure 21. Arrayed Coaxial Cavity Antenna Radiation Patterns for the Horizontal Probe Pairs, 4 to 4.8 GHz.

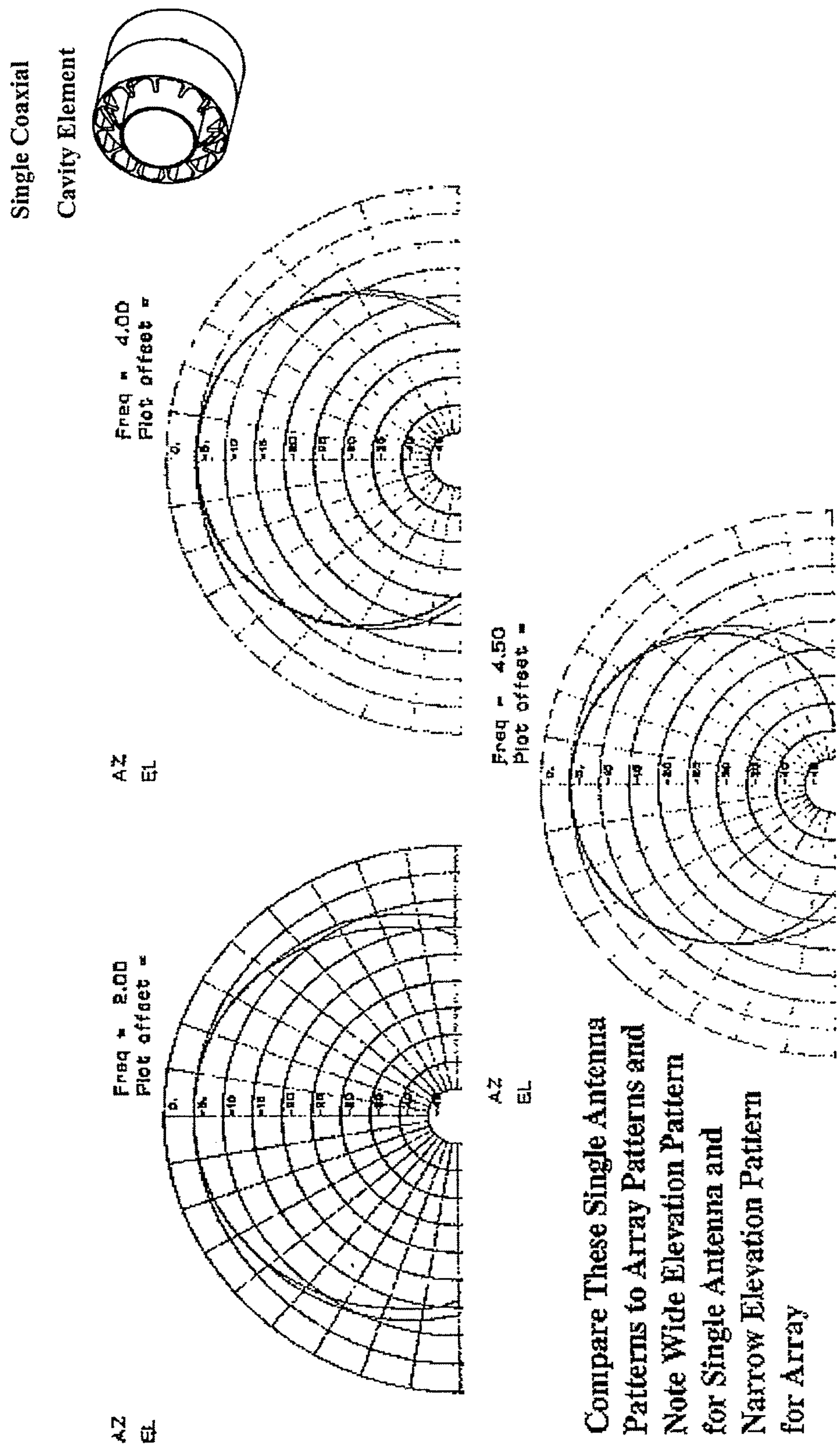

Figure 22. Single Coaxial Cavity Antenna Radiation Patterns for Comparison of Wide Elevation Versus Narrow Elevation for Arrayed Antennas.

Direction Finding Application:

An effort is being performed where the coaxial cavity elements are used in a 2 to 18 GHz 360 degree DF antenna. The goal is to illustrate a working 360 degree DF antenna in a diameter less than 12 inches. Figure 23 illustrates the DF antenna using these elements in the 2 to 18 GHz frequency configuration. The data of figure 23 shows the frequency range to be 1 to 18 GHz which is expected if a comparison is made to a spiral and appropriate gain roll-off out of band is allowed.

A modification has been made to the configuration of figure 23 that still works over the 1 to 18 GHz frequency range, but is only 9.0 inches in diameter. Both of these configurations are being built and tested over the next 12 to 18 months. The expected Angle of Arrival Accuracy (AOA) is expected to be approximately 0.5 degrees as seen in previous measurements.[6,7]

The coaxial cavity elements are considered medium gain elements since they are between the spiral and the horn. The expectation is for increased range with a smaller size 360 degree DF antenna.

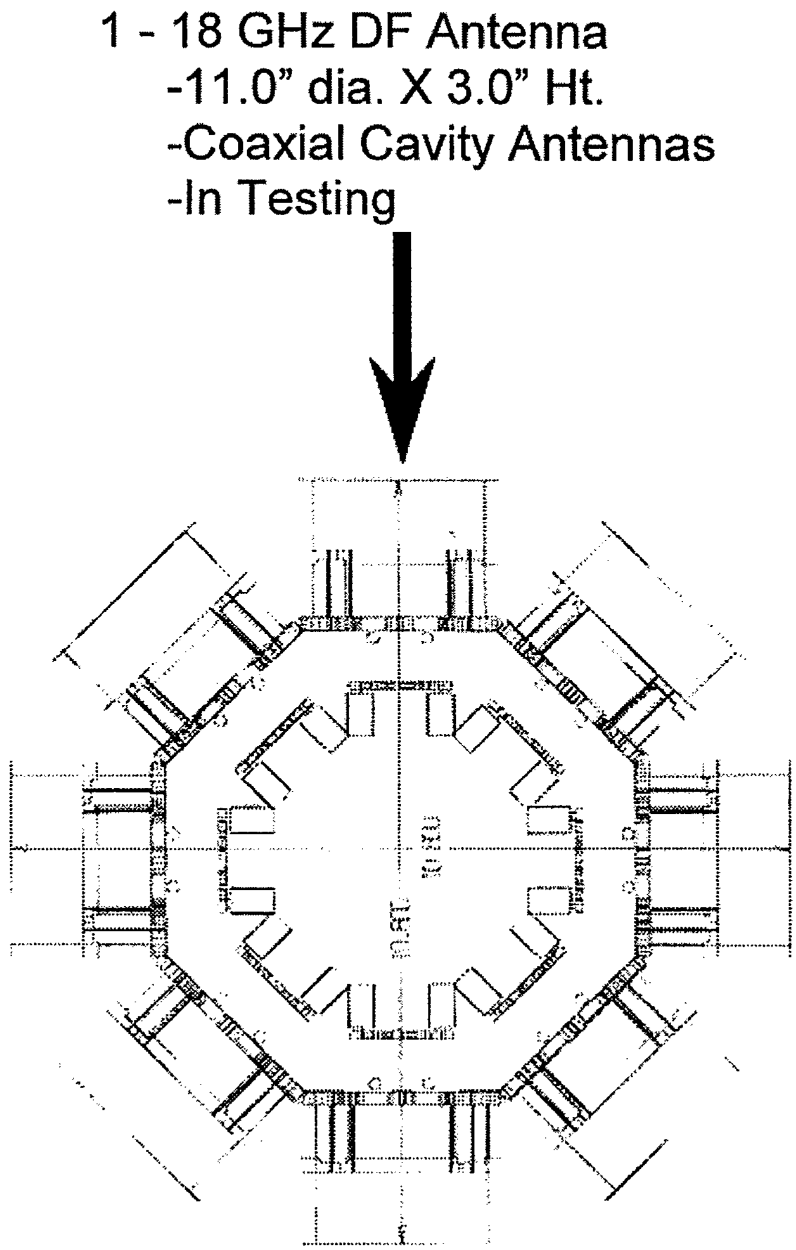

Figure 23. Circular Direction Finding Antenna Using the Coaxial Cavity Antennas.

Conclusions:

The coaxial cavity antenna has been described and data illustrating its low dispersion performance have been presented. The coaxial cavity antenna is scaleable as shown over octave, multi-octave and any other desired frequency band as shown with the band 3, 4, 5 versions and the RWR antenna that covers 2 to 40 GHz in a 2.0 inch aperture. This antenna has excellent phase and amplitude tracking over both field of view and the operational frequency range. This makes it an excellent antenna choice for use in interferometers, polarimeters and circular direction finding antennas. Recent data indicates that the coaxial cavity antenna has desirable properties in the arrayed configuration. The lack of coupling, the butting up of the cavities to each other is illustrated by the gain data having an almost theoretical 3 dB increase over the single element. This also verifies that the coaxial cavity antenna is a high efficiency antenna.

An example is shown using the coaxial cavity elements in a polarimeter. This data illustrates the problems that are encountered when building a polarimeter and what is desired in the elements used in this type of sub-system.

Ongoing work is being performed in the 360 degree circular DF antenna where the size is already down to 11.0 inches in diameter and a novel approach has been discovered for decreasing the size to a 9.0 inch diameter. This 360 degree DF antenna version works over the frequency range of 1 to 18 GHz taking advantage of the roll off as in a spiral antenna.

Design curves and scaling data for impedance matching and frequency band determination have been developed. This data and antenna design are in patent pending.[5]

Acknowledgment:

The author wishes to thank the personnel, attached to the Raytheon - Antenna Engineering Laboratory, Garland, Texas, where all of this work has been accomplished and is presently continuing.

References:

1. A. W. Love, Electromagnetic Horn Antennas, IEEE Press, New York, 1976.

2. R. G. Corzine and J. A. Mosko, Four-Arm Spirals, Artech House, Norwood, MA, 1990.

3. C. H. Walter, Traveling Wave Antennas, Dover Publications, Inc., New York, 1965.

4. Y. Mushiake, Self-Complimentary Antennas: Principle of Self-Complementary for Constant Impedance, Springer-Verlag, New York, 1996.

5. R. Jaeger, T. Holzheimer, R. Rudd and R. Ackerman, "Coaxial Cavity Antenna," Patent Pending, 20 October, 1998.

6. T. R. Holzheimer, "An Implementation of a 0.5 to 2.0 GHz Circular 360 Degree Direction Finding Antenna," 1999 Antenna Applications Symposium, Allerton Park, Monticello, Illinois, 17-19 September, 1999, pp. 374-404.

7. T. R. Holzheimer, "High Accuracy DF Antenna Using COTS Hardware," 1995 Antenna Applications Symposium, Allerton Park, Monticello, Illinois, 20-22 September, 1995, pp. 12-1-12-30.

A CANTED SECTOR ANTENNA WITH BROAD IMPEDANCE BANDWIDTH FOR HIGH PERFORMANCE ARRAYS

J. T. Bernhard, N.-W. Chen, R. Clark, P. Mayes, and E. Michielssen
Electromagnetics Laboratory and Center for Computational Electromagnetics
Department of Electrical and Computer Engineering
University of Illinois at Urbana-Champaign
Urbana, IL 61801

Abstract: This work details the development of a planar canted sector antenna element that exhibits broad impedance bandwidth and wide-beam radiation patterns. The angle of the element over the ground plane largely determines both the matching impedance of the element as well as the impedance bandwidth. The angle and shape of the sector also play a role in the impedance characteristics. Measurement and simulation data show radiation patterns suitable for broadside operation over a wide band and endfire operation over an even wider band. However, use of the simple canted element for array scanning over all angles will be limited by radiation pattern variation in the higher frequencies of operation. Approaches for minimizing this variation as well as the issues involved in arraying these elements are discussed.

1. Introduction

The growing demand for multipurpose phased arrays translates into antenna specifications that often dictate large instantaneous or switched impedance bandwidths as well as flexible radiation patterns. These specifications also necessitate new ways of arraying these elements to minimize sidelobe levels, mitigate blind angles, and maximize gain for a given array size. Moreover, large-scale fabrication of antenna arrays requires elements that are as nearly planar as possible.

In this paper, we examine a canted sector antenna element that promises to meet some of these requirements. Several groups have considered placing antenna elements at an angle to the ground plane in order to increase bandwidth [1-3]. However, all of these antennas have been rectangular or square patch antennas, which are inherently narrowband. In contrast, our approach uses a triangular sector fed from the apex to achieve a large instantaneous impedance bandwidth.

2. Antenna Structure

The basic structure of the canted sector antenna element is presented in Figure 1. The canted element has a radius *R*, an external edge of length *B*, and an axial length *L* and is fed at the apex as shown. All of the antennas in this study have a sector angle (between the radial edges) of 80^0. The sector is placed over the ground plane at an angle α and a corresponding height *h*. The feed point of the sector is placed as close to the ground plane as possible and fed with a coaxial cable. Made out of copper, the conducting sector is supported with foam to maintain accurate cant angle α during fabrication.

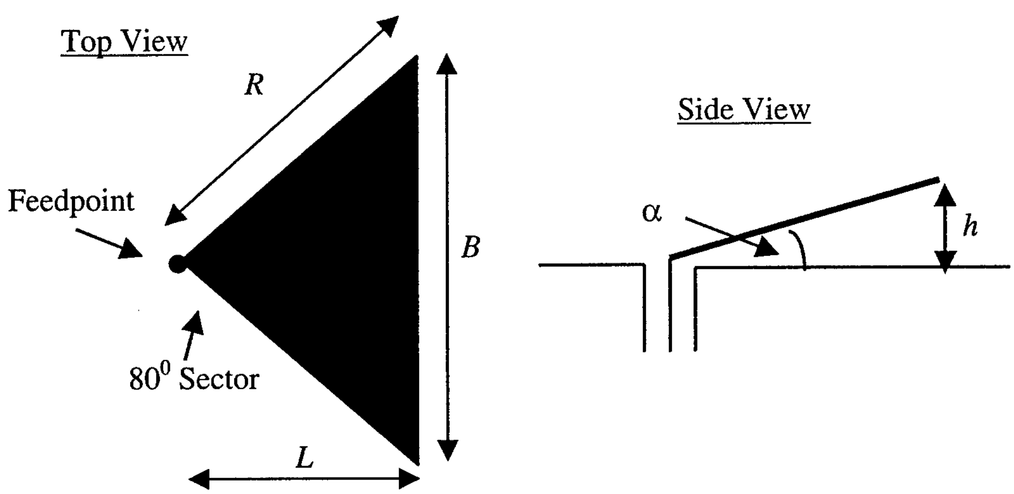

Figure 1: Canted antenna element structure.

3. Impedance Bandwidth Investigations

Experiments and simulations indicate that the canted antenna operates in different modes depending on the length of the element relative to wavelength. The different modes of operation and their approximate impedance bandwidths as a function of size are summarized in Table 1.

Operation Mode	Impedance Bandwidth (%)	Size
Resonant	~10%	$< \lambda/2$
Multi-resonant	~50%	$< \lambda/2$
Semi-resonant	~2:1 (71%)	$\sim \lambda$
Non-resonant	>2:1*	$> \lambda$

Table 1: Description of modes of operation of canted sector antennas and their respective impedance bandwidths as a function of size (L) in wavelengths. *Note that the operating bandwidth may be determined by pattern/directive gain requirements.

All canted sector antennas studied herein were analyzed using a triangular patch method of moments code developed in the Center for Computational Electromagnetics at UIUC. This code allows for the modeling of conducting surfaces with wire connections. Wires can possibly be loaded. Fine geometrical details (e.g., coax feeds) can be handled through the use of so-called "loop-star/tree" decompositions. This code is capable of operating both in the frequency and in the time domain (where it delivers broadband data with a single program run).

Examination of the impedance plot of a triangular sector antenna with a cant angle of 10^0 and a length L of 5.0 cm shown with its ground plane image in Figure 2 helps to distinguish the modes of operation. The first two crossings of the real axis on the Smith chart occur at the lower frequencies where the impedance locus is closest to the rim of the chart. The location of these crossings is indicative of a high-Q resonance with the inherent narrow bandwidth. As frequency increases, the impedance locus forms loops of relatively small size, further away from the rim of the chart. The real-axis crossings and near-crossings then represent resonances of lower Q and wider bandwidth. These resonances of lower Q may be close enough together that several of them can be included in a single operating band, hence the name semi-resonant. As frequency continues to increase, the impedance locus converges into a very small area on the chart approaching the point that corresponds to the impedance of a sector with no reflections, e.g. one that is infinitely long. In this case, the influence of resonances is no longer seen.

Confidence in the results of the simulations was reinforced through use of a second, albeit older and less powerful, code. The second code was a modified version of the Finite Element Radiation Model (FERM) developed at the Lincoln Laboratory of the Massachusetts Institute of Technology [4]. Figure 3 shows FERM results for the input impedance of the 80-degree sector when canted at 10 and at 15 degrees. The similarity to the results in Figure 2 is evident. It is also evident that the cant angle is an important parameter that can be used to control the level of the mean impedance, the value of 15 degrees yielding a very good match to 50 ohms.

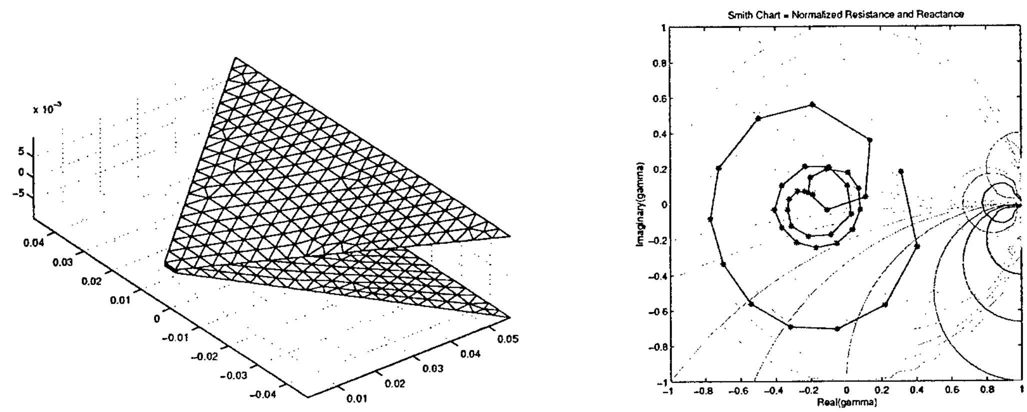

(a) (b)

Figure 2: (a) 10^0 canted sector element (described in more detail above) and (b) its input impedance from 2-7 GHz in 0.125 GHz steps.

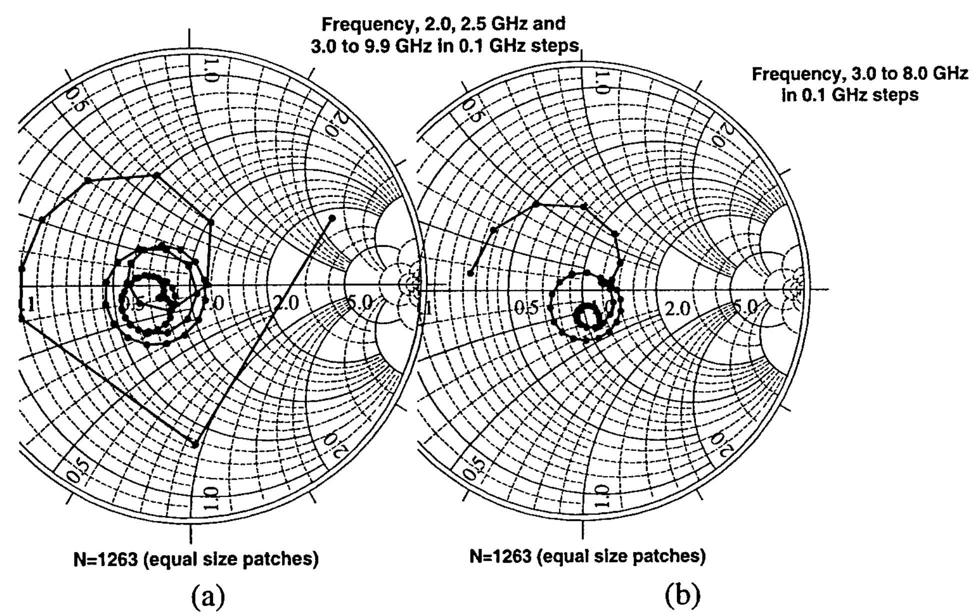

(a) (b)

Figure 3: Input impedance for 80-degree sectors with cant angles of 10 (a) and 15 degrees (b), computed using the FERM code.

We also performed experiments on the effects of cant angle α on the impedance level and bandwidth. These results are summarized in Figure 4. As expected, the match to 50 ohms improves and the 2:1 VSWR impedance bandwidth increases with increasing values of α. Therefore, a compromise exists between the total height of the antenna above the ground plane (which has an impact on fabrication complexity and cost) and the achievable impedance bandwidth.

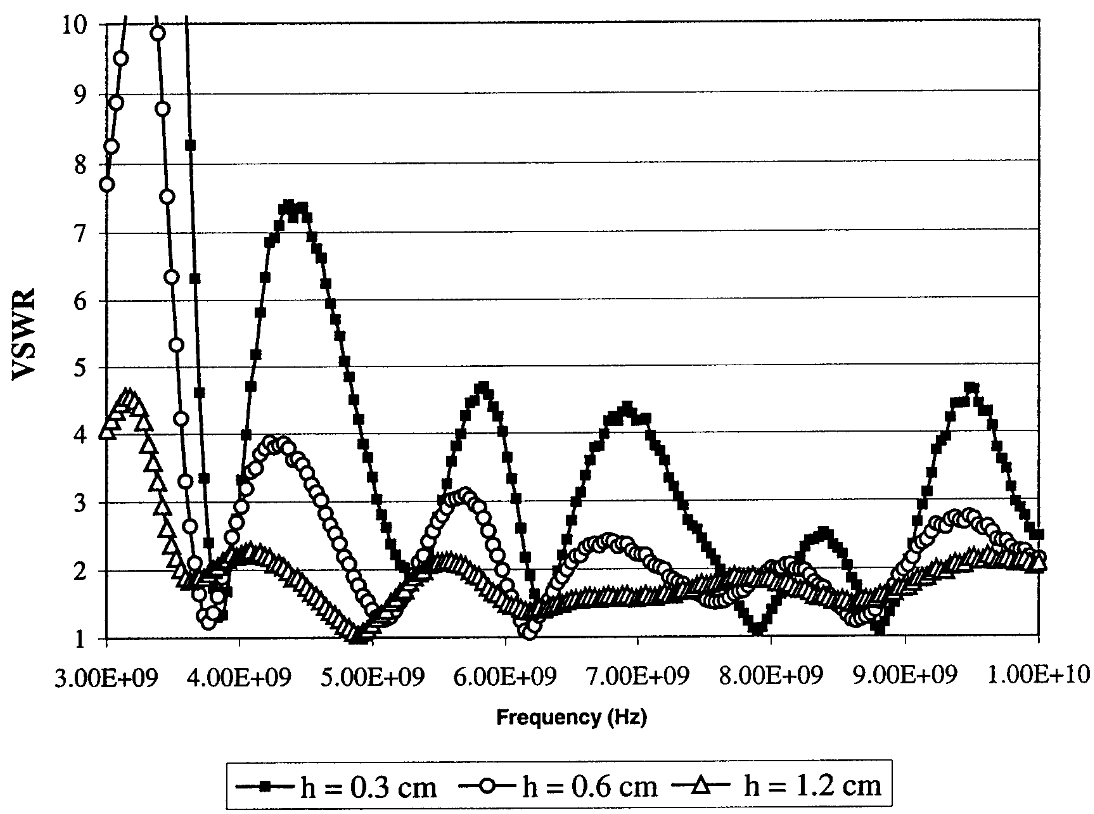

Figure 4: Measurements of VSWR for three canted sector antennas with h = 0.3 cm (α= 3^0), with h = 0.6 cm (α = 6^0), and h = 1.2 cm (α = 12.4^0). For all sectors, the sector angle was 80^0, R = 7.3 cm, B = 9.4 cm, and L = 5.6 cm.

4. Radiation Pattern Investigations

It is apparent that, if there is no restriction on the size in wavelengths, the impedance bandwidth of the sector antenna is very large. However, the radiation pattern is likely to behave in the opposite way. For a small sector the pattern is

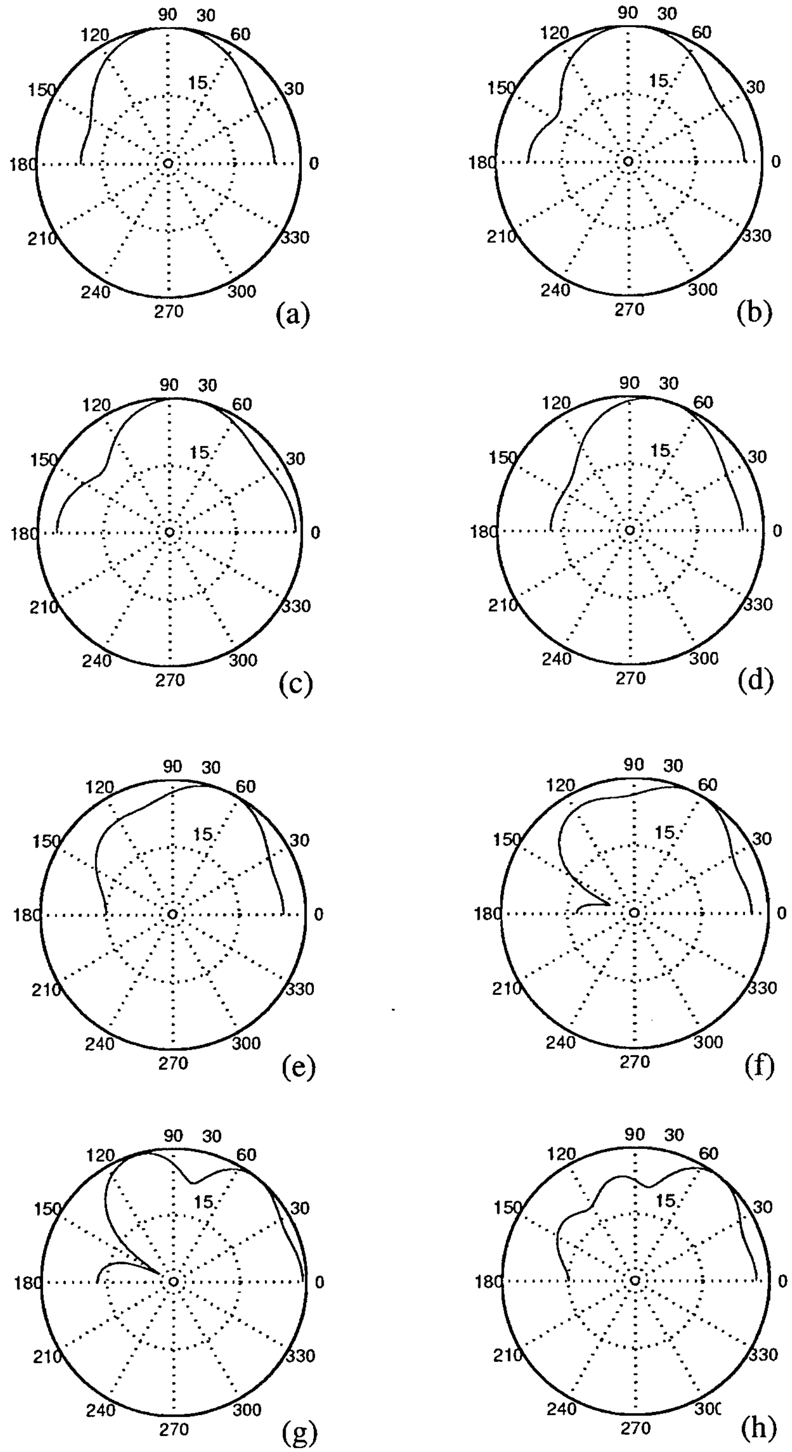

Figure 5: E-plane patterns of the canted sector antenna depicted in Fig. 2 at (a) 2.51, (b) 2.90, (c) 3.28, (d) 3.92, (e) 4.56, (f) 5.21, (g) 5.85, (f) 7.00 GHz.

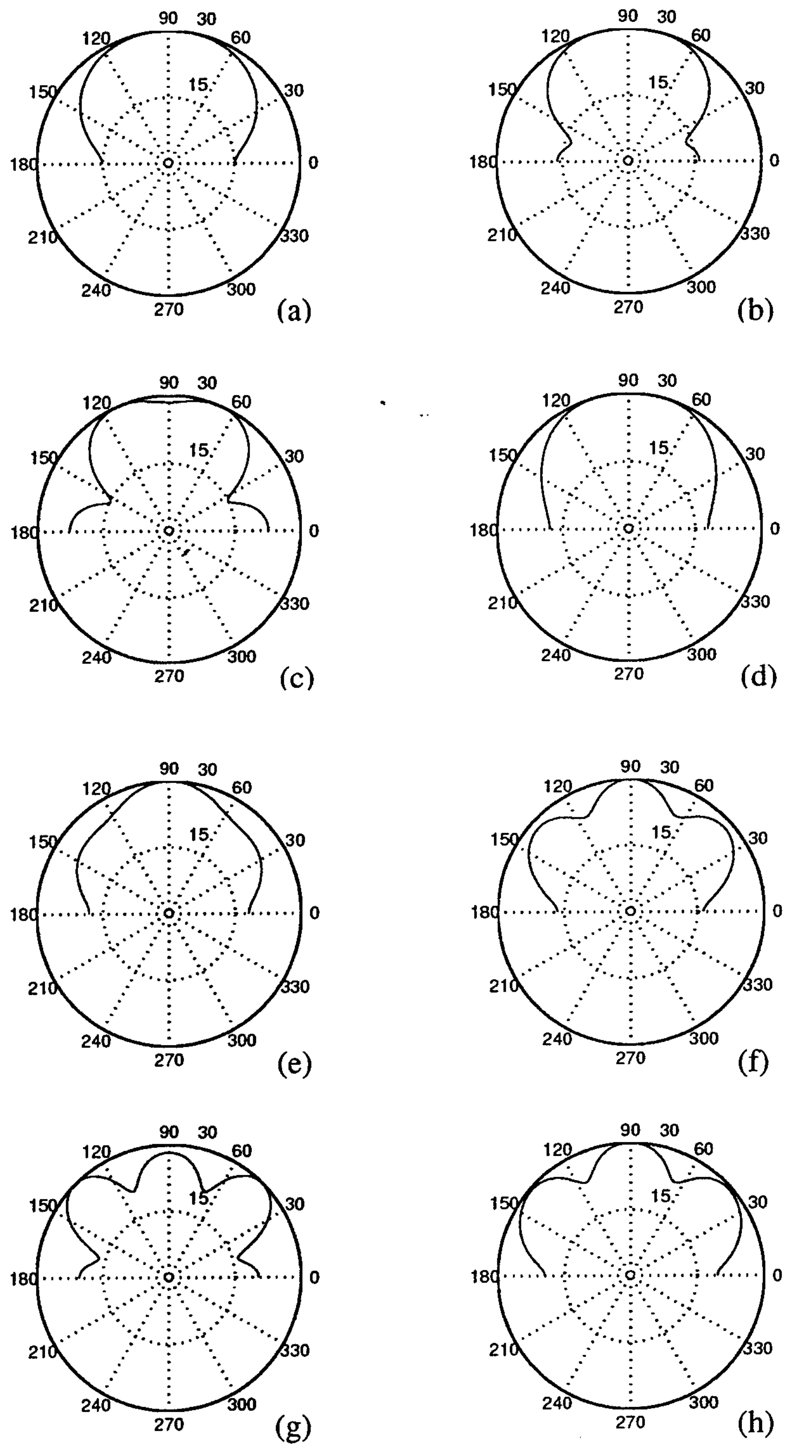

Figure 6: H-plane patterns of the canted sector antenna depicted in Fig. 2 at (a) 2.51, (b) 2.90, (c) 3.28, (d) 3.92, (e) 4.56, (f) 5.21, (g) 5.85, (f) 7.00 GHz.

expected to be well-formed and stable with changes in frequency. As the frequency increases, and the sector becomes large compared to the wavelength, the pattern is likely to develop multiple lobes. To examine these effects, patterns of several sectors of different parameters were computed using both of the simulation codes.

Figures 5 and 6 show E-plane and H-plane radiation patterns for 10 degree canted sectors across the frequency band 2.51 to 7 GHz. In this frequency range, the element is useful for broadside operation. The pattern does deteriorate somewhat near broadside near the higher end of the band. We have observed, however, that the deterioration of the pattern is more outspoken when several canted sectors are placed together (apex clustered) for polarization control as described below in Figure 7.

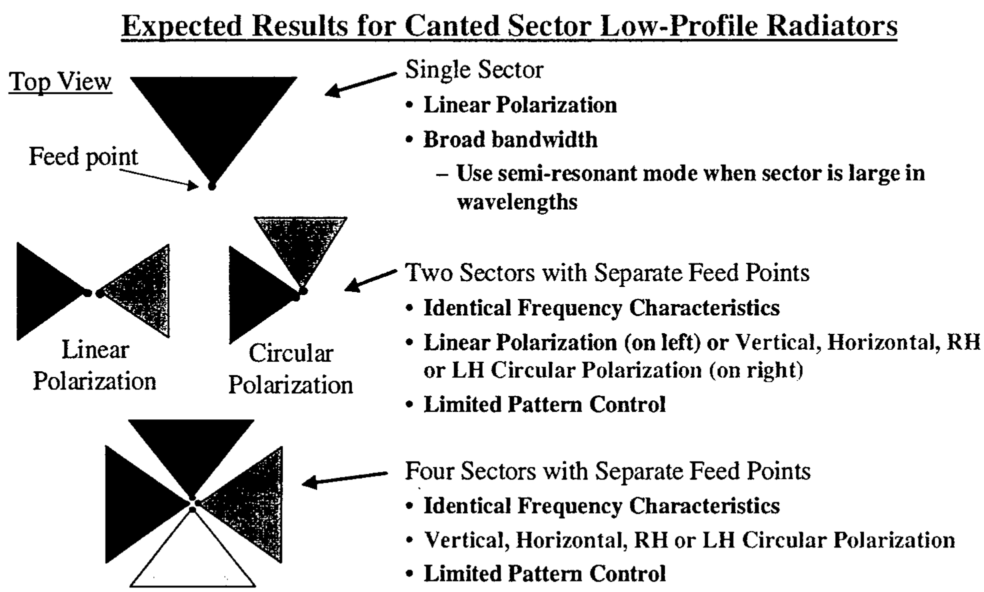

Figure 7: Radiators composed of multiple sectors around a common feed region.

For broadside arrays the boresight gain of the element is important. One way to evaluate the pattern bandwidth of an array element is to look at the variation in the boresight gain of the element relative to the maximum gain. Figure 8 is a comparison of this quantity for 80-degree sectors with cant angles of 10 and 15 degrees.

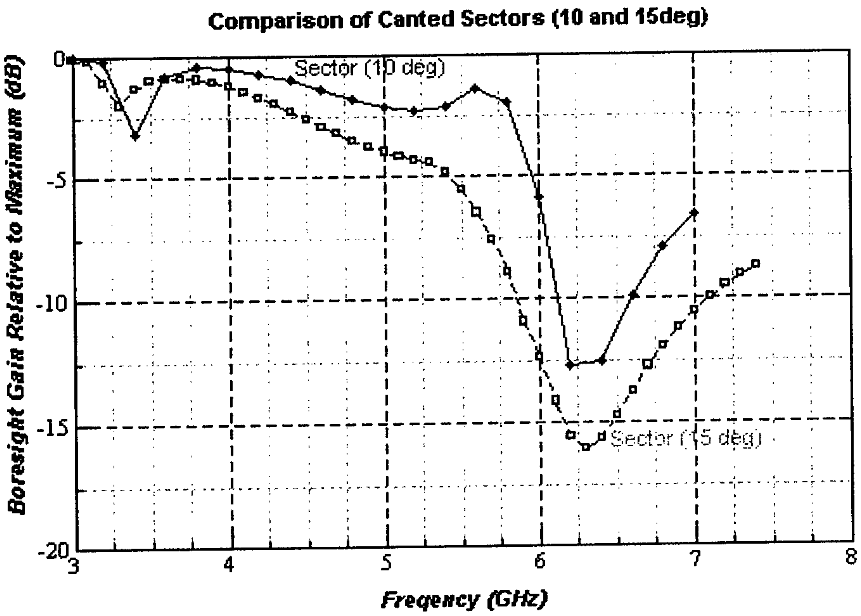

Figure 8: Boresight gain relative to maximum for 80-degree sectors with cant angles of 10 and 15 degrees.

It is clear from this comparison that the sector with 10-degree cant angle has less pattern variation over a wider band than the sector with 15-degree cant angle. The lower band limit is established by the SWR in Figure 3 at 3.6 GHz. Assuming a 5-dB variation in boresight/maximum gain is permissible, the upper band limit for the sector with 10-degree cant angle is approximately 6 GHz. The operating band for this element, which has a height of only 1 cm, is about 50%. Furthermore, extension of the upper band limit through pattern improvements appears within reach.

Sector elements can also provide wide-angle coverage, even to endfire, in one direction. The coverage at wide angles is maintained over a bandwidth much greater than that for broadside.

5. Array Considerations

When operated in any of its broader impedance bandwidth modes, the canted antenna element will be too large to be suitable for periodic arrays due to the creation of grating lobes. Therefore, we are considering arrangement of these elements in an aperiodic, or random array [5]. The benefits and costs of a random array constructed with these canted elements versus a periodic array of broadband tapered slots are summarized in Table 2.

Property	Periodic Tapered Slot Antenna Array	Aperiodic Canted Antenna Array
Lateral Element Size relative to a Wavelength	Small size required (-)	Large size permissible (+)
Lateral Element Spacing	Half-wavelength (-)	Large in Wavelengths (+)
Mutual Coupling	High (blind angles) (-)	Low (no blind angles) (+)
Grating Lobes	Yes (-)	No (+)
Frequency Independent Array Factor	No (-)	Yes (+)
Suitable for High Volume Fabrication	No (-)	Yes (+)
Gain per unit Aperture Area	High (+)	Moderate (-)

Table 2: Comparison between array performance using two elements with wide impedance bandwidths (tapered slots and canted sectors) arranged in periodic and aperiodic (random) arrays, respectively.

Implementation of canted sector antennas in aperiodic arrays lowers grating lobes, mitigates blind angles, and provides a frequency-independent array factor. The one drawback of the aperiodic array configuration remains the lower gain per unit aperture area as compared with a uniform array. However, for the same total array aperture area, the random array requires a greatly reduced number of elements with uniform excitation to each element to achieve reasonable sidelobe levels.

Using the theory of uniform and random arrays, it is possible to compare performance of uniformly- and nonuniformly-spaced arrays with given sidelobe performance. Suppose that a rectangular aperture is available with dimensions, a

= 6 m, b = 22 m. At 10 GHz, the aperture is 200 x 733 wavelengths. The formula for the maximum gain of a uniformly illuminated aperture of this size gives a value of 1.84×10^6 (62.7 dB). For half-wave spacing, 586,400 elements are required.

The Lo and Lee handbook [5] indicates that only 1.8×10^4 elements are needed in the given aperture in order to produce –30 dB sidelobes. Such an array would indeed be sparse, the average spacing between elements being 2.86 wavelengths. Such an array would permit the use of elements much larger than the canted sectors described above. The array would perform over a very wide band, but with gain reduced because fewer elements are used. It is not wise, therefore, to use fewer elements than possible to fit into the available aperture if the objective of the array is to achieve high gain. There are two options for increasing the number of elements: (a) make the element smaller while maintaining element performance over the desired band, or (b) make the aperture larger.

In large random arrays, it is conceivable that half of the single-sector elements could provide wide-angle scanning in one azimuth direction; the other half, in the opposite direction.

6. Conclusions and Directions for Future Work

This work presents preliminary results of our investigations into canted sector antennas that can be used as broadband array elements. The wide beams of the antenna make it appropriate for applications that require broadside as well as endfire radiation. Individual sectors can be used for limited scanning capability, while the sectors arranged in opposing pairs can be used for wider scan angles. Improved scanning capabilities will be sought through variations in the antenna geometry. When two or four sectors are arranged around a common apex point, the polarization of the distant field can be selected by switches in the feed system. Various arrangements of sectors that will be studied are shown in Figure 7.

Future work planned for these antennas includes analysis and design of random arrays of these elements, as well as further characterization to arrive at a design-oriented model of the element that will permit scaling of the design for any frequency band or substrate material.

7. References

[1] D. R. Poddar, J. S. Chatterjee, and S. K. Chowdhury, "On some broad-band microstrip resonators," *IEEE Trans. on Antennas Propagat.*, vol. 31, pp.193-194, Jan. 1983.

[2] R. K. Mishra and S. S. Pattnaik, "Resonant frequency of wedge shaped microstrip antenna," *Electron. Lett.*, vol. 26, pp. 912-913, 21 June 1990.

[3] Y.-M. Jo, "Broad band patch antennas using a wedge-shaped air dielectric substrate," *Proc. IEEE Int. Symp. Antennas Propagat.*, vol. 2, pp. 932-935, 1999.

[4] S. Lee, "Numerical Modeling of RCS and Antenna Problems," Technical Report 785, Lincoln Laboratory, Massachusetts Institute of Technology, Lexington, Massachusetts, Dec. 1987.

[5] Y.T. Lo, S.W. Lee, Editors, *Antenna Handbook: Theory, Applications, and Design*, Van Nostrand Reinhold Company, 1988.

PLANAR INVERTED F ANTENNA COVERED WITH A DIELECTRIC LAYER

J.W. HE and K.S. CHUNG

School of Electrical and Computer Engineering
Curtin University of Technology
GPO Box U 1987, Perth 6845
Western Australia
Email: rjianwei@cc.curtin.edu.au; tchungks@cc.curtin.edu.au

Abstract: Small and low-profile antennas play increasingly important roles in the growing infrastructures for cellular and wireless data systems. Such antennas may require a cover over the radiating elements to provide protection from physical damage and harsh environments, as well as to keep them ergonomically attractive. The inverted F antenna (IFA) is known to allow a flexible impedance match in a low profile design. Also, it allows both vertically and horizontally polarised electric fields to be received, improving receiver performance in environments where strong multi-path fading effects exist, such as urban and in-door areas.

In this paper, a modified planar inverted F antenna (PIFA) covered with a dielectric layer is presented. In this application, the dielectric layer is used as a radome to protect the antenna. Due to the effects of loading, the performance, measured with respect to such as the resonant frequency, bandwidth, and efficiency of the antenna, changes. Therefore, in the design of this kind of PIFA the presence of a dielectric cover layer must be taken into consideration.

Simulations based on the Method of Moments (MOM) are used to evaluate the performance of the antenna. The effects caused by a dielectric layer of different thickness, dielectric constant and loss tangent are examined. The results presented may be adopted in the design of a PIFA covered by a protective radome. Experimental results obtained compared well with the computer simulated results. Finally, a transmission line model is used to provide a quick approximate analysis for the design of such dielectric-covered antennas.

1. Introduction

Small and low-profile antennas are attractive for use in modern-day miniature radio equipment. Because of its compactness and small size, the planar inverted F antenna (PIFA) has attracted significant attention for this type of application[1]-[3]. Often, a dielectric radome is used to protect the antenna. Such a dielectric cover will, however, alter the impedance matching and radiation efficiency of the antenna.

This paper investigates the effects of a dielectric layer on the performance of a PIFA in term of the resonant frequency, bandwidth and efficiency. The properties of the dielectric-antenna system are explored using computer simulations based on a Method of Moments (MOM). Prototypes have been fabricated and tested in order to validate the MOM simulations. Furthermore, a transmission line model is used to provide a quick analysis for such dielectric-covered antennas.

2. Structure

The antenna structures under investigation are based around a PIFA with a top dielectric cover layer as shown in Figure 1. In Figure 1 (a), the PIFA consists of a ground plane, a top plate element parallel to the ground plane, a feed wire attached between the ground plane and the top plate, and a shorting strip which connects the top plate to the ground plane. The antenna is mounted on a finite ground plane. Since the addition of the shorting strip allows a good impedance match to be achieved with a top plate that is typically less than $\lambda/4$ long, the resulting PIFA is more compact than a patch antenna. The dimensions of the top plate are L_1 x L_2 at a height H above the finite ground plane. The width of the shorting strip is W. The distance between the feed point and the shorting strip is d_f. The distance between the edge of the ground plane and the shorting plate of the PIFA is D. In Figure 1 (b), the PIFA is fabricated underneath a dielectric layer, which is also used as a radome to protect the antenna. The thickness of the dielectric layer is d. In Figure 1 (c), an air gap G is kept between the top plate of the PIFA and the dielectric cover layer.

3. Computational Results

To obtain computational results for our investigations, the three-dimensional electromagnetic stimulation tool (IE3D), developed by Zeland Software, Inc., was used to study the performance of the dielectric-covered PIFA. It is an integral equation-based full-wave analysis approach. The basic principle of this method is

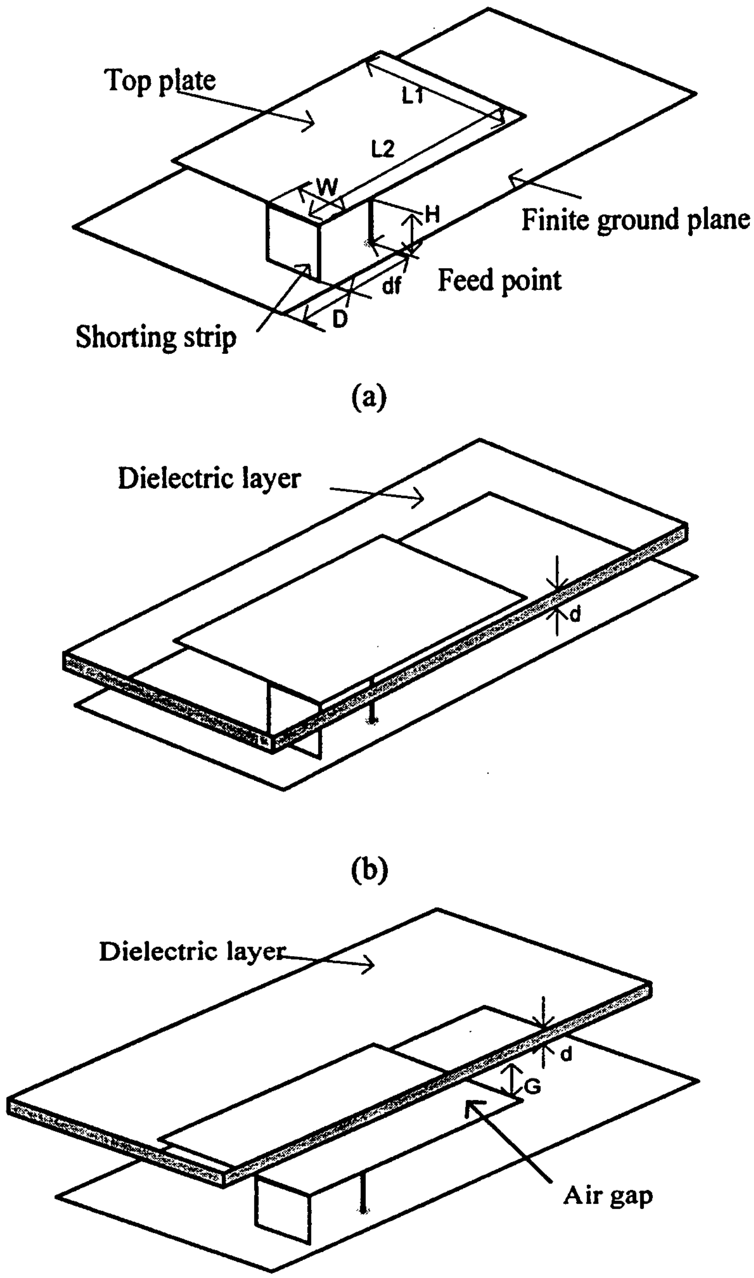

(c)

Figure 1. Antenna structures under investigation (a) Planar Inverted F Antenna (PIFA), (b) Dielectric-covered PIFA without an air gap, (c) Dielectric-covered PIFA with an air gap.

to expand the current distribution on the metallisation of an antenna using a set of basis functions with unknown coefficients. The Method of Moments (MOM) is then employed to discretise the integral equation into a matrix equation. Solving the matrix equation yields the current distribution. All the parameters, such as scattering parameters and far fields can then be extracted from the current distributions.

In section 3.1, the design of a Planar Inverted F Antenna (PIFA) for the test purpose at 900MHz is described. In the remaining sections, the effect of the dielectric layer on the performance of the PIFA for different thickness, dielectric constant and loss tangent as well as different separations from the top plate is analysed.

3.1 Planar Inverted F Antenna (PIFA)

The design variables for this PIFA as shown in Figure 1 (a) are the height, width, and length of the top plate, the width of the shorting strip and the location of the feed wire. A description of some of the design parameters which affect the resonant frequency and bandwidth of the PIFA is given in [1].

For the test antenna the radiating top plate dimensions are (L_1, L_2)=(56.5 mm, 30 mm) with a height H=13.33 mm. The width of the shorting strip is W=5 mm. The feed point is d_f = 11.2 mm away from the shorting strip. The dimensions of the finite ground plane are 110 mm x 50 mm.

In order to identify the effects on resonant frequency and bandwidth of the location of a PIFA on the finite ground plane, an investigation was performed. The PIFA input impedance and VSWR for a 50 Ω match for the different locations are plotted in Figures 2 and 3, respectively. It can be observed that as the distance D (See Figure 1 (a)) deceases, the antenna resonant frequency decreases and the antenna bandwidth increases. When D is set to 6 mm for this PIFA, a bandwidth of 8.33% for a VSWR$\leq$2 is achieved at the resonant frequency f_r of 905.5 MHz. The input impedance and VSWR of this PIFA are shown as solid-line curves in Figure 2 and Figure 3, respectively.

3.2 Dielectric Covered PIFA without a Gap

When the PIFA is covered by a dielectric layer without a gap as shown in Figure 1 (b), the input impedance, bandwidth and efficiency of the antenna change as a function of the dielectric constant, loss tangent and thickness of the layer. Figures 4 and 5 show the input impedance characteristics of the PIFA with

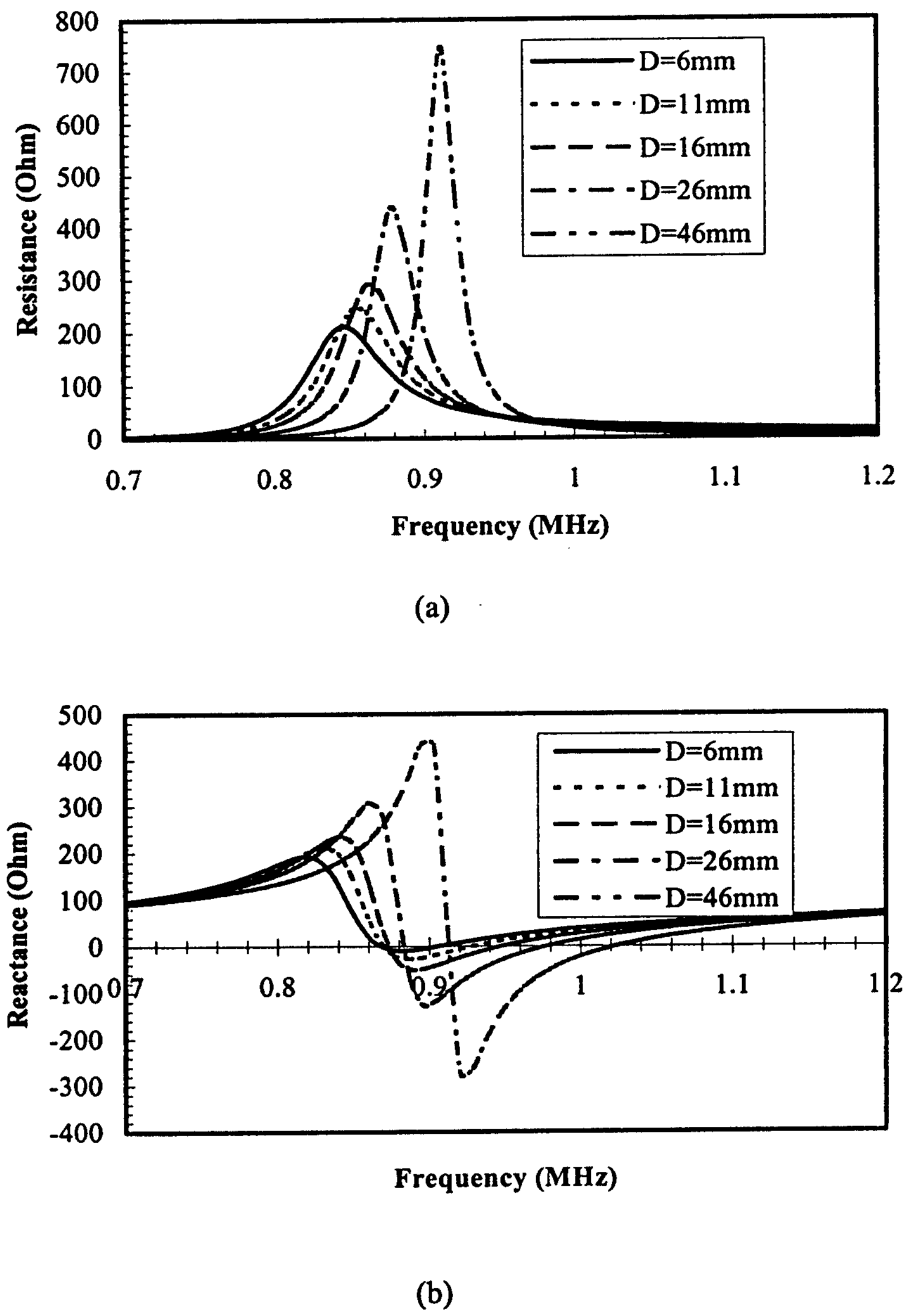

Figure 2. Impedance characteristics for a PIFA mounted for different values of D. (a) Resistance, (b) Reactance.

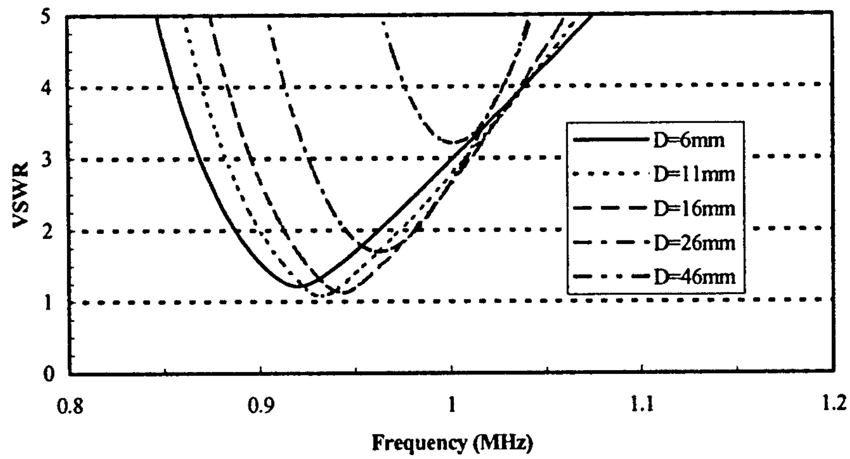

Figure 3. VSWR (for a 50 Ω match) as a function of frequency with the PIFA mounted at different locations of the finite ground plane.

different dielectric materials R4003 and FR-4, respectively. The R4003 material from Rogers has a dielectric constant of 3.38 and a low loss tangent of 0.0027. The FR-4 material has a dielectric constant of 4.4 and a loss tangent of 0.07. It is observed that the resonant frequency of the antenna decreases when it is covered with a dielectric layer. The more the dielectric constant increases or the greater the thickness of the dielectric layer, the more the resonant frequency decreases. Also it can be seen that the material with a small loss tangent does not seem to affect the resonant frequency of the antenna much. However, it can be seen from Table 1 the material with a large loss tangent, such as FR-4, significantly affects the efficiency of the antenna.

Table 1 Simulated results of the effect of the dielectric cover on the performance of the PIFA.

Condition	Resonant Frequency (MHz)	Bandwidth (MHz)	Impedance (ohm)	Efficiency (%)
d=0.06", ε r=4.4, lossless	851.5	59	41	86.1
d=0.032", ε r=4.4, lossless	875.5	64	47	87.4
d=0.06", ε r=4.4, tan δ =0.07	846.5	62	47	76.3
d=0.032", ε r=4.4, tan δ =0.07	867	66	52.5	81
d=0.06", ε r=3.38, lossless	864.5	62	45	87.3
d=0.032", ε r=3.38, lossless	880	67	51	88.2
d=0.06", ε r=3.38, tan δ =0.0027	864	62	45.5	87
d=0.032", ε r=3.38, tan δ =0.0027	880	66.5	51	87.9

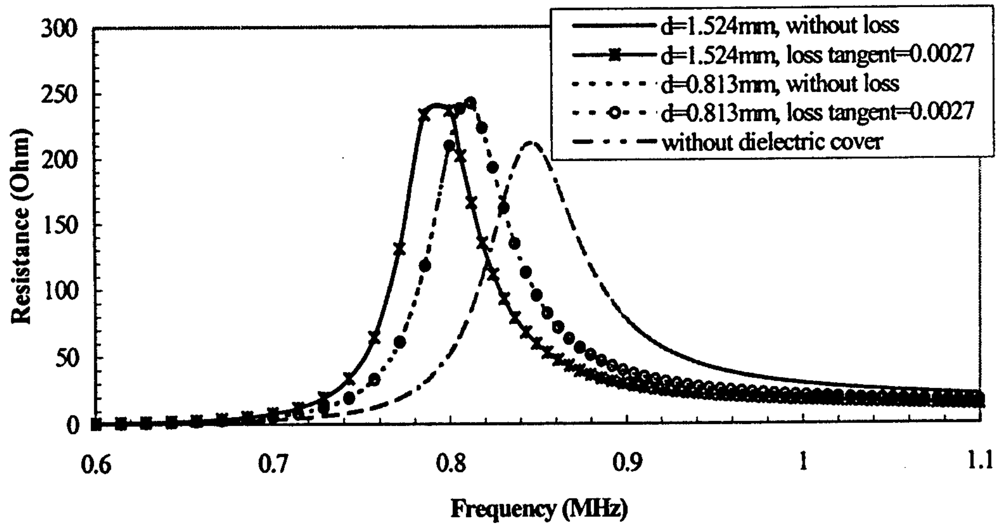

(a)

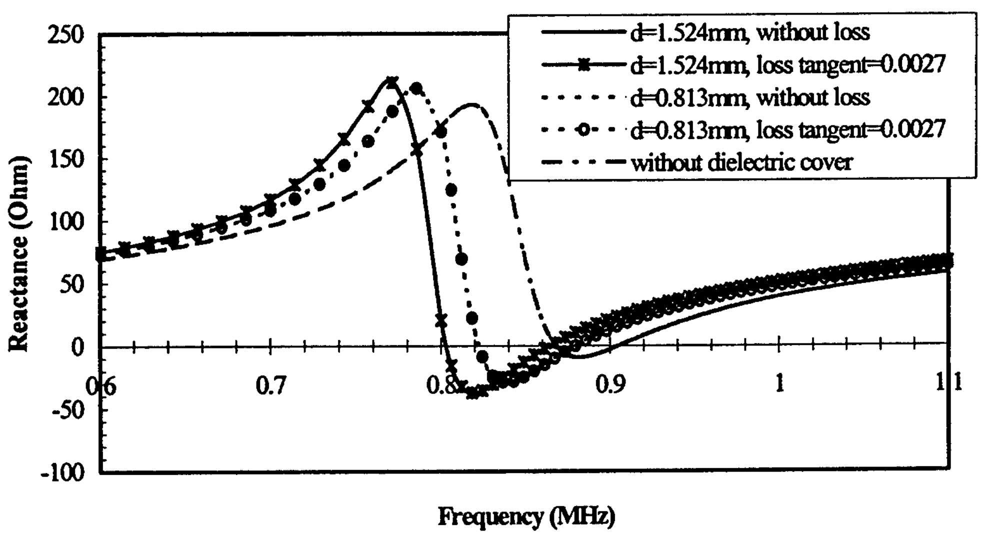

(b)

Figure 4. Input impedance of the PIFA covered with a Rogers R4003 material. (a) Resistance, (b) Reactance.

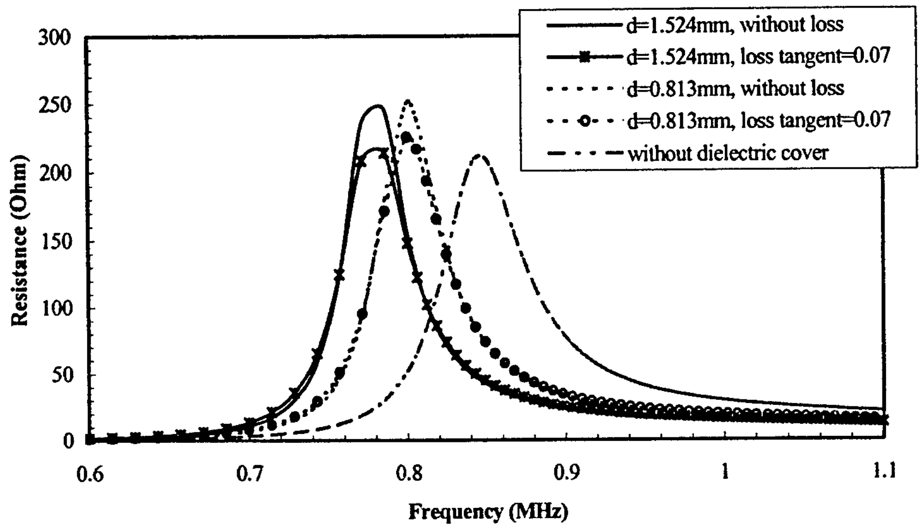

(a)

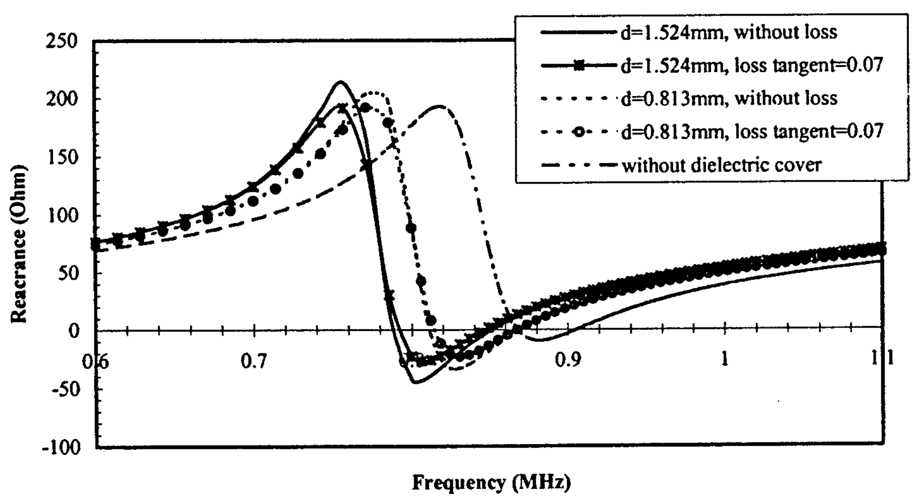

(b)

Figure 5. Input impedance of the PIFA covered with a FR-4 material. (a) Resistance, (b) Reactance.

3.3 Dielectric Covered PIFA with a Gap

In this section, the presence of an air gap G between the top plate of the PIFA and the dielectric cover, as shown in Figure 1 (c), is investigated. Figures 6 (a) – 6 (c) give the input impedance, resonant frequency and bandwidth of the dielectric covered PIFA as a function of the air gap G. In these simulations, a Rogers R4003 dielectric sheet with a thickness 1.524mm is used. From Figure 6, it can be observed that the effect of the dielectric layer may be ignored while the gap G is larger than a certain value. For example, in this case G ≥ 10 mm.

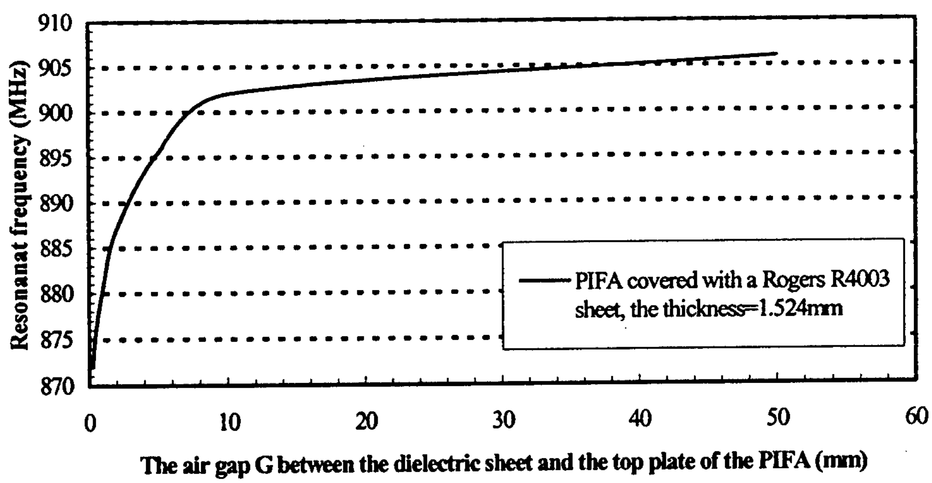

(a)

Figure 6. (a) Resonant frequency of the dielectric-covered PIFA as a function of the air gap G.

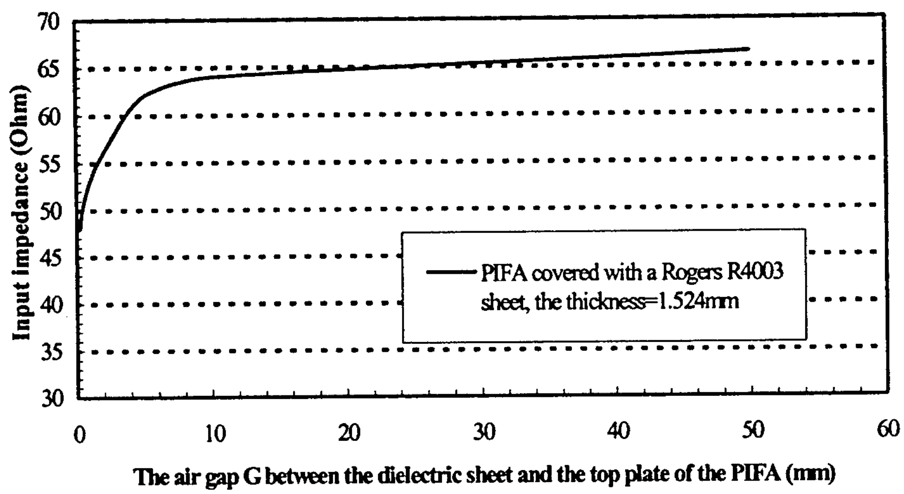

(b)

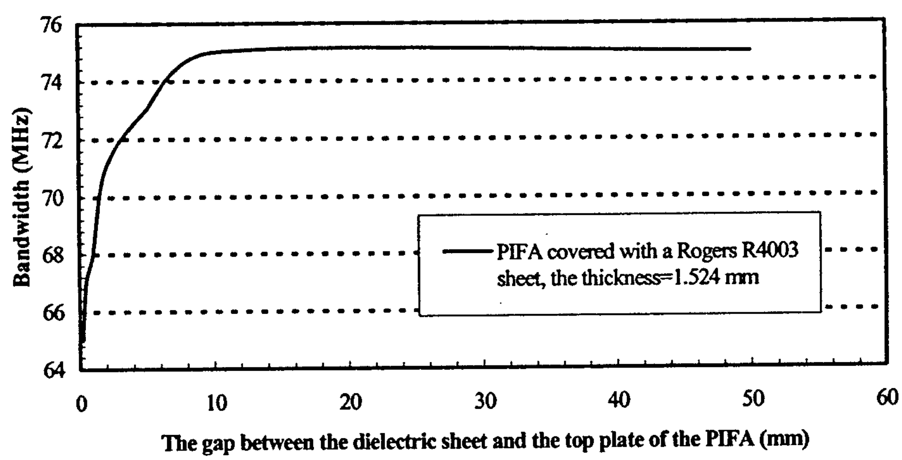

(c)

Figure 6. (b) Input impedance and (c) bandwidth of the dielectric covered PIFA as a function of the air gap G.

4. Measured Results

In order to verify the simulated results given in section 3, a series of experiments were carried out. First, a PIFA based on the dimensions of the test antenna shown in Figure 1(a) was fabricated and measured. Figures 7 (a) and (b) show the measured and simulated VSWR and return loss of the PIFA. The computed VSWR and return loss agree well with measurements. The measurements and simulations predict the same bandwidth and centre frequency. In the second experiment (See Figure 1 (b)), a dielectric sheet (265mm x 80mm) was placed on the PIFA with the help of styrofoam block ($\varepsilon_r \cong 1.05$) such that the dielectric sheet was in good contact with the surface of the top plate of the PIFA. A comparison of the simulated and experimental results for this dielectric covered PIFA is presented in Table 2. Finally, a styrofoam block with a thickness of 11mm is inserted between the dielectric sheets and the top plate of the PIFA. The styrofoam block produces a gap filled by the material with the dielectric constant very close to air (See Figure 1 (c)). The simulated results for this case are given in Table 3. Tables 2 and 3 show that both the measured and simulated results agree fairly well.

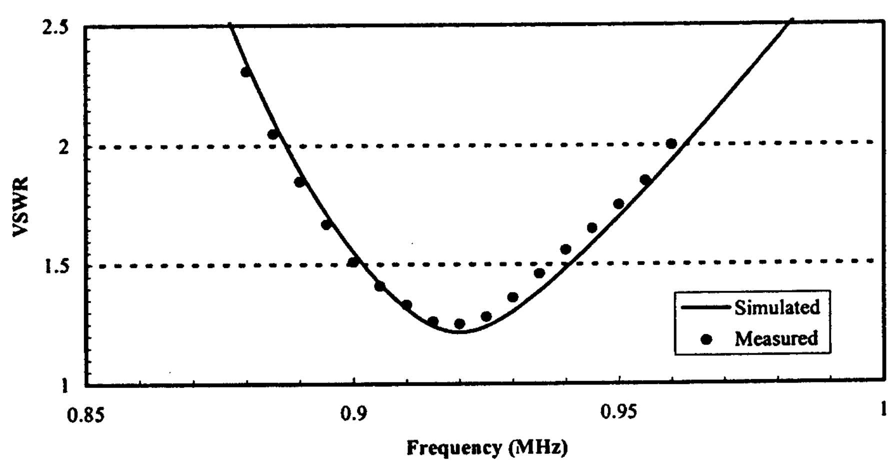

Figure 7 (a). Comparison of the MON simulated and measured VSWR (for a 50 Ω match) for the PIFA as shown in Figure 1 (a).

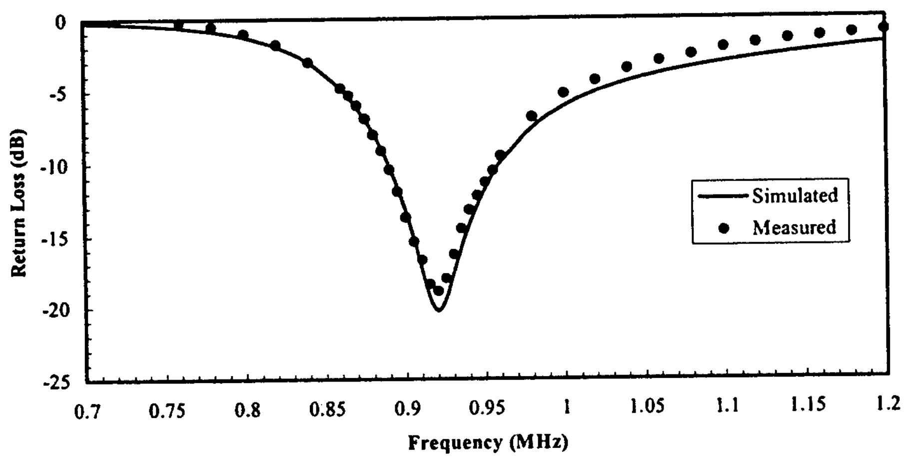

(b)

Figure 7 (b). Comparison of MOM simulated and measured return loss for the PIFA in Figure 1 (a).

Table 2. Comparison between simulated and measured results for the dielectric-covered PIFA without a gap (Figure 1 (b)).

Dielectric Cover	ε_r	d (mm)	fr (MHz)		Δ fr/fr (%)		Impedance (Ohm) at resonance		Bandwidth (MHz)	
			Measured	Simulated	Measured	Simulated	Measured	Simulated	Measured	Simulated
Air	1		909.9	905.5	0	0	69.5	70.5	72.05	75
Styrofoam	1.05	11	906.85	902	0.34	0.39	66.7	66.5	71.85	73
FR4	4.4	1.524	857.2	846.5	5.79	6.52	55.3	47	60.9	62
		3.048	829.2	816	8.87	9.88	45.6	42	56.8	56
R4003	3.38	1.524	865.4	864	4.89	4.58	53.2	45.5	63.2	62
		3.048	839.2	839.5	7.78	7.29	48.1	38.5	57.2	55

Table 2. Comparison between simulated and measured results for the dielectric-covered PIFA with a styrofoam gap of 11 mm (Figure 1 (a)).

Dielectric Cover	ε_r	d (mm)	fr (MHz)		Δ fr/fr (%)		Impedance (Ohm) at resonance		Bandwidth (MHz)	
			Measured	Simulated	Measured	Simulated	Measured	Simulated	Measured	Simulated
Air	1		909.9	905.5	0	0	69.5	70.5	72.05	75
Styrofoam	1.05		906.85	902	0.34	0.39	66.7	66.5	71.85	73
FR4+styrofoam	4.4	1.524	896.55	896	1.47	1.05	68.75	61.5	64.9	72
		3.048	889.15	892	2.28	1.49	66.25	58	61.2	70.5
R4003+styrofoam	3.38	1.524	898.3	897.5	1.27	0.88	69.65	62.5	64.5	72.5
		3.048	890	894	2.18	1.27	66.7	60	61.5	71

5. Transmission Line Model

Instead of the MOM simulation, a transmission line model analysis may be used to provide a quick approach to determine the fractional change in the resonant frequency of a PIFA covered by a dielectric layer. This simple analysis model could be useful in the design for this kind of antenna.

For a PIFA without a dielectric cover, resonance is given by [1]

$$L1 + L2 + H - W = \frac{\lambda}{4} \tag{1}$$

where λ is the free space wavelength, L_1 and L_2 are the length and width of the top plate of the PIFA, H and W are the height and the width of the shorting strip of the PIFA respectively. See Figure 1 for the details.

When a PIFA is covered with a dielectric layer, it can be treated as an inverted microstrip line model. In this case, the resonance is expressed by

$$L1 + L2 + H - W = \frac{\lambda e}{4} \tag{2}$$

where λe is the effective wavelength, which changes as a function of the dielectric constant, loss tangent and thickness of the layer.

For an inverted microstrip line, the effective dielectric constant is given by [4]

$$\sqrt{\varepsilon_{re}} = 1 + \frac{d}{H}\left(a - b\ln\left(\frac{L2}{H}\right)\right)\left(\sqrt{\varepsilon_r} - 1\right) \tag{3}$$

where

$$a = \left(0.5173 - 0.1515\ln\left(\frac{d}{H}\right)\right)^2$$

$$b = \left(0.3092 - 0.1047\ln\left(\frac{d}{H}\right)\right)^2$$

where ε_r and d are the dielectric constant and the thickness of the dielectric sheet respectively, ε_{re} is referred to as the effective dielectric constant.

As a result, the change in the resonant frequency of a dielectric-covered PIFA (Figure 1 (b)) relative to the uncovered PIFA (Figure 1 (a)) can be calculated by using the following expression:

$$\frac{\Delta f_r}{f_r} = 1 - \sqrt{e_{re}} \tag{4}$$

Table 3 presents the values of the fractional change in the resonant frequency based on the MOM simulations, measurements and calculations using the transmission line model for the dielectric-covered PIFA as shown in Figure 1 (b).

Table 3 Values of MOM simulated, measured and TLM calculated results of $\Delta f_r / f$ for the dielectric-covered PIFA as shown in Figure 1 (b).

Dielectric Cover	ε_r	d (mm)	Δ fr/fr (%)		
			Measured	MOM Simulated	TLM Calculated
Styrofoam	1.1	11	0.34	0.39	0.43
FR4	4.4	1.524	5.79	6.52	5.7
		3.048	8.87	9.88	8.55
R4003	3.4	1.524	4.89	4.58	4.42
		3.048	7.78	7.29	6.67

6. Conclusions

The effects of dielectric loading on the performance of PIFAs have been investigated both theoretically and experimentally. The resonant frequency, input impedance and bandwidth of a PIFA covered with a dielectric layer can be predicated accurately using the Method of Moments (MOM) technique. Simulated and experimental results have been found to be in good agreement. The resonant frequency, input impedance and bandwidth of the PIFA covered with a thick sheet of high dielectric constant are drastically affected by the cover. For example, the fractional change in the resonant frequency is more than 9%, when the PIFA is covered by the dielectric sheet with a thickness of 3.048 mm and a dielectric constant of 4.4. This is out of the original bandwidth. Also, the material with a low loss tangent does not seem to affect the resonant frequency of the antenna much. However, the material with the large loss tangent affects the efficiency of the antenna significantly. These observations are important so that appropriate corrections can be made in the design of such dielectric-covered antennas. However, it has been observed that these effects will be reduced if an air gap is kept between the dielectric sheet and the radiator element.

Finally, a transmission line model is applied to provide a quick prediction of the fractional change of the resonant frequency of the PIFA covered with a dielectric sheet. This simple model is shown to provide a good approximate value for the resonant frequency but does not require much computation time.

7. Acknowledgment

The authors would like to thank Mr. Keith Rainbow for helpful discussions and insight.

8. References

[1] K. Hirasawa and M. Haneishi, *Analysis, Design, and Measurement of Small and Low-Profile Antennas,* pp. 161-180, Boston, Artech House, 1991.

[2] J.P. Loahos and I. Pankinaho, "Electrically Tuning of Integrated Mobile Phone Antennas", *Proc.23th Antenna Applications Symposium,* pp. 69-97, 1999.

[3] Z.D. Liu, P.S. Hall and D. Wake, "Dual-Frequency Planar Inverted-F Antenna", *IEEE Trans. Ant. Propagat.,* vol. AP-45, pp.1451-1457, October, 1997.

[4] K.C. Gupta, R. Garg, I. Bahl and P. Bharta., *Microstrip Lines and Soltlines,* pp. 115-117, the 2nd edition, Boston, Artech House, 1996.

Strip-Slot-Air-Mercury Patch Microwave Antennas

Dr. Yogeshwar Prasad Kosta and Shakti Kosta*
Scientist/Engineer
Space Applications Centre, Indian Space Research Organization,
Ahmedabad, INDIA

ABSTRACT

This paper describes the design and development of a working prototype Strip-Slot-Air-Mercury Patch Microwave (SSAMP) Antenna at Ku-band. Using the SSFIP principle, Mercury patch antenna was designed and developed at 9.775 Ghz. Here Mercury is used as the basic radiator of electromagnetic signals. Various antenna parameters such as radiation pattern, return loss, resonant frequency has been studied and experimentally verified. Also the effect of temperature on the resonant frequencies and return loss have been investigated. The study was further extended by using log-periodic technique to increase the gain and bandwidth of the SSAMP. This was done by stacking mercury parasitic patches. The results of the experimental investigations are tabulated and depicted in the graphs in this paper. A topic on "Futuristic Applications" of electrically conducting liquids (Mercury) has been discussed. This details, the proposed fabrication techniques that will be utilized to exercise control on some of the critical Antenna Parameters such as Gain, Return loss, Resonant frequency, Polarization, Beam Shaping and Scanning by means of exercising suitable control over temperature/s and pressure/s.

1.0 Introduction:

An exploratory study of experimental nature was undertaken to investigate the feasibility of using electrically conducting liquids such as mercury & salt solution at microwave frequencies. The aim was to design, fabricate and develop working prototypes of various microwave passive functions such as: Antenna structures, Couplers , ID filters & Microstrip Transmission Lines. Successful attempts have been made earlier towards the development of microwave functions such as microwave patch antenna at 8.35 Ghz and 10.46 Ghz [11], Stripline I.D.Filter at 2.225 Ghz [12], Microstrip transmission lines and other microwave circuits [14] and their applications [13]. These developments demonstrates that its possible to design and develop microwave functions using electrically conducting liquids such as mercury and salt solution and these could find suitable use in certain strategic applications... in future may be.... In view of these developments, here in this paper another attempt is made to develop a Strip-Slot-Air-Mercury Patch (SSAMP) Antenna. The study is further extended to investigate the effect of parasitic patches stacked onto the antenna. The design details regarding

* **Shakti Kosta is a Post Doctoral Fellow at the Lawrance Berkeley National Lab, Berkeley.**

calculations of slot dimensions, patch size, spacing between slot and patch is available in literature along with theoretical design and experimental results [1] to [6], and in text books on Microstrip Antennas [8] to [10].

2.0 Reliazation of the Strip-Slot-Air-Mercury Patch (SSAMP)

2.1 Designed circuit dimensions:

The SSAMP system was designed at to operate at the center frequency of 10.0 Ghz. The radiator, mercury patch single antenna element was designed at 10 Ghz using Teflon ($\epsilon r = 2.2$) substrate material of 1mm thickness. While, the exitation circuit, consisting of the microstrip line feed and the exitation slot was realized on Rogers RT Duriod 5870.

The design dimensions of the mercury patch was, length 9.6 mm (L) and 8.45 mm (W) respectively, while the dimensions of the feeding slot was, length 9.8 mm and width 0.38 mm respectively.

The dimensions and spacings between parasitic elements of mercury is calculated based on the frequency independent log-periodic technique. This technique suggests that the dimensions of the patches and the spacings between them needs to be progressively reduced. The lengths, widths and the spacing between the elements were reduced by a multiplication factor of 0.90 for each parasitic added. The equation to calculate the values of the parasitics and the spacings betweeen them is given below:

$$L_{n+1} = L_n * 0.90$$
$$W_{n+1} = W_n * 0.90$$
$$S_{n+1} = S_n * 0.90$$

Where:
"L" is the length of the patch,
"W" is the width of the patch,
"S" is the spacing between the patches.
"n" is an integer

The calculated values are as follows:

Lengths of the first, second, third parasitics = 8.640mm , 7.776mm , 6.9984mm.
Width of the first, second, third parasitics = 7.605mm , 6.8445mm , 6.16005mm.
Spacing between the patch and first parasitic, first and second, second and third = 0.90mm , 0.81mm , 0.729mm.

2.2 Fabrication of Circuit Elements:

The basic radiator, the mercury patch was fabricated by inundating mercury under pressure inside a capillary type rectangular glass cavity. The dimensions of the cavity is 0.2 to 0.3 mm in thickness, with length and width of 9.6mm X 8.50mm respectively. The variations in the fabricated dimensions are between ± 0.30mm. The overall thickness of the glass confining mercury was varying between 0.9mm to 1.10mm. The fabrication was tailor made to requirements. This was realized with some R&D along with modifications based on an ongoing fabrication process of manometers and thermometers in factories. Initially, the first step is to fabricate the glass capillary cavity of the required dimensions. The second step is to inundate the cavity with the liquid, which in this case is mercury and finally the third step is to pressurize and seal the cavity. The glass capillary confining mercury under pressure was then pushed fit and stuck by means of glue onto a recessed teflon material of 2.0mm thickness.

The exitation circuit was realised by etching a slot on the ground plane along with a microstrip line using photolithographic techniques. Tuning pads are provided for stub tuning of the circuit.

2.3 Antenna Assembly Process

The exploded view of the SSAMP consisting of various circuit elements that are to be cascaded by stacking is shown in figure # 1. The complete assembly along with parasitics is shown in figure # 2. Before the actual antenna system is ready for final assembly, measurments are done to optimize various antenna parameters such as return loss, gain and bandwidth. Once the optimun combinations is determined, the circuit elements are then cemented and cured. This forms one complete antenna system.

3.0 Experimental Investigations and Test Results

After the antenna assembly is optimized for its required RF performances. The measurements have been carried out many times and repeatibility of the measured results have been checked. The return loss of the SSAMP were measured on Scalar Network Analyser [*hp* 8757C] and their resonant frequencies on Spectrum Analyser [*hp* 8566B]. The measured resonant frequency was 9.775 Ghz.

These are tabulated in table # 1 below:

Table # 1

Frequency in Ghz	Return loss in dB	Patch Antenna	Temperature in deg. C
9.775	-18.46	Mercury	26.0 *
9.546	-21.32	Mercury	60.0 **
9.987	-25.78	Mercury	0.0 **

(**) Indicates Measurement taken after three hours stabilization.

The effect of temperature on the resonant frequency and return loss of the fabricated SSAMP is experimentally investigated and studied. The results of the experimentation have been ploted in figure # 3 and # 4 respectively. As observed from the table # 1 above, that, there is shifts in the resonant frequency of the SSAMP by a few tenths of megahertzs from its resonant frequency at room temperature. This variation in the resonant frequency is plotted in figure # 4. This shift in resonant frequency is due to the slight space available within the capillary confining mercury and due to temperature changes in the environment in which the antenna system is operating. The changes in the environmental temperature initiates expansion of the mercury, and favourably, due to the space available for expansion, mercury expands. Thus resulting in shift/s in the resonant frequency of the antenna system. The effect of temperature on the return loss is also studied and the observations plotted in figure # 3. Radiation patterns, both E-Palne and H-Plane of the patch antenna is plotted in figure # 5 and # 6 respectively. The gain of the SSAMP measured is 5.15 dB.

The log-periodic technique is applied to improve the gain and bandwidth of the SSAMP. The effect of parasitic loading on Strip-Slot-Air-Mercury Patch (SSAMP) by stacking with mercury parasitics has been investigated, and as expected, from the principles of frequency independent log-periodic characteristics improvement in gain and bandwidth on loading the SSAMP with parasitics is observed. The results of the experimental investigations are summarised and tabulated in table # 2 below;

Table # 2 : Frequency : 9.775 Ghz (SSAMP - Stacked with mercury parasitics)

No. of parasitics	Gain in dB	Bandwidth in MHz	VSWR (1 : 2)
One	1.30	2440	23.32%
Two	1.70	2350	22.46%
Three	0.78	2300	21.98%

4.0 Conclusive results of the experiment

1. Experimental results clearly demonstrates that its possible to design and develop microwave antennas using liquids such as mercury.
2. As observed, and confirmed here that the concept of log-periodic technique can be utilized to improve the bandwidth and the gain of the SSAMP.
3. Experimentally and as predicted theoritically there is a significant improvement in bandwidth, upto a minimum of 20% atleast as compared with the unloaded mercury patch antenna.
4. During the course of the experimental investigations, it was observed that there is no significant improvement in gain and bandwidth , on loading the SSAMP beyond three parasitics.
5. Pressurization of the confined mercury decides the cut-off temperature limit/s for the thermal expansion of the liquid.
6. Experimental observations have also shown that ,Off-axial alignment of the parasitics show improvement in gain and reduction of bandwidth.
7. Its possible to shift the resonant frequency of the antenna system by exercising suitable control over pressurization of the confined liquid (mercury) during fabrication and the temperature.

5.0 Futuristic Applications

5.1 VARIABLE FREQUENCY LIQUID PATCH MICROWAVE ANTENNAS

5.1.1 Basic Microstrip Patch Antenna

A microstrip patch antenna consists of a dielectric material sandwiched between a metallized ground plane at the bottom side and a patterned metallization on the top side of a specific shape and size as shown in the figure # 7a, to obtain a required antenna characteristics. The microstrip patch antenna is generally realized using photolithography techniques. Arrangements is made to exite the patch via a coaxial connector, with the center pin of the connector extending and making electrical contact with the patch at a specific location, as shown in the figure # 7b.

5.1.2 Liquid (Mercury) Patch Microwave Antenna (LPMA)

5.1.2.1 Description and Constructional Features

The figures # 8a (Top-View) and 8b (Side-View) depicts the configuration of the liquid patch microwave antenna. This antenna structure consists of a low loss dielectric material confining electrically conducting liquids, in this case "mercury", on the topside of the dielectric material as shown in figure # 8a. The electrically conducting liquid: Mercury, is confined within this capillary type cavity at some specific atmospheric pressure, depending on the application requirements. The other side of the dielectric material, that is the bottom side is fully metallized; this forms the ground plane of the antenna structure. The ground plane can also be formed by electrically conducting liquid: Mercury. Finally arrangement is made to provide electrical contact with the patch by means of a coaxial connector. This is done by extending the center pin of the coaxial connector into the pressurized cavity confining mercury as shown in figure # 8a & b. Other types of excitation of the patch is also possible, one example is of the coupled line excitation as depicted in figure 7c.

The liquid patch of mercury could be of any specific shape and size depending upon the requirements of antenna characteristics such as: Radiation pattern, VSWR, Gain, Frequency of operation. For example: The liquid patch could be circular, triangular, rectangular, square, polygon, ellipse, rods like structures also called as dipoles.

5.1.2.2 Working principle and the definition of the temperature technique

Its well known to physicists that temperature changes causes expansions /contractions in the physical lengths/volumes of most materials. The effect is quite pronounced/significant in the case of liquids. The fabrication of these patch antennas using electrically conducting liquids such as mercury or salt solution (0.1 Normal) is based on the "making of the thermometer", where the confined mercury under pressure inside the capillary is responsible for its controlled and calibrated expansions. Microstrip antennas designed and fabricated using the phenomenon of thermal expansions of electrically conducting liquids under pressures is called the temperature technique.

5.1.3 Mechanism of affect:

5.1.3.1 Change in the resonant frequency of the antenna structure

The liquid patch is a capillary type structure confining mercury under specific pressure. The variations in the temperature cause the effective area of the patch to vary in sympathy with temperature. Thus in the microwave sense these variations in the patch area shift the resonant frequency of the mercury patch microwave antenna. The variations of the resonant frequency of the patch can be engineered by exercising suitable control over pressurization of the cavities during the design phase and subsequently by keeping suitable control over temperatures.

5.1.4 Comparison between conventional patch and the liquid patch antennas

Conventional Patch Antenna	Liquid Patch Antenna
1. Single fixed resonant frequency	1. Multiple frequency operation by means of: Exercising suitable control over Temperature, and by varying the temperatures.
2. No such affect	2. Superconducting Patches, as: Mercury is a superconductor

Concluding that:

Its to change the resonant frequency of the patch antenna using electrically conducting liquids such as mercury, by utilizing the property of thermal expansions, using the temperature technique as described here.

5.2 VARIABLE GAIN LIQUID PATCH MICROWAVE ANTENNA ARRAY

5.2.1 Basic Microstrip Patch Antenna Array

The basic microstrip patch antenna array is a series of physically identical microstrip antennas cascaded by means of microstrip transmission lines on a single substrate above a common ground plane. The configuration of the array is depicted in figure # 9.

5.2.2 Description and Constructional Features:

A microstrip patch antenna array consists of a dielectric material sandwiched between a common metallized ground plane at the bottom side and a series of physically identical patterned metallization on the topside of a specific shape and size as shown in the figure # 9. These antennas are electrically connected by means of microstrip transmission lines as shown in the figure to obtain a required antenna characteristics. These antennas generally have very high gains. Such antennas find applications in the direct broadcast communications systems for avionics, military and satellite. They are generally fabricated by using photolithography techniques. Arrangements are made to exite the patch antenna array from the side, via a coaxial connector as shown in figure. The electrical contact is established by extending the center pin of the connector over the transmission line making a physical contact and then soldering the pin onto the line for a permanent contact with the array circuit.

5.2.3 Liquid (Mercury) Patch Microwave Antenna Array

5.2.3.1 Description of Constructional Features

The figures # 10 and figure # 11, depict the configurations of the liquid patch microwave antenna array. This antenna structure consists of a low loss dielectric material confining electrically conducting liquids, in this case "mercury". The confinement by capillary type cavities, at the near topside of the dielectric material is shown in figures # 10 and 11. The electrically conducting liquid: Mercury, is confined within these capillary type cavities at some specific atmospheric pressure, depending on the application requirements. The other side of the dielectric material, that is the bottom side is fully metallized; this forms the ground plane of the antenna structure, fig # 10. The ground plane can also be formed by electrically conducting liquid: Mercury, as shown in fig # 11. Finally arrangement is made to provide electrical contact with the patch by means of a coaxial connector. This is done by extending the center pin of the coaxial connector into the pressurized cavity confining mercury as shown in figures. However, other types of excitation of these patches are also possible.
The liquid patches of mercury could be of any specific shape and size also the microstrip transmission lines feeding the array of patches could be of different hierarchy and weights depending upon the requirements of antenna characteristics such as: Radiation pattern , VSWR, Gain, Frequency of operation. Possible examples are: The liquid patch arrays could be circular, triangular, rectangular, square, polygon, ellipse, and rods like structures also called as dipoles.

5.2.3.2 Working principle and the definition of the temperature technique

Its well known to physicists that temperature changes causes expansions /contractions in the physical lengths/volumes in/of most materials. The effect is quite pronounced in the case of liquids. The fabrication of these patch antenna arrays using electrically conducting liquids such as mercury is similar/based on the "making of the thermometer", where the confined mercury under pressure inside the capillary is responsible for its controlled and calibrated expansions. Microstrip antenna arrays designed and fabricated using "the phenomenon of thermal expansions of conducting liquids under pressures" is called the temperature technique.

5.2.4 Mechanism of affect:

5.2.4.1 Change in the Gain of the antenna array utilizing the temperature technique

The liquid patch antenna arrays is fabricated as single connected capillary type structure confining mercury under specific pressure. As explained above, the variations in the temperature causes the expansion of the electrically conducting liquid: mercury. The expansion of the mercury results in the activation of the patch antenna cavities, from patch # 1 to patch # 4 , depending upon the number of patches in the array, as shown in the figure # 10. Each activated patch contributes to adding extra gain to the antenna system, thus increasing the performance of the system.
Now by properly engineering the pressure required into the cavities during the design phase and by exercising suitable control over temperature, the following parameters can be varied to our advantage:

1. To have suitable control over the Gain. That is to increase or decrease the gain of the antenna array at will.
2. To have superior system performance by improving and maintaining the required G/T ratio of the system.
3. To activate and deactivate the antenna array structure at some specific temperature. This is possible due to the pressurization of the antenna array structure cavities. The required pressure is calculated during the design phase and the structure is fabricated according to the specified pressures.

5.2.4.2 Working principle and the definition of the pressure technique

In any microwave circuits or functions or systems application, pressure technique can be easily applied. The pumping in and out of an electrically conducting liquid under pressures to activate and deactivate various microwave circuits, functions, or systems either partially, or fully by means of an electronically driven pump is called as the "Pressure Technique".
The "Pressure Technique" can be defined as, doing the following systematic activities:
1. Pressurizing cavities for the required applications requirements.
2. Pumping electrically conducting liquids such as mercury under pressure into cavities (inundating).

3. Partially and or fully activating the required specific part/s of the circuit/s, function/s or system/s as per application requirements or demand/s.
4. Depressurization of cavities.
5. Pumping out the electrically conducting liquid such as mercury from the cavities partially and or completely as per applications and demand/s.

The above five steps may be realized using an electronically operated pump system, along with a switching network. A simplified bock diagram of a typical system is shown in the figure # 12.

5.2.4.3 Mechanism to apply pressure technique to microwave antenna circuits functions and systems.

General Procedure:

In order to successfully apply pressure technique, the following procedure is adopted:

1. Locate or Identify a neutral point within the circuit/s.
2. Derive/Draw a channel through the neutral point.

Condition is: The Neutral point should have total access in terms of connectivity of the complete circuit.

Definition of Neutral Point:

This is the point in the circuit, that has the following characteristics:

1. It dose not alter/affect the Electrical or the Microwave performance of the circuit/s, or function/s, or system/s
2. It dose not change the characteristics of the circuits, or function/s, or system/s.
3. It dose not contribute to any major changes in the electrical & mechanical designs of the circuit/s.
4. It dose not call for any major modifications in the mechanical configurations of the system.
5. Dose not makes the system complicated and complex.

5.2.5 Mechanism of affect and the mechanisms to operation and application of pressure technique to liquid microwave antenna array systems to control and vary the gain of the antenna system.

The mechanism of application of this technique is based on the general application procedure given above. Firstly a neutral point is located in the antenna array structure. This is point A, as depicted in figure # 11. A very fine (narrow width) capillary type channel is derived from this. One end of this point connects to the complete antenna array circuit, while, the other end provides access to the electronically operated pumping system depicted in figure # 12. Technically speaking point "A" of the circuit is a high impedance line presenting open circuit at the point of contact, that at point "A". This dose not allow any RF or Microwave signals to propagate into this fine capillary channel, that is to say it acts as a "bypass", thus isolating this point "A", as if it did not exists. Hence this point only serves the purpose of providing path for pressurizing, depressurizing, activating and deactivating the antenna system. An example of such a point on a single patch antenna could be the non-radiating edges of the patch antenna. Further this liquid patch antenna arrays is fabricated as a capillary structure confining mercury under specific pressure. As explained above, the individual patches could be inundated with mercury with this fine narrow channel as and when required to increase the gain of the antenna system and obtain higher system performance of the antenna system by improving G/T of the system. The G/T improves due to increased gain. This is possible by activating the patches one by one. Each activated patch contributes to adding extra gain to the antenna system .

5.2.6 Comparison between the conventional patch antenna arrays and the liquid antennas arrays

Conventional Patch Antenna	Liquid Patch Antenna
1. Fixed system Gain	1. Variable system Gain by means of using: • Temperature technique • Pressure technique
2. Antenna/Radar Visible	2. By utilizing the pressure technique The antenna structure or Radar Can be made Invisible
3. No such effect	3. Superconducting Patches, as : Mercury is a superconductor
4. G/T is fixed	4. G/T can be varied to our advantage using both the techniques mentioned.

Concluding that:

Its possible to control and vary the gain of the patch antenna array using electrically conducting liquids such as mercury, by utilizing the property of thermal expansions, using the temperature technique as described here. Also it possible to control and vary the gain of the antenna system by utilizing the pressure technique as described above. A further advantage of this technique is that it's possible to make the ***antenna system invisible*** by withdrawing the liquid when the antenna system is not in use.

5.3 POLARIZATION SWITCHED LIQUID PATCH MICROWAVE ANTENNAS

5.3.1 Basic Dual Polarization Microstrip Patch Antenna

A dual polarized microstrip patch antenna consists of a dielectric material sandwiched between a metallized ground plane at the bottom side and a patterned metallization on the top side of a specific pattern shape and size as shown in the figure # 13a, to obtain a required antenna characteristics. The microstrip patch antenna is generally realized using photolithography techniques. Arrangements is made to exite the patch via a coaxial connector, with the center pin of the connector extending and making electrical contact with the patch at a specific location, as shown in the figure # 13b.

5.3.2 Dual Polarized Liquid (Mercury) Patch Microwave Antenna (LPMA)

5.3.2.1 Description and Constructional Features

The figures # 14 a (Top-View) and 14 b (Side-View) depicts the configuration of the liquid patch microwave antenna. This antenna structure consists of a low loss dielectric material confining electrically conducting liquids, in this case "mercury", on the topside of the dielectric material as shown in figure # 14 a. The electrically conducting liquid: Mercury, is confined within this capillary type cavity at some specific atmospheric pressure, depending on the application requirements. The other side of the dielectric material, that is the bottom side is fully metallized; this forms the ground plane of the antenna structure. The ground plane can also be formed by electrically conducting liquid: Mercury. Finally arrangement is made to provide electrical contact with the patch by means of a coaxial connector. This is done by extending the center pin of the coaxial connector into the pressurized cavity confining mercury as shown in figure # 14 a and figure # 14 b. Other types of excitation of the patch also exists but are not discussed here.

The liquid patch of mercury is of a basic specific shape not all shapes can produce dual polarization switching. The size depending upon the frequency of operation. The two combined, that is the shape and size dictates the requirements of antenna characteristics such as: Radiation pattern, VSWR, Gain, Frequency of operation.

5.3.2.2 Working principle of temperature technique and its definition

Its well known to physicists that temperature changes causes expansions /contractions in the physical lengths/volumes of most materials. The effect is quite pronounced in the case of liquids. The fabrication of these patch antennas using electrically conducting liquids such as mercury is based on the "making of the thermometer", where the confined mercury under pressure inside the capillary is responsible for its controlled and calibrated expansions. Microstrip antennas designed and fabricated using the phenomenon of thermal expansions of conducting liquids under pressures is called the temperature technique.

5.3.3 Mechanism of affect:

5.3.3.1 Switching of Polarization of the antenna structure using temperature technique

The liquid patch is a capillary type structure confining mercury under specific pressure. The variations in the temperature cause the effective area of the patch to vary in sympathy with temperature. Initially the shaded portion is completely filled with conducting liquid: mercury, under specified atmospheric pressure. This pressure is determined by the polarization switching requirements, say X deg.C. Upto this temperature or below these temperature ranges the polarization is linear. This temperature is also called as the Cut-in temperature or the liquid activation temperature (LTA). The cut-in temperature or LTA is defined as that temperature beyond which the mercury confined within the capillary type cavity starts to expand. The linear polarization comes from the shaded portion shown in the figure # 14 a. Now in order to switch to circular polarization, the temperature of the antenna system or the surrounding is modified beyond or above the X deg.C value. This causes the mercury to expand and fill the remaining area, that is the stub/notch, the unshaded portion. The shape/configuration thus obtained produces circular polarization.

Hence it's concluded that : The controlled temperature variations of the patch antenna fills the remaining area. This affects to change the polarization of the patch antenna, thus switching the polarization of the antenna from linear to circular polarization. The switching of the polarization can be affected by exercising suitable control over pressurization of the cavities during the design phase and subsequently by keeping suitable control over temperatures.

5.3.4 Comparison between the conventional patch antenna and the liquid antennas

Conventional Patch Antenna	Liquid Patch Antenna
1. Polarization cannot be switched	1. Polarization can be switched at a particular temperature (LTA) by utilizing temperature technique

Concluding that:

Its possible to switch to different polarization of the patch antenna using electrically conducting liquids such as mercury, by utilizing the property of thermal expansions, using the temperature technique as described

5.4 Conclusion

Based on the fabrication method/technique/s discussed above, we conclude, that its possible to vary the antenna characteristics such as resonant frequency, gain, polarization etc. by exercising suitable control over temperature and pressure. This is achieved by appropriately choosing the techniques, viz: temperature and pressure as discussed.

However it is emphasized that the use of electrically conducting liquids such as mercury, to realize microwave circuits, antennas and systems need sophisticated fabrication and laboratory techniques. These processes at the movement are extremely costly and not available easily in the industry.

REFERENCES:

[1] Lee, R.Q., K.F.Lee, and Bobinchak, "Characteristics of a Two-Layer Electromagnetically Coupled Rectangular Patch Antenna", Electronics Letters, Vol. 23, 1987, pp. 1070-1072.

[2] Zurcher, B., J.F. Zurcher, and F. Gardiol, "Broadband Miicrostrip Radiators, the SSFIP Concept", Electromagnetics, Vol. 9, 1989, pp. 385-393.

[3] Kossiavas, G., F. Croq, D. Lan Sun Luk, and A. Papiernik, "Large Bandwidth Stacked Printed Antennas", Proc. ISAP' 89, Tokyo, 1989, pp. 21-24.

[4] Sullivan,P.L., and D.H.Schaubert, " Analysis of an Aperture Coupled Microstrip Antenna", IEEE Trans. on Antennas and Propogation, Vol. 34, #8, Aug. 1986, pp # 977-984

[5]Pozar, D. M., and S.D. Targonski, " Improved Coupling for Aperture Coupled Microstrip Antennas", Electronics Letters, Vol. 27, 1991, pp. 1129-1131.

[6] Lo, Y. T., D. Solomon, and W.F. Richards, "Theory and experiments on Microstrip Antennas", IEEE Trans. On antennas and propogation, Vol. 27, 1979, pp. 137-145.

[7] Hall, R. C., "Full-Wave Aperture Coupled Patch Antenna", Electronics Letters, Vol. 29, 1993, pp. 2073-2074.

[8] Microstrip Antenna Design by K.C.Gupta and Abdelaziz Benalla, by Artech House, 1988.

[9] Microstrip Antennas by Bhal, I.J, and Bhartia,P, Artech House, 1980.

[10] Microstriplines and slotlines by K.C.Gupta, Garg R and Bhal, I,J, Artech house 1979.

[11] A Liquid Patch Microwave Antenna by Kosta Y.P., B.K.Chaturvedi et al., Proceedings of the NACONECS-1989. Tata McGrawhill, Nov. 2-4, 1989, pp. 43-47, Dept. of Electronica & Computer Engg., University of Roorkee.

[12] Reliazation of Interdigital Filter Using Mercury Resonators by Y.P.Kosta, Special Issue (Part 2) of IETE on Antennas, Microwave Components, MIC/MMIC, Microwave Solid State Deveces, Microwave Tubes of IETE, Vol. 16, #2, March-April 1999, pp# 177-180.

[13] Mercury Patch Microwave Antenna, by Y.P.Kosta, Space Applications Centre, Proceedings of the International Conference on Smart Materials, Structures and Systems, 7-10 July, Indian Institute of Science, 1999, Bangalore, pp # 701-706.

[14] Ph.D Thesis in Telecommunication Engineering, 1998 of University of Jabalpur, M.P.,by Y.P.Kosta.

Exploded Configuration

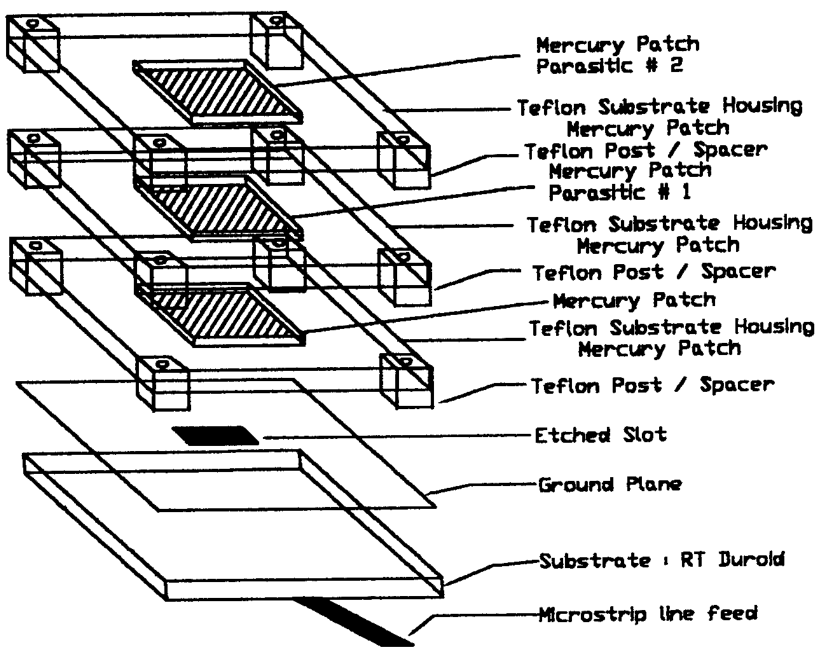

Figure # 1. Configuration of Exploded View of Strip-Slot-Air-Mercury Patch (SSAMP)

Assembled Configuration

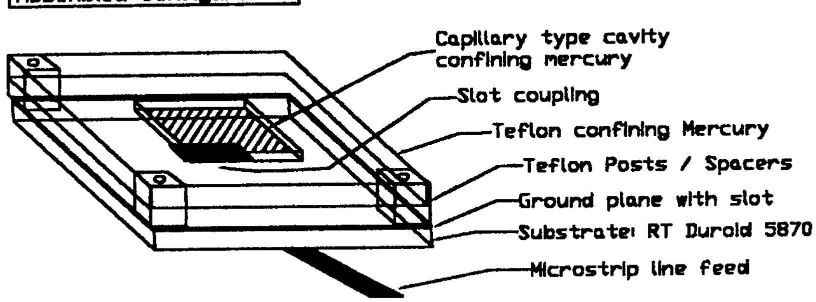

Figure # 2. Configuration of Assembled Strip-Slot-Air-Mercury Patch (SSAMP)

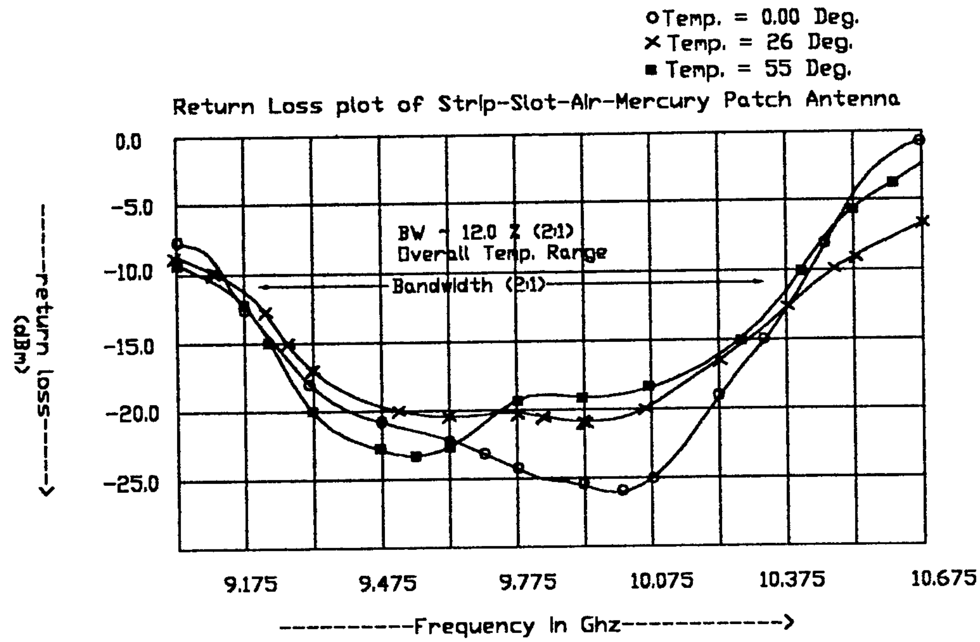

Figure # 3: Return loss of SSAMP with Temperature

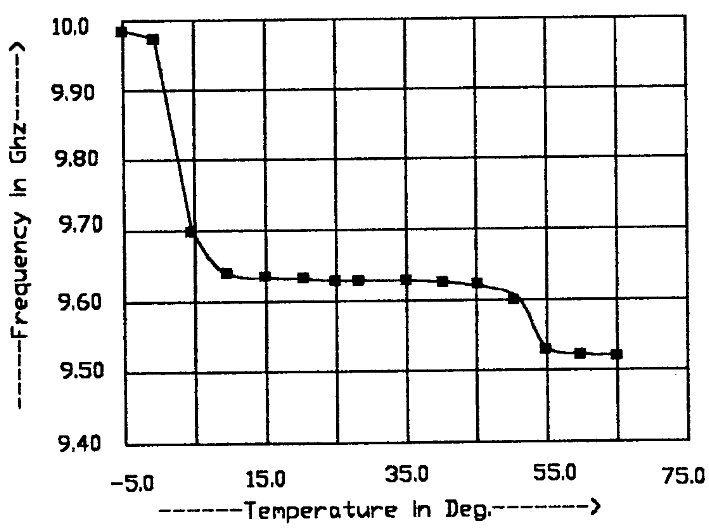

Figure # 4: Variation of Resonant Frequency with Temperature of SSAMP

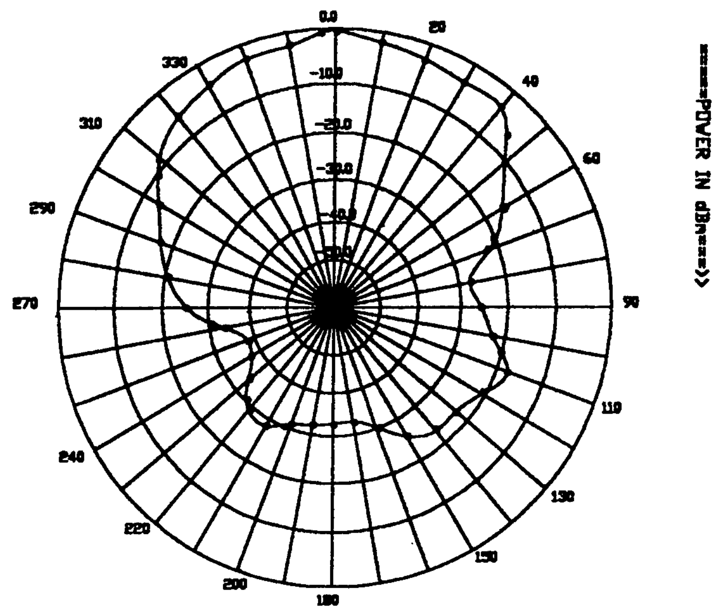

Figure # 5 : E-Plane Radiation Pattern at 9.775 Ghz

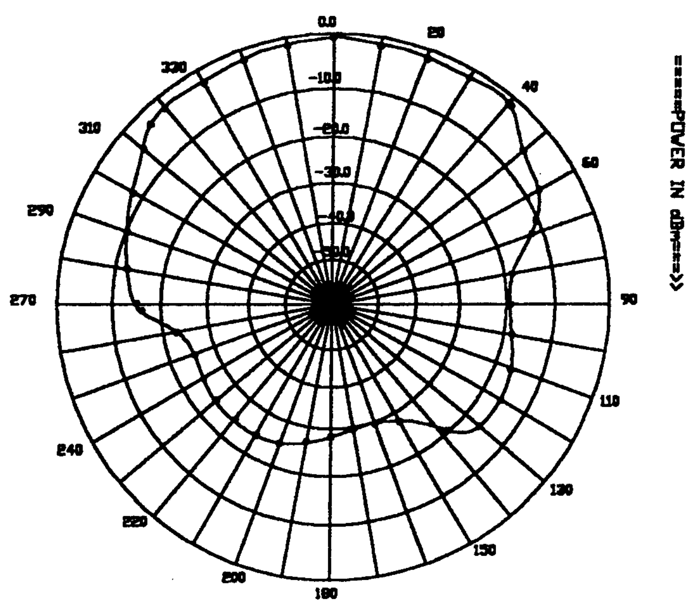

Figure # 6 : H-Plane Radiation Pattern at 9.775 Ghz

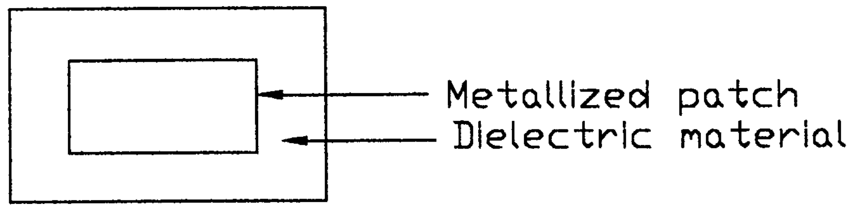

Fig. # 7 a : Conventional Microwave Patch Antenna (Top-View)

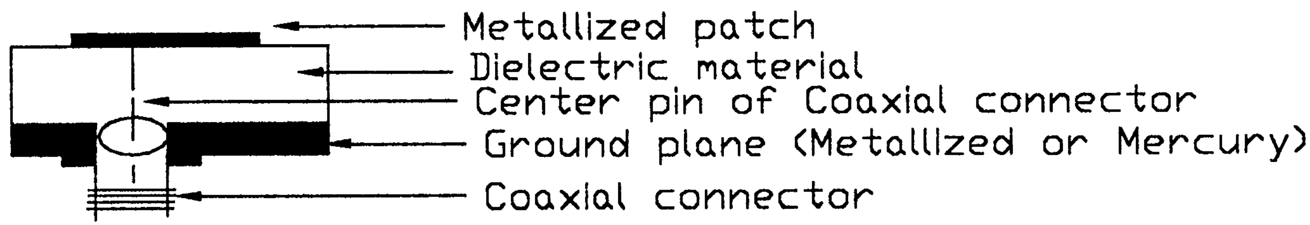

Fig. # 7 b : Conventional Microwave Patch Antenna (Side-View)

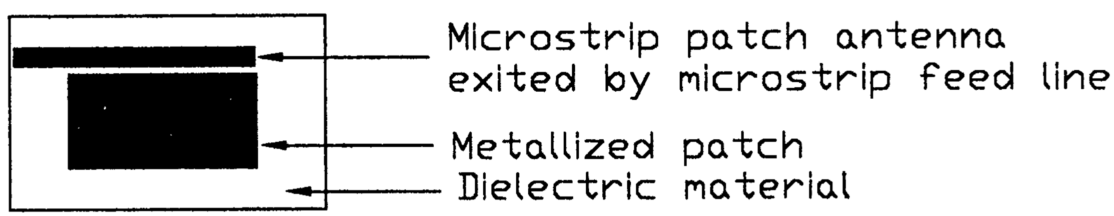

Fig. # 7 c : Conventional MPA with feed line exitation (Top-View)

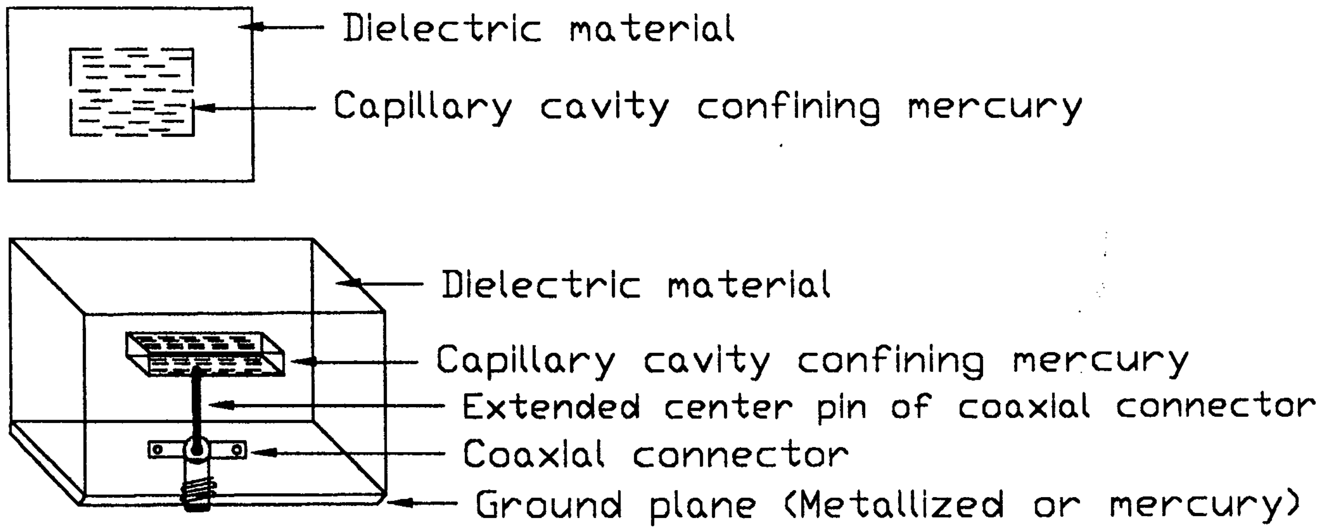

Fig. # 8 a : Mercury Patch Antenna (Top-Side view and Isometric View)

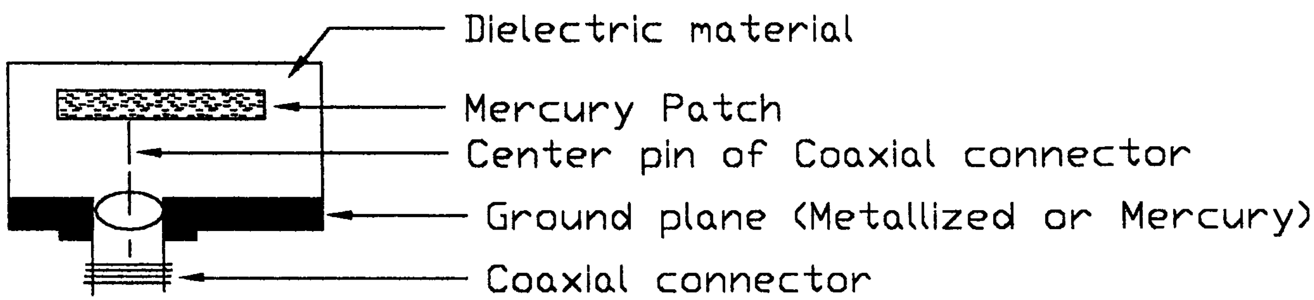

Fig. # 8 b : Mercury Patch Antenna (Side-View)

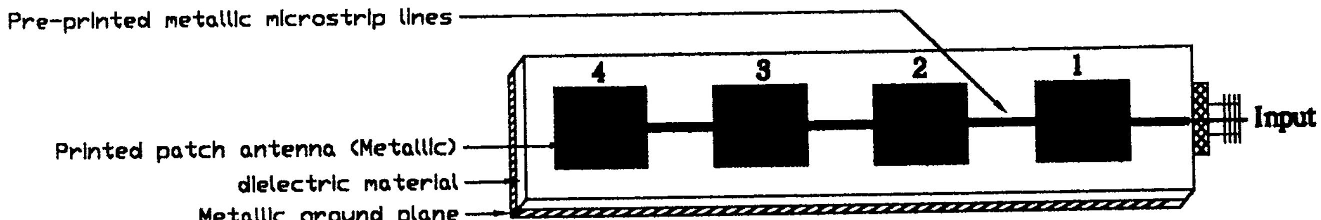

Figure no. 9 Conventional Patch Microstrip Patch Antenna Array

Temperature Controlled Compensation for Gain

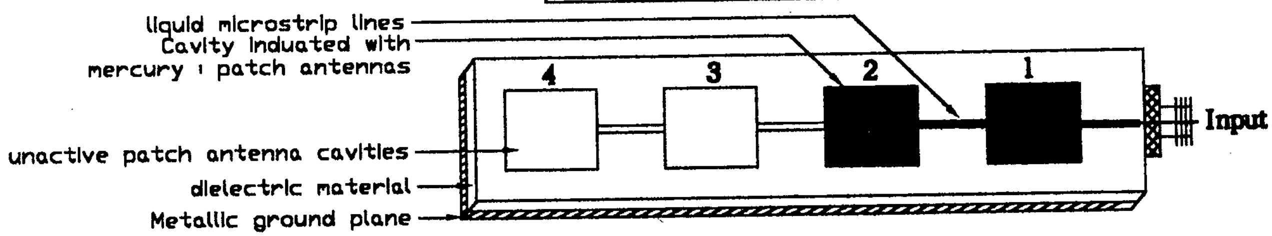

Figure no. 10 Liquid Patch Microstrip Patch Antenna Array

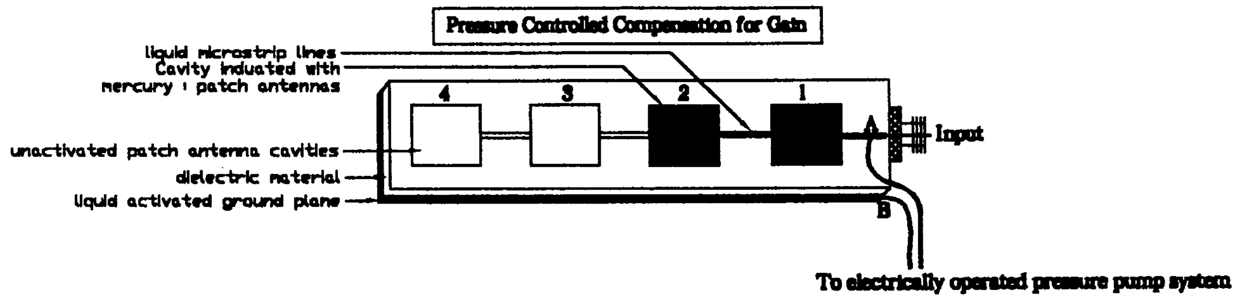

Figure no. 11' Liquid Patch Microstrip Patch Antenna Array

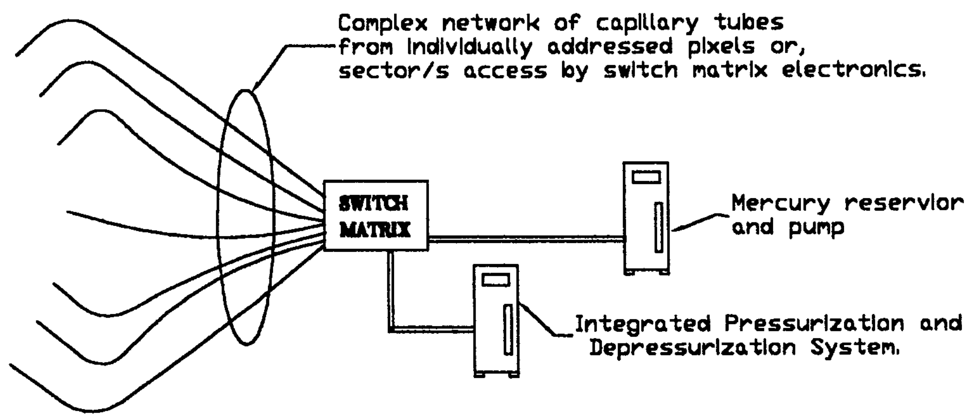

Figure no. 12' Typical configuration of system & circuits utilizing Pressure control system

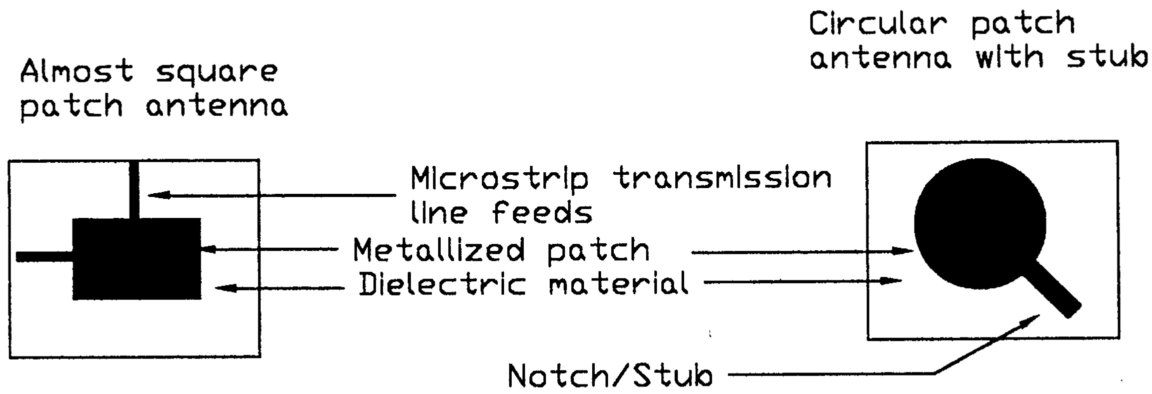

Fig. no. 13 a : Conventional Circular Polarized Microwave Patch Antenna (Top-View)

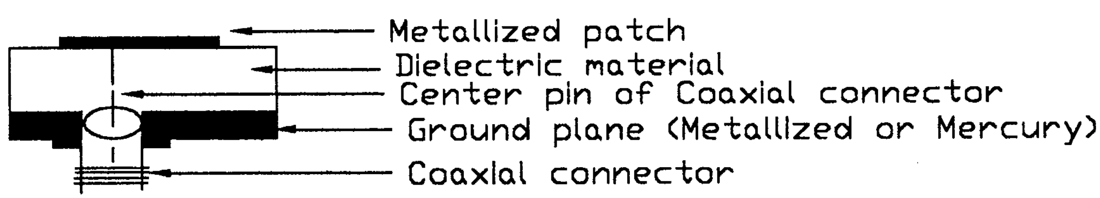

Fig. no. 13 b : Conventional Circular polarized Microwave Patch Antenna (Side-View)

[Top-Side and Isometric View]

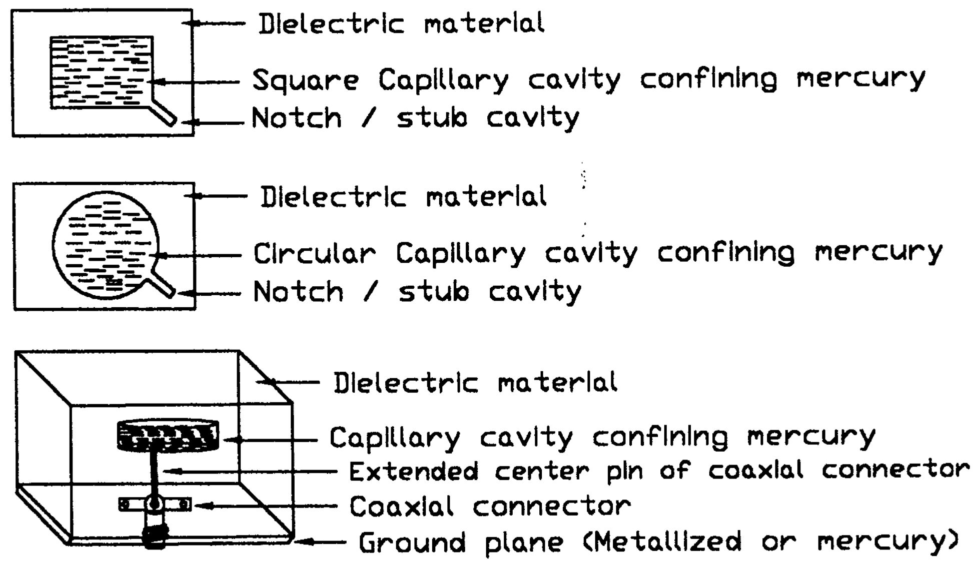

Fig. no. 14 a : Dual Polarized Mercury Patch Microwave Antenna

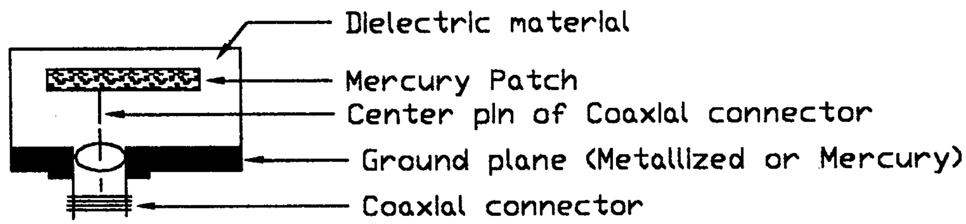

Fig. no. 14 b : Dual Polarized Mercury Patch Microwave Antenna [Side-View]

PAGES 360 - 372 INTENTIONALLY LEFT BLANK

Space Based Lens Vs Corporate Antenna Distortion Comparison

Daniel Davis and Jon A. Moellers
Northrop Grumman Corporation, ESSS
Baltimore, Maryland

Abstract: This paper presents requirements for a space-based radar antenna. This is followed with design concepts developed for a lens antenna and a corporate array configuration, that meet the specified requirements. Error calibration and compensation are assumed to be measurable points on both assemblies and that it is possible to calibrate and compensate distortion errors in software.

Surface distortion errors are developed for a set of the most probable error situations. This leads to the development of parametrics that relate distortion errors to electrical performance. These are described and incorporated into an analytical tool, which make it possible to vary the correction accuracy and then evaluate overall performance. The analytical tool is used to trade-off requirements, calibration methods and calibration benefits.

1. Introduction

It is frequently thought that lens antenna surface distortion errors are "self correcting" since displacements compensate between input and output and therefore have an advantage over rigid corporate configurations. That notion led to this study and analysis.

The antenna distortion errors for two antenna configurations, a lens fed by an array and a rigid corporate array, are compared in terms of surface distortions. The two antennas are developed with the same mission that is, to operate as a Surveillance Radar in a LOE orbit. With this in mind, a general set of radar system requirements was developed. The system requirements shown in Table 1, were evolved into a set of antenna requirements shown in Table 2. Based on these requirements, two antennas are configured and analyzed in terms of distortion errors.

Table 1. Radar Requirements

Parameter	Value
Operating Band	S-Band
Altitude	1000 km, LEO Orbit
Power Aperture Product	2500 kW-m2

Table 2. Antenna Requirements

Parameter	Value
Power Radiated	5 kW Ave
Aperture	50m x 10m
Beamwidth	0.14° Az 0.65° El
Scan	±45° Az ±20° El

Error calibration / compensation begins with measuring points on the array and analyzing the data in software to calibrate and compensate the antenna. Distortion parametrics, which relate distortion errors to electrical performance are described and incorporated into an analytical tool. The analytical tool is used to trade-off requirements, calibration methods and calibration benefits.

2. Basic Design

Based on the antenna requirements two configurations are developed, a lens design and a corporate design. Both antennas operate at 3.2 GHz, with an instantaneous bandwidth of 1% and operating band of 0.6 GHz.

2.1 Lens Configuration

The lens configuration is shown in Figure 1. The lens is 50m by 10m and is fed by a phased array feed 25m from the lens surface. The lens system block diagram is shown in Figure 2. An active lens is fed by a multi-beam feed array. The feed is designed to create 64 uniformly illuminated beams, 16 in azimuth by 4 in elevation, with beamwidth spacing in both planes. The feed is configured with a Rotman lens in both planes. 64 inputs feed the Rotman lens, each forming a 64-sin x/x beams. The choice of an active lens was based on computing the two-way

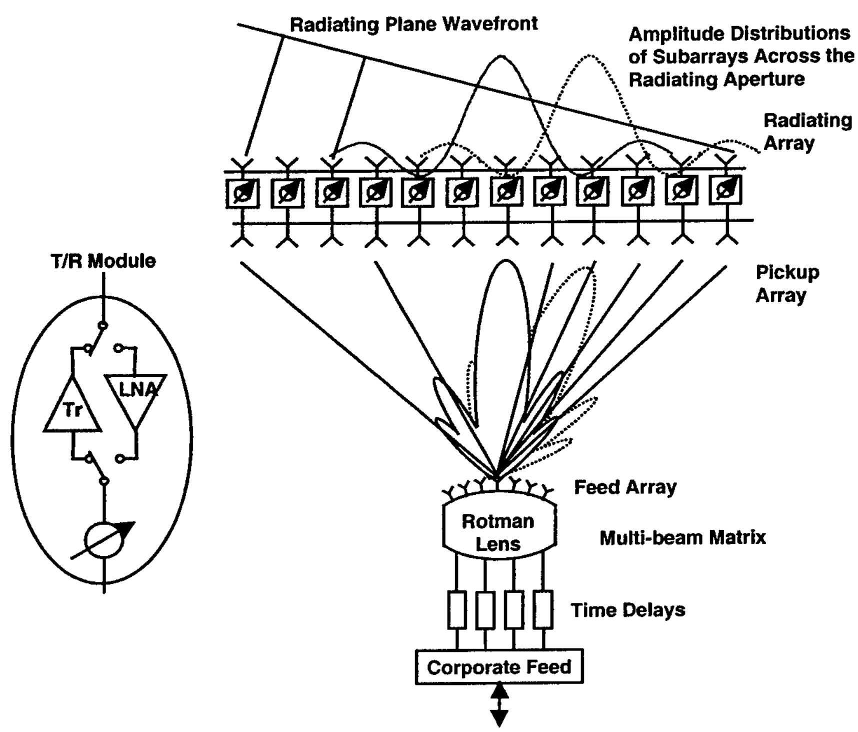

Figure 1. Array Fed Lens With Time Delay Units in Beam Feeds

path losses, the receiver noise figure and the total prime power requirements. This is a complex payload and bus problem, but the prime power requirements point in favor of an active lens; therefore, that approach was chosen.

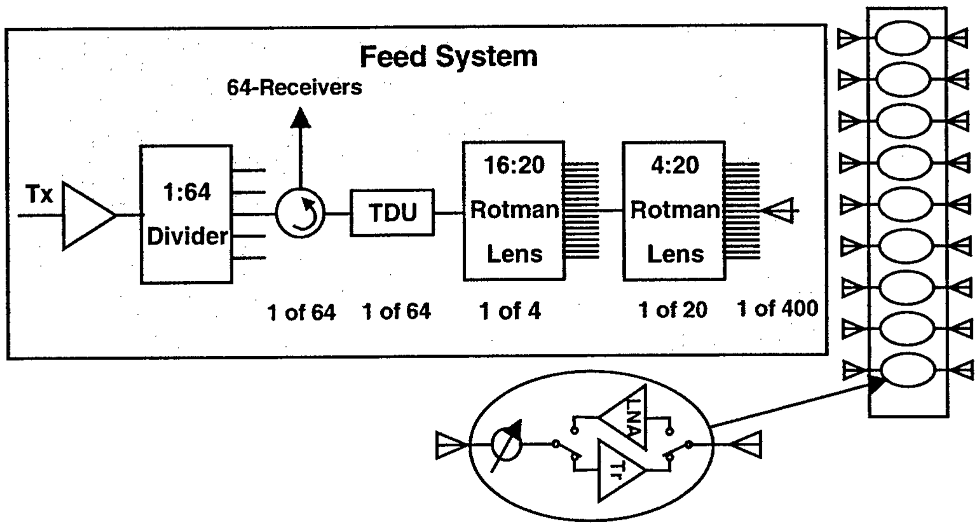

Figure 2. Lens Block Diagram

2.2 Corporate Configuration

The corporate system configuration, shown in Figure 3, is 50m by 10m, with 85 rigid panels. Pairs of panels create overlapped patterns forming 16 by 4 overlapped distributions. A block diagram of the corporate array in Figure 4 offers more detail on its configuration.

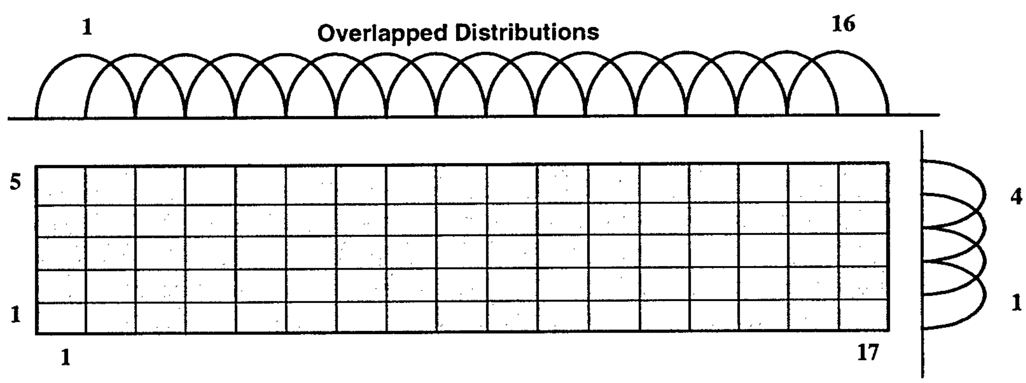

Figure 3. Corporate Array Aperture

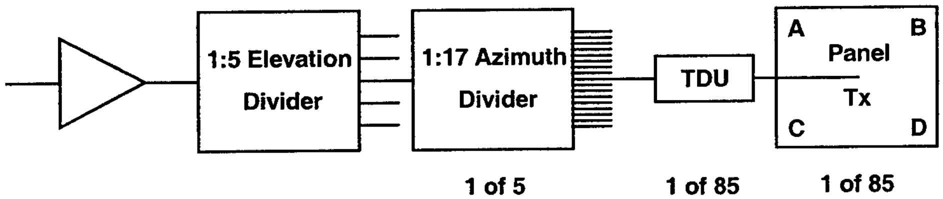

Figure 4. Corporate Array Block Diagram

3. Error Models

The first step is to develop an error model expressing the phase as a function of distortion error.

3.1 Lens Displacement Effect on Phase

The lens displacement effect on phase error is quite forgiving. Using the geometry in Figure 5 to examine the z-displacement, the difference in path length and the resulting phase error is given in equation (1):

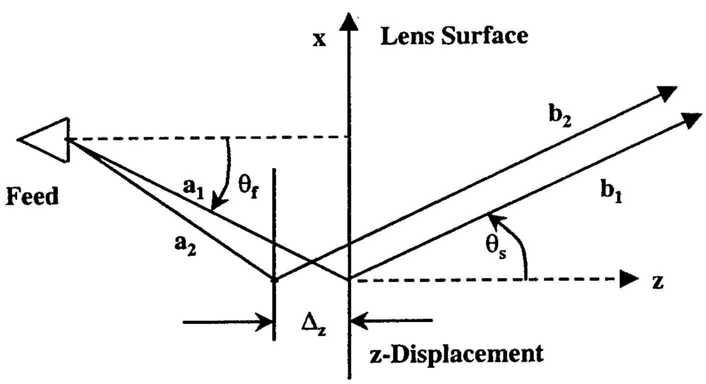

Figure 5. z-Lens Displacement Geometry

$$
\begin{aligned}
\Delta\varphi_z &= \frac{2\pi}{\lambda}[(a_1 + b_1) - (a_2 + b_2)] \\
&= \frac{2\pi}{\lambda}[(a_1 - a_2) - (b_2 - b_1)] \\
&= \frac{2\pi}{\lambda}\left[\Delta_z \cos\theta_f - \Delta_z \cos\theta_s\right] \\
&= \frac{2\pi\Delta_z}{\lambda}\left[\cos\theta_f - \cos\theta_s\right]
\end{aligned} \tag{1}
$$

A similar analysis follows for errors in the x-dimension given in equation (2) and shown in Figure 6.

$$
\begin{aligned}
\Delta\varphi_x &= \frac{2\pi}{\lambda}\left[(a_1 + b_1) - (a_2 + b_2)\right] \\
&= \frac{2\pi}{\lambda}\left[(a_1 - a_2) + (b_1 - b_2)\right] \\
&= \frac{2\pi}{\lambda}\left[\Delta_x \sin\theta_f + \Delta_x \sin\theta_s\right] \\
&= \frac{2\pi\Delta_x}{\lambda}\left[\sin\theta_f + \sin\theta_s\right]
\end{aligned} \tag{2}
$$

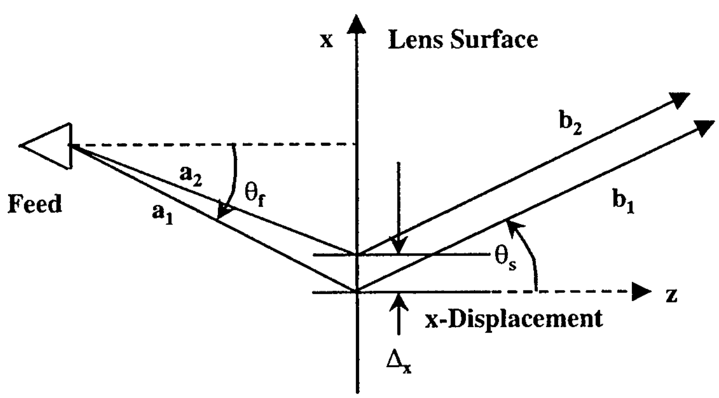

Figure 6. x-Lens Displacement Geometry

These simple equations are very helpful in predicting pattern effects due to distortion, in that the phase error across the aperture directly affects pattern performance. Several distortion errors are most likely to occur with a lens configuration.

4. Analytical Process

The progression of steps to develop an analytical process to compare the two antenna configurations are:

1) Develop an error model expressing distortion error effects on phase error

2) Compute resulting patterns
3) Extract electrical parameters from patterns
4) Fit polynomial functions to pattern parameters
5) Incorporate polynomial error functions into a analytical tool

Eight distortion error types are determined and the resulting phase errors across the aperture are computed for a 10 cm displacement error and steering angles of 0°, 22.5° and 45°. 2-D error models in azimuth and elevation are used to demonstrate the effects of errors on electrical parameters. This approach permits a simpler relationship between distortion and electrical parameter that can be plotted in 2-dimensions while also giving a general flavor for the effect. The cross coupling of errors in both dimensions is not treated in this analysis.

4.1 Lens Displacement Errors

Lens displacement errors are shown conceptually in Figure 7. We look at both x and z distortions for four types of errors across the lens aperture using equations (1) and (2), taking each error individually:

a) Feed offset both in depth "z" and in plane "x", in terms of peak error
b) Linear variation such as a tilt error would cause in the "z"-plane or linear stretch or shrinkage in the "x" plane, in terms of peak error
c) Quadratic variation as if the surface were blown in or out in the "z"-plane or quadratic stretch or shrinkage error in the "x" plane, in terms of peak error
d) Periodic sinusoidal variation in the "z"-plane as would occur if there were multiple gores or stiff boundaries around regions of the lens where the lens could be blown in or out within the region, in terms of peak error

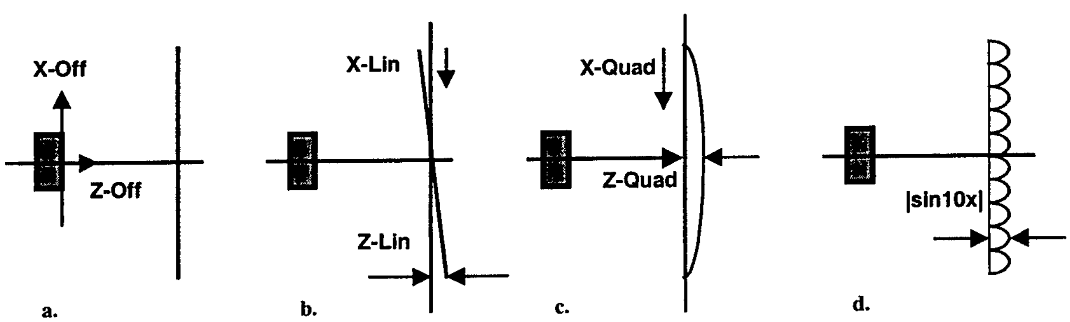

Figure 7. Lens Distortion Types

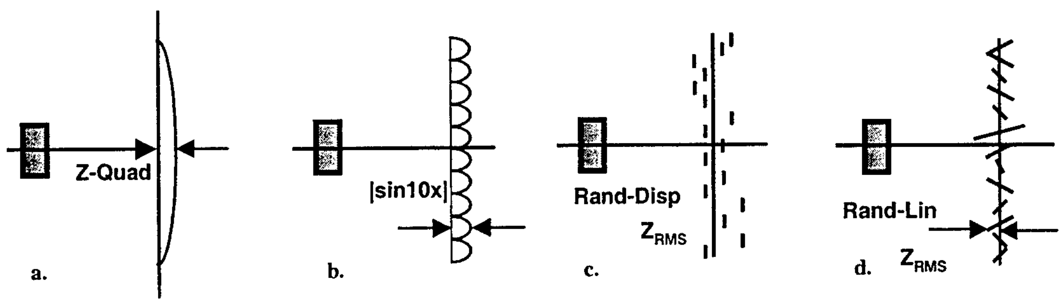

Figure 8. Corporate Distortion Types

4.2 Corporate Displacements Errors and Phase

Since the corporate array panels are rigid, the displacements effect the phase directly and the models are simple and need not be shown. The most prominent corporate errors are shown in Figure 8. Errors are developed for:

a) Quadratic error in the "z"-plane. The surface is deformed in or out from a plane held by a rigid perimeter frame, in terms of peak error
b) Sinusoidal variation in the "z"-plane, as when there is a rigid grid of stiff boundaries around each sub-panel, in terms of peak error
c) Random "z" plane sub-panel displacement about the desired surface, such as if sub-panels are independently supported and adjusted, in terms of RMS error
d) Random linear "z" plane sub-panel tilt about the desired surface, such as if the ends of each sub-panel are independently adjusted within a tolerance, in terms of RMS error

4.3 Phase Distributions Error

Figure 9 shows an example of the phase distributions across the lens aperture for each error type. In these plots we assume a 10 cm maximum error (20cm peak-to-peak for the linear case). On each plot the aperture error is determined for three scan angles, 0°, 22.5° and 45°.

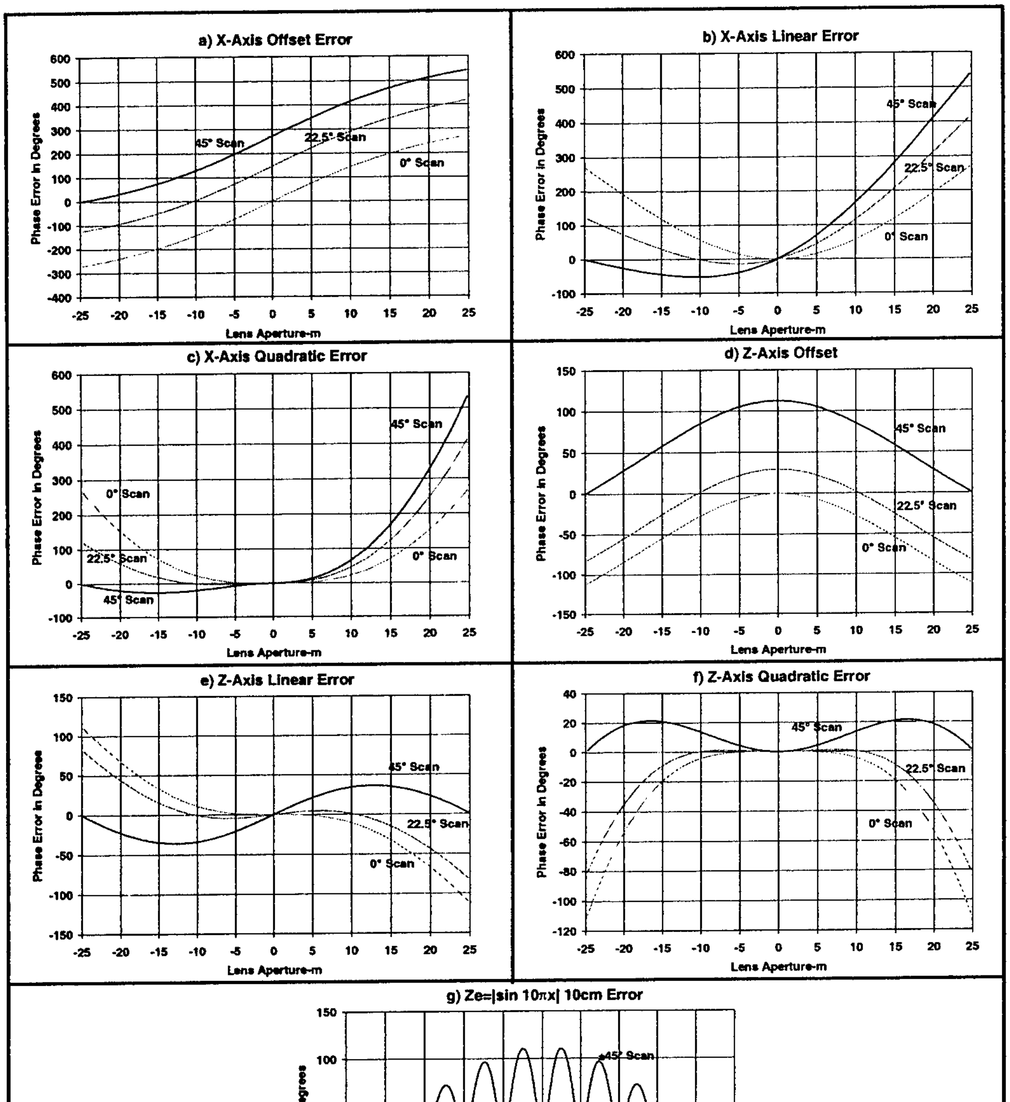

Figure 9. 10cm Distortions Effect on Phase Error Across 50m Lens Aperture a) X-Offset, b) X-Linear, c) X-Quadratic, d) Z-Offset, e) Z-Linear, f) Z-Quadratic, g) Z-Truncated Sinusoid

4.4 Effect of Distortion on Patterns

The errors in Figure 9 result in the patterns shown in Figure 10, when a –45dB Taylor distribution weighting is applied. Receive pattern examples are shown for

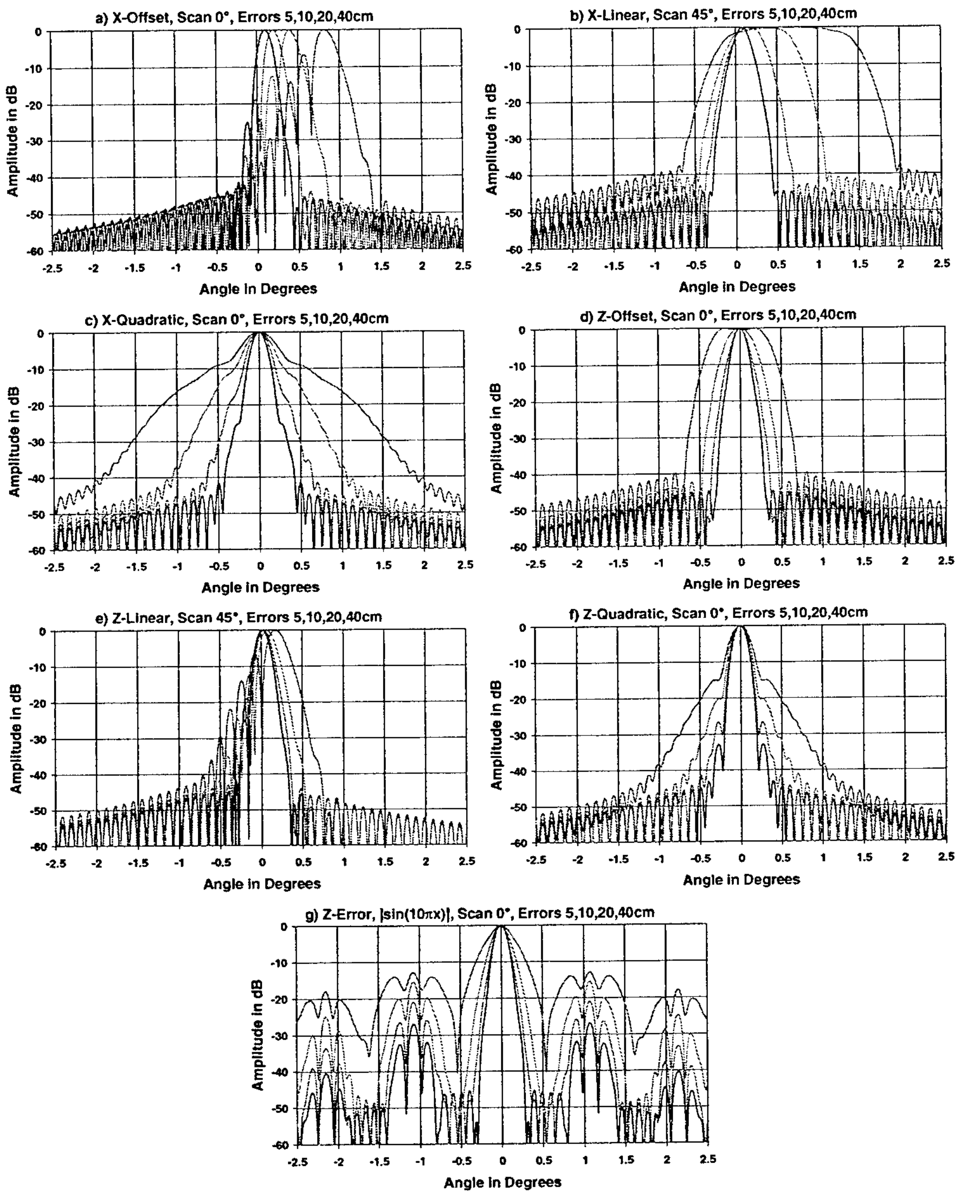

Figure 10. 5, 10, 20, 40cm Distortions Effect on Lens Azimuth Receive Patterns: a) X-Offset (Any Scan), b) X-Linear(45° Scan), c) X-Quadratic (0° Scan), d) Z-Offset(0° Scan), e) Z-Linear(45° Scan), f) Z-Quadratic(0° Scan), g) Z-Truncated Sinusoid

distortions resulting from errors of 2, 4, 8 and 16 cm. Patterns "b" and "e" are for 45° scan, while the other patterns are for 0° scan.

4.5 Effect on Electrical Parameters

Patterns like those above were computed over the range from 5 cm to 40 cm in 5 cm steps to characterize the effect of errors on electrical performance. From each pattern six electrical parameters are extracted.

The effect of the errors described above is related to pattern parameters:

1) Efficiency
2) Peak location
3) -3dB
4) –15dB beamwidth
5) Peak sidelobe
6) RMS sidelobe

Figure 11 shows plots for the lens and Figure 12 shows plots for the corporate configuration. These plots are curve fitted to determine simple polynomials for use in the analytical tool. Some judgement was required to set a polynomial form to simply characterize each case. Generally low order polynomials are used to insure that the function errors are on the conservative side. Patterns like those in Figure 10 were computed for electrical performance for transmit and receive in azimuth and elevation. From each pattern set, six electrical parameters are extracted (the examples shown in Figures 11 and 12, are for receive azimuth).

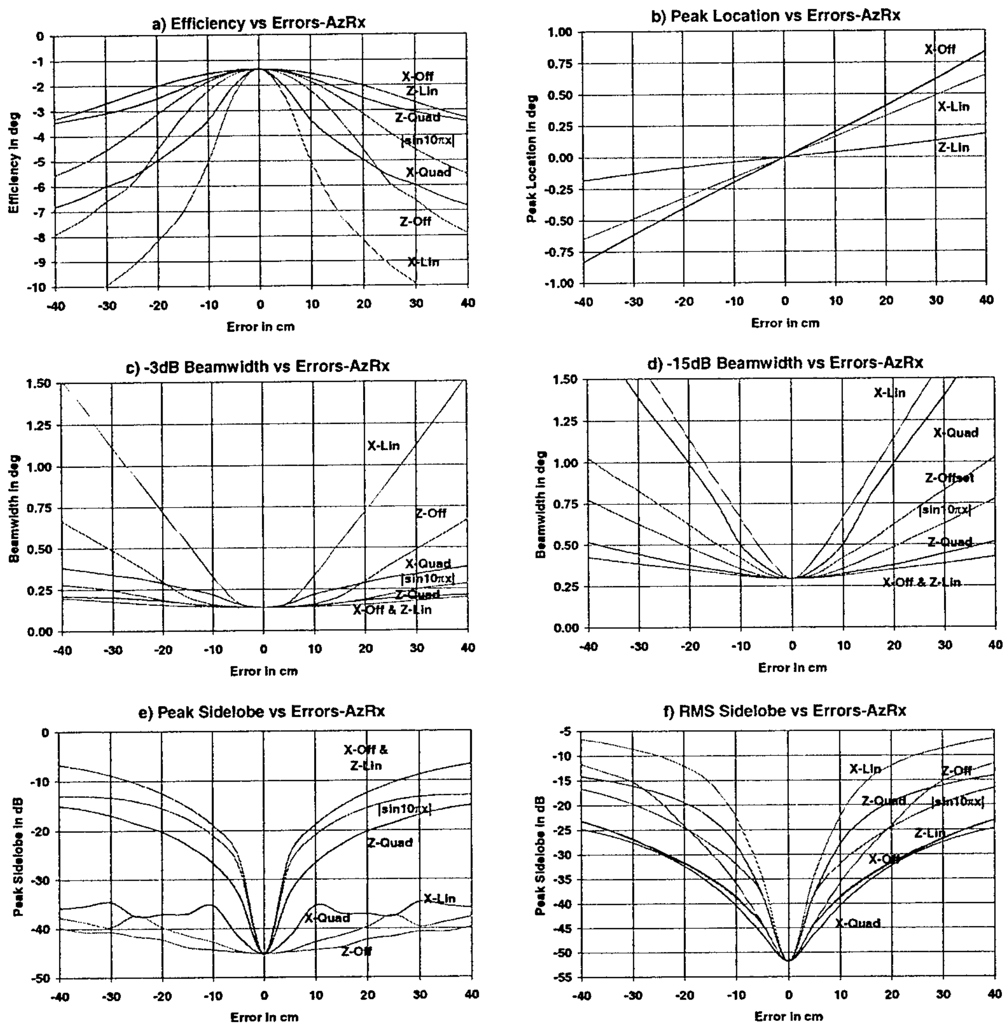

Figure 11. Lens Azimuth Receive Electrical Parameters vs Error; a) Efficiency, b) Peak Location, c) –3dB Beamwidth, d) –15dB Beamwidth, e) Peak Sidelobe

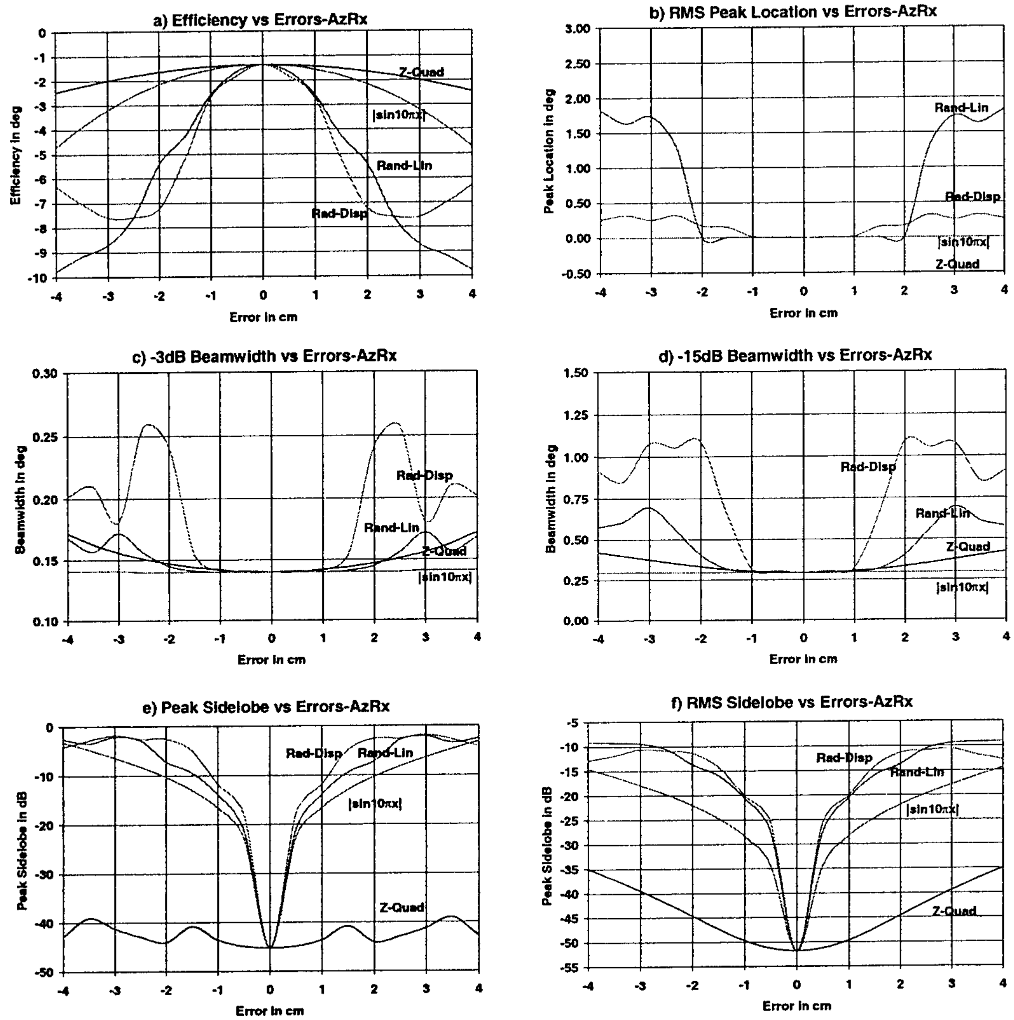

Figure 12. Corporate Azimuth Receive Electrical Parameters vs Error; a) Efficiency, b) Peak Location, c) –3dB Beamwidth, d) –15dB Beamwidth, e) Peak Sidelobe

5. Aperture Design and Performance Summary

The performance of both apertures can be summarized, for a reasonable system, in Tables 3 and 4. These summaries are needed to set electrical limits for use in the distortion analysis that follows.

Table 3. Sidelobe and Beamwidth Pattern Performance				
	Az-Rx	**El-Rx**	**Az-Tx**	**El-Tx**
BW -deg	0.140	0.606	0.094	0.496
Theo SL-dB	-45.000	-30.000	Unif	Unif
N-Bar	7	2		
Comp SL –dB	-38.501	-23.164	-11.931	-11.725

Table 4. Gain Summary		
	Gain-dB	
	Tx	**Rx**
Aperture Gain-dB	58.548	58.548
Efficiency	-2.051	-0.288
Spillover	-0.012	-0.264
Reflection	-0.200	-0.626
Total	56.285	57.370

6. Comparative Error Limits

Error functions, such as those in Figures 11 and 12, are reduced to simple polynomials and the resulting error functions are incorporated into an analytical tool. The error limits are derived from the "Aperture Design and Performance Summary" (Tables 3 and 4) and entered in the "Error Limits" cells in the spreadsheet.

It is assumed that measurements can be made to calibrate the distortion errors. These measurements will be made on panels, sub-sections multiple groups of sections and expressed in simple polynomial or harmonic forms. This enables compensation to lower error levels.

The Lens and Corporate Error Trade-Off are shown in Tables 6 and 7. The "Azimuth" or "Elevation Mechanical Distortion Error Limits" corresponding to the errors described in Figures 7 and 8 are entered as inputs to the tables. This allows the errors to be appropriately proportioned among the possible sources. The polynomial functions are evaluated resulting in an electrical error due to that parameter. Then the results of all the errors are RSS[ed] and brought to a common column. If these exceed the respective “Error Limits”, the cell changes color. The numbers represent the residual errors after calibration and compensation.

Table 5. Lens Distortion Error Trade Off

		Distortion Effects				Limits			
		Az-Rx	El-Rx	Az-Tx	El-Tx	Az-Rx	El-Rx	Az-Tx	El-Tx
	Gain Loss-dB	0.092	0.008	0.071	0.013	0.200	0.200	0.200	0.200
	Pk Shift-Deg	[illegible]	0.057	0.001	0.011	0.014	0.061	0.009	0.050
	3dB BW Increase-deg	0.001	0.001	0.002	0.001	0.014	0.061	0.009	0.050
	15dB BW Increase-deg	0.003	0.004	0.053	0.113	0.147	0.657	0.091	0.453
	Pk SL Increase-dB	4.974	1.903	0.450	0.082	5.000	5.000	5.000	5.000
Exceedance	RMS SL Increase-dB	4.741	1.158	0.669	0.139	5.000	5.000	5.000	5.000
	Type Error	RSS Δ	X-Off	Z-Off	X-Lin	Z-Lin	X-Quad	Z-Quad	|sin10x|
	Err in cm		0.530	1.000	0.600	0.550	0.800	0.700	0.600
	Azimuth Receive								
	Efficiency-dB	0.092	-0.001	-0.009	-0.036	-0.001	-0.084	-0.002	-0.002
	Pk Shift-Deg	0.016	0.011	0.000	0.010	0.002	0.000	0.000	0.000
	3dB BW Deg	0.001	0.000	0.000	0.001	0.000	0.000	0.000	0.000
Azimuth	15dB Az Rx BW-deg	0.003	0.000	0.001	0.002	0.000	0.002	0.000	0.000
	Pk SL-dB	4.974	2.551	0.007	0.006	2.644	0.381	2.069	2.612
	RMS SL-dB	4.741	0.928	1.655	2.540	0.961	2.673	0.828	1.915
	Azimuth Transmit								
	Efficiency-dB	0.071	-0.001	-0.017	-0.035	-0.001	-0.059	-0.006	-0.004
	Pk Shift-deg	0.001	0.001	0.000	0.001	0.000	0.000	0.000	0.000
	3dB BW-deg	0.002	0.000	0.001	0.002	0.000	0.002	0.000	0.000
	15dB Az Rx BW-deg	0.053	0.000	0.029	0.028	0.000	0.034	0.002	-0.001
	Pk SL-dB	0.450	0.035	0.102	0.209	0.380	0.043	0.018	0.014
	RMS SL-dB	0.669	0.003	0.020	-0.668	0.004	-0.004	0.026	0.029
	Type Error	RSS Δ	X-Off	Z-Off	X-Lin	Z-Lin	X-Quad	Z-Quad	|sin2x|
	Err in cm		1.000	10.000	1.200	4.000	0.400	10.000	10.000
	Elevation Receive								
	Efficiency-dB	0.008	0.000	-0.004	-0.006	0.000	0.000	-0.002	-0.002
	Pk Shift-deg	0.057	0.023	0.000	0.047	0.024	0.000	0.000	0.000
	3dB BW-deg	0.001	0.000	0.001	0.000	0.000	0.000	0.000	0.000
	15dB Az Rx BW-deg	0.004	0.000	0.002	0.004	0.000	0.000	0.001	0.000
Elevation	Pk SL-dB	1.903	0.077	0.659	0.037	1.428	0.076	0.052	1.064
	RMS SL-dB	1.158	0.000	0.252	1.084	0.033	0.212	0.093	0.220
	Elevation Transmit								
	Efficiency-dB	0.013	0.000	-0.007	-0.009	0.000	-0.001	-0.005	-0.002
	Pk Shift-deg	0.011	0.002	0.000	0.006	0.009	0.000	0.000	0.000
	3dB BW-deg	0.001	0.000	0.000	0.001	0.000	0.000	0.000	0.000
	15dB Az Rx BW-deg	0.113	0.000	0.001	0.106	0.000	0.038	0.001	0.000
	Pk SL-dB	0.082	0.001	0.036	0.053	0.046	0.000	0.011	0.015
	RMS SL-dB	0.139	0.000	0.050	0.110	0.002	0.056	0.036	0.017

Electrical Error Limits

Azimuth Mechanical Distortion Error Limits

Elevation Mechanical Distortion Error Limits

Table 6. Corporate Distortion Error Trade Off

		Distortion Effects				Limits			
		Az-Rx	El-Rx	Az-Tx	El-Tx	Az-Rx	El-Rx	Az-Tx	El-Tx
	Gain Loss-dB	0.040	0.110	0.033	0.122	0.200	0.200	0.200	0.200
	Pk Shift-Deg	0.004	0.033	0.004	0.018	0.015	0.069	0.009	0.047
	3dB BW Increase-deg	0.000	0.002	0.001	0.007	0.015	0.069	0.009	0.047
	15dB BW Increase-deg	0.008	0.050	0.003	0.153	0.147	0.657	0.091	0.453
Exceedance	Pk SL Increase-dB	4.968	5.001	0.217	0.437	5.000	5.000	5.000	5.000
	RMS SL Increase-dB	0.511	3.318	0.582	0.775	5.000	5.000	5.000	5.000

Electrical Error Limits

	Type Error	RSS Δ	Z-Quad	|sin10x|	Rnd-Disp	Rnd-Lin
	Err in cm		0.100	0.055	0.046	0.046
	Azimuth Receive					
	Efficiency-dB	0.040	-0.003	0.002	-0.018	-0.036
	Pk Shift-deg	0.004	0.000	0.000	0.004	0.000
	3dB BW-deg	0.000	0.000	0.000	0.000	0.000
Azimuth	15dB Az Rx BW-deg	0.008	0.000	0.000	-0.007	-0.003
	Pk SL-dB	4.968	0.072	2.490	3.133	2.942
	RMS SL-dB	0.511	0.015	0.102	0.389	0.315
	Azimuth Transmit					
	Efficiency-dB	0.033	0.001	0.002	-0.017	-0.028
	Pk Shift-deg	0.004	0.000	0.000	0.004	0.000
	3dB BW-deg	0.001	0.001	0.000	0.000	0.000
	15dB Az Rx BW-deg	0.003	0.000	0.000	0.003	0.000
	Pk SL-dB	0.217	0.005	-0.121	0.180	-0.016
	RMS SL-dB	0.582	0.000	0.145	0.405	0.392

Azimuth Mechanical Distortion Error Limits

	Type Error	RSS Δ	Z-Quad	|cos5x|	Rnd-Disp	Rnd-Lin
	Err in cm		0.400	0.103	0.086	0.090
	Elevation Receive					
	Efficiency-dB	0.110	-0.023	0.002	-0.088	-0.062
	Pk Shift-deg	0.033	0.000	0.000	0.033	-0.001
	3dB BW-deg	0.002	0.002	0.000	0.000	0.000
	15dB Az Rx BW-deg	0.050	-0.003	0.000	-0.049	0.012
Elevation	Pk SL-dB	5.001	0.386	2.536	3.135	2.931
	RMS SL-dB	3.318	1.685	1.457	1.806	1.669
	Elevation Transmit					
	Efficiency-dB	0.122	-0.019	0.002	-0.099	-0.068
	Pk Shift-deg	0.018	0.000	0.000	0.018	-0.001
	3dB BW-deg	0.007	0.006	0.000	0.003	0.000
	15dB Az Rx BW-deg	0.153	0.145	0.000	0.047	-0.009
	Pk SL-dB	0.437	0.145	-0.206	0.354	0.054
	RMS SL-dB	0.775	0.323	0.113	0.547	0.430

Elevation Mechanical Distortion Error Limits

7. Lens and Corporate Limits/Requirements/Real World Comparison Summary

The results from the Tables 5 and 6 are transferred to Table 7 where they are summarized. This table also shows the "Real World/Uncompensated" errors estimated from past experience. The "Requirements from Trade-Off Analysis" shows the error requirements needed to perform the task and thus says that they must be achieved through calibration and then compensation.

Table 7. Limits/Requirements/Real World Comparison

Absolute Maximim Limits if Only One Error is Assumed

Lens Configuration		
Error	Az	Elev
X-Off Peak	0.699	2.664
Z-Off Peak	3.134	27.870
X-Lin ±Peak	0.864	1.545
Z-Lin ±Peak	1.074	9.402
X-Quad Peak	1.530	4.536
Z-Quad Peak	1.787	43.086
|sin10x| or |sin2x| Peak	1.190	26.644

Corporate Configuration		
Error	Az	Elev
Z-Quad Peak	1.108	1.108
|sin10x| or |cos5x| Peak	0.111	0.203
Rnd-Disp RMS	0.089	0.137
Rnd-Lin RMS	0.102	0.157

Requirements from Trade-Off Analysis

Lens Configuration		
Error	Az	Elev
X-Off Peak	0.530	1.000
Z-Off Peak	1.000	10.000
X-Lin ±Peak	0.600	1.200
Z-Lin ±Peak	0.550	4.000
X-Quad Peak	0.800	0.400
Z-Quad Peak	0.700	10.000
|sin10x| or |sin2x| Peak	0.600	10.000

Corporate Configuration		
Error	Az	Elev
Z-Quad Peak	0.100	0.400
|sin10x| or |cos5x| Peak	0.055	0.103
Rnd-Disp RMS	0.046	0.086
Rnd-Lin RMS	0.046	0.090

Calibrate and Compensate

Real World/Uncompensated

Lens Configuration		
Error	Az	Elev
X-Off Peak	[illegible]	[illegible]
Z-Off Peak	[illegible]	2.250
X-Lin ±Peak	0.300	0.150
Z-Lin ±Peak	[illegible]	1.140
X-Quad Peak	0.300	0.150
Z-Quad Peak	[illegible]	2.250
|sin10x| or |sin2x| Peak	0.300	1.200

Corporate Configuration		
Error	Az	Elev
Z-Quad Peak	[illegible]	[illegible]
|sin10x| or |cos5x| Peak	[illegible]	[illegible]
Rnd-Disp RMS	[illegible]	[illegible]
Rnd-Lin RMS	[illegible]	0.060

Acknowledgements

This contract was funded and supported by the AFRL, Sensor's Directorate at Hanscom AFB under contract F19628-99-C-0033. The authors thank J.P. Turtle, for Program Management and for technical input from the Antenna Technology Branch. The authors acknowledge assistance given from within Northrop Grumman Corporation by J.V. Arnts, L.R. Payton, and G. Gallegro.

UPLINK C/I-SIMULATIONS OF MULTI-BEAM ANTENNAS IN AN LMDS SYSTEM

Ulrika Engstrom[1], Martin Johansson[1], Anders Derneryd[1], Bjorn Johannisson[1], Gino Masini[2]

[1] Ericsson Research, Corporate Unit
Ericsson Microwave Systems AB
SE-431 84 Molndal, Sweden

[2] Ericsson Lab Italy
Microwave Product Unit
Via Cadorna 73
I-200 90 Vimodrone (MI), Italy

Abstract: Carrier-to-interference performance is simulated for a local multipoint distribution system (LMDS). Conventional wide beam sector node antennas are compared with multi-beam antennas. The performance improvement provided by the use of narrow beam antennas in terms of up-link interference rejection is evaluated. The simulations show a potential improvement in C/I of 5 dB using three-beam antennas instead of the current 90-degree sector node antennas.

1. Introduction

Telecommunication operator requirements for access systems as well as users´ increased demands for bandwidth are the driving forces behind the development of new broadband access systems. In this context, broadband wireless systems are competitive and complementary techniques to copper and fiber access.

A high-capacity wireless local multipoint distribution system (LMDS), operating in the 24 to 30 GHz band is considered. The LMDS follows a cellular deployment structure in which multiple square sectors cover a certain geographical area. Within each sector, there is at least one radio node with up to 64 fixed Access Terminations (AT) communicating over the air interface with a maximum bit-rate of 37.5 Mbps in both up- and down-link. The ATs, which require line-of-sight paths to the node, can be located anywhere within the sector coverage area.

The present system is uplink-limited with three major AT interfering directions. With a frequency reuse of two and two orthogonal polarization directions, the worst interference occurs when the three major co-channel interferers are located at the sector borders four sectors away. The introduction of a multi-beam node antenna has the potential to reduce the interference level by exploiting narrow beams.

Simulations of carrier-to-interference ratio (C/I) performance of multi-beam antennas have been carried out. In the simulations, multi-beam node antennas are compared with sector node antennas regarding effects on up-link C/I performance in the network.

2. Cell structure

The sectors of an LMDS-network are laid out in a regular square pattern in order to have a simple and clear case in the simulations. A cell plan consisting of 3 by 3 radio hubs is shown in Figure 1. Each hub is equipped with four node antennas. Sector diagonals are typically in the range 2 to 6 km.

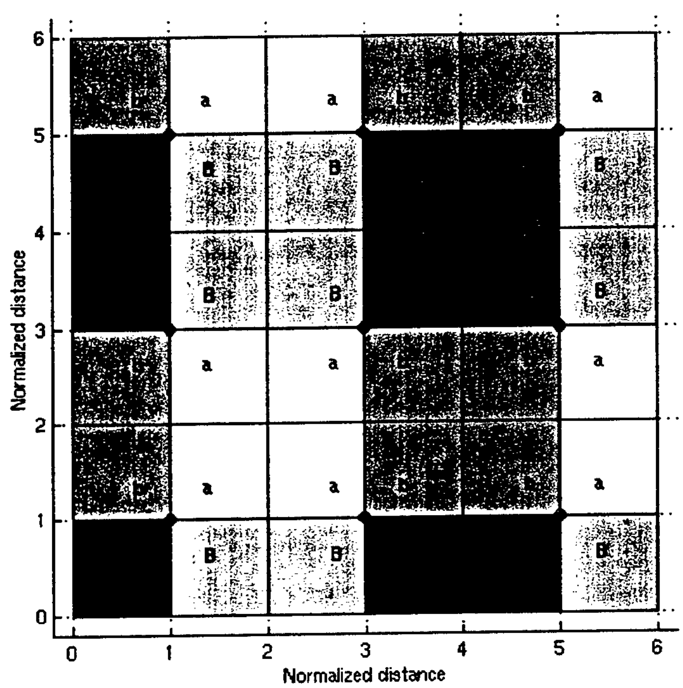

Fig. 1 A square cell plan with 3 by 3 radio hubs indicated with ⊗. Separate letters denote two different frequencies. Upper and lower cases represent orthogonal polarization directions.

Both horizontal and vertical polarization directions and a frequency re-use scheme of two are usually implemented in a network, i.e. both frequencies (denoted A/a and B/b) are re-used with two orthogonal polarization directions as represented with upper and lower cases in the figure.

At each radio hub, four 90° sector node antennas covering 360° in azimuth are currently used. Such wide beam node antennas used today in MINI-LINK BAS for vertical and horizontal polarization are shown in Figure 2. In down-link, from node antenna to AT, the node antenna radiates over the whole sector. In up-link, the node antenna receives information from one AT per time slot, exploiting time division multiple access (TDMA). The MINI-LINK BAS AT antennas are highly directive parabolic antennas in a compact outdoor unit as shown in Figure 3 with a half-power beam-width of a few degrees.

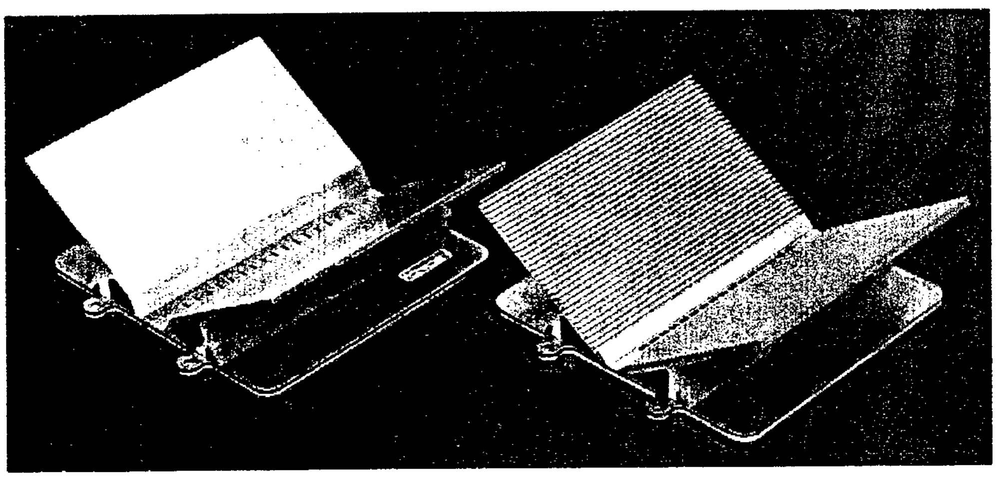

Fig. 2 MINI-LINK BAS wide beam node antennas (left: vertical polarization, right: horizontal polarization). The baffles are used for beam shaping.

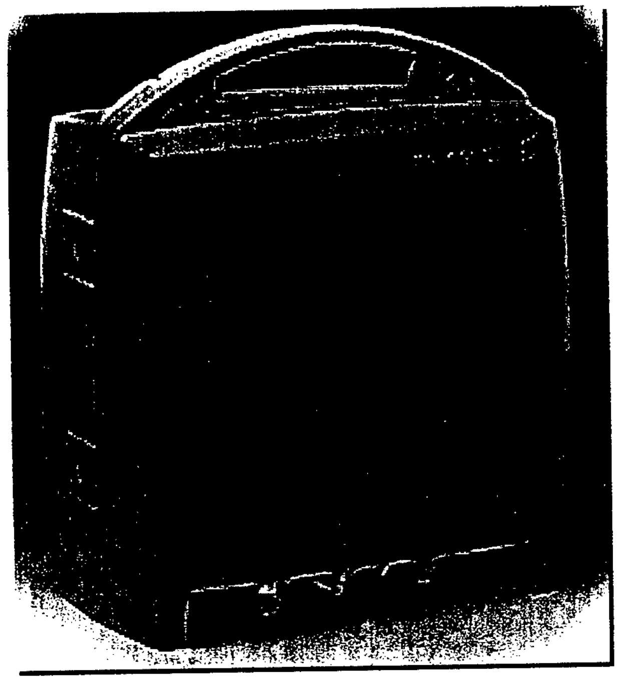

Fig. 3 Outdoor part of the MINI-LINK BAS Access Termination (AT).

The ATs are spread over the sector area and for the active AT, one or more TDMA time slots in the frame are assigned. In the simulations, we have assumed that all sectors are under maximum load condition, i.e., all time slots in a frame are used by an AT somewhere in the sector. The active AT is in the simulations randomly chosen on a time slot by time slot basis. Another assumption is that the ATs are under remote transmit power control such that the power received at their connected radio node by each AT has the same level. This means that the AT output power level is adjusted to compensate for distance as well radio node antenna directive gain.

When we consider a given time slot in the TDMA frame, it can be interfered by a user connected to a radio node in another cell that uses the same frequency channel and the same polarization direction at the same time. In down-link, the major interference is from the radio node towards an AT located four sectors away as illustrated by the white arrow in Figure 4.

In up-link, there are three major interference directions shown as black arrows in the figure. The reason is that ATs positioned in these directions point directly toward the considered radio node that is in the same direction as the connected one. The highest interference signals occur when these three major co-channel interferers are located at sector boundaries four sectors away.

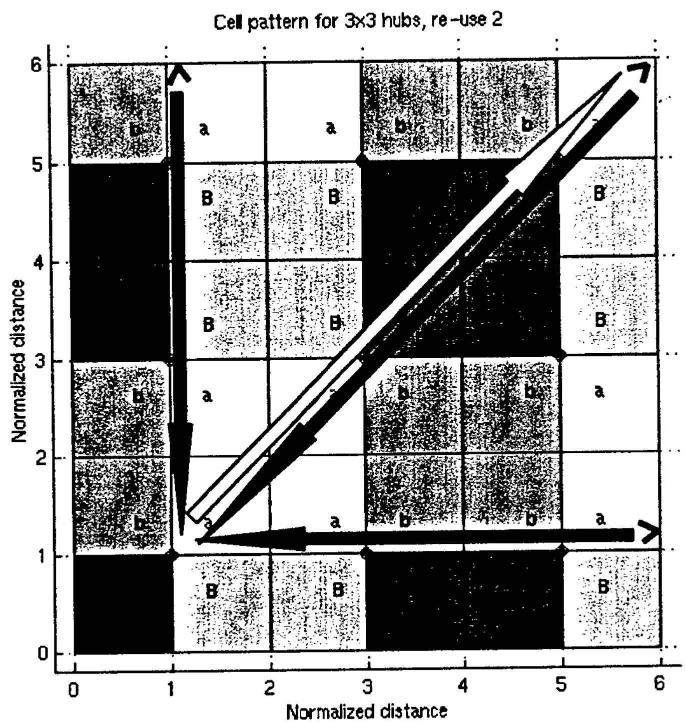

Fig. 4 Interference directions in a square cell plan with 3 by 3 radio hubs using a frequency re-use plan of two and two polarization conditions. White arrow represents down-link and black arrows represent up-link.

3. Theoretical worst cases

The interference level within a network depends on the position of the ATs and the gain of the antennas. The C/I-ratio has been estimated for ATs placed in the worst positions in order to get a rough estimate of the highest interference levels that can be generated by a frequency re-use plan of two. A single AT positioned at the border of the nearest interfering sector is indicated by one of the black arrows in Figure 4 (3 by 3 radio hub network). This results in a minimum C/I-ratio in up-link of 14 dB assuming line-of-sight, no atmospheric attenuation and transmit power control. With more interfering AT-signals arriving simultaneously at the considered node, the C/I-ratio decreases to 11 dB and 9.2 dB for two and three interfering directions, respectively, i.e., a degradation of 3 dB and 4.8 dB, respectively. This shows that there is a potential improvement in C/I in up-link by the introduction of multi-beam node antennas as a replacement for sector beam antennas, since one or two of the major interfering signals can be suppressed.

4. Simulations

Simulations have been performed for up-link C/I calculations in a 3 by 5 hub network with each hub equipped with four radio node antennas. The assumptions are flat land, line-of-sight, clear sky, no antenna down-tilt and a sector diagonal of 2.4 km. In every sector there are 64 ATs randomly distributed over the area, see Figure 5.

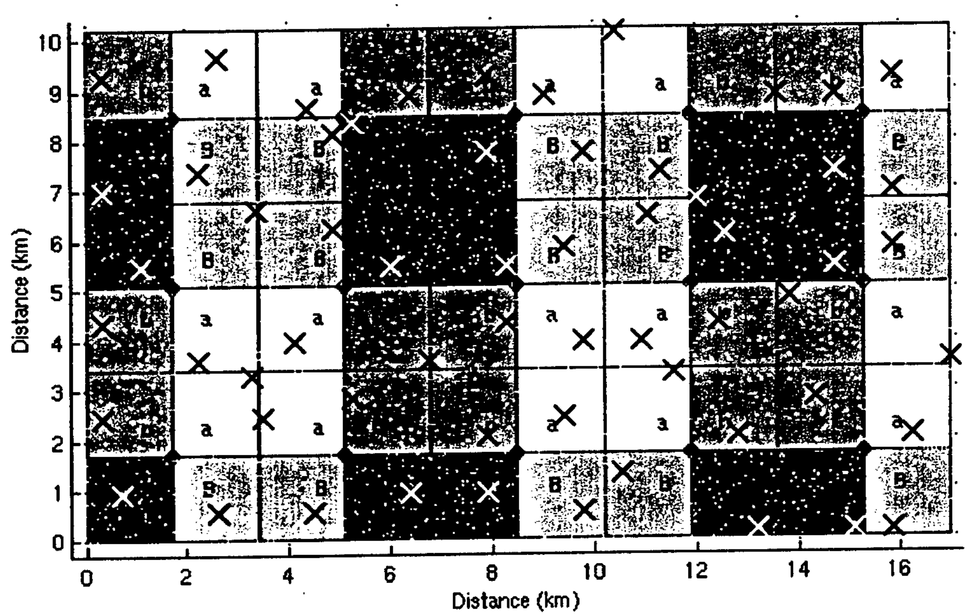

Fig. 5 A square cell plan with 3 by 5 radio hubs indicated with ⊗. Separate letters denote two different frequencies. Upper and lower cases represent orthogonal polarization directions. Crosses indicate active ATs (one per sector and time slot), while white dots represent inactive ATs.

All node antennas in the network have the same radiation characteristics (wide beam or multi-beam) in the simulations. Illustrations of the radiation patterns of the radio node antennas used are plotted in Figures 6 and 7. Node antennas with one to four beams evenly distributed across the 90° sector have been evaluated. The cross-over level between the beams is set to –4 dB. The cross-polarization level within the main beam is assumed to be –25 dB.

The cumulative distribution function (CDF) has been obtained by calculating the up-link C/I-ratio for all the radio node antennas including co-channel, adjacent channel and cross-polarization radiation interference for each of 1000 time slots. In every sector, the transmitting AT was chosen randomly for each time slot.

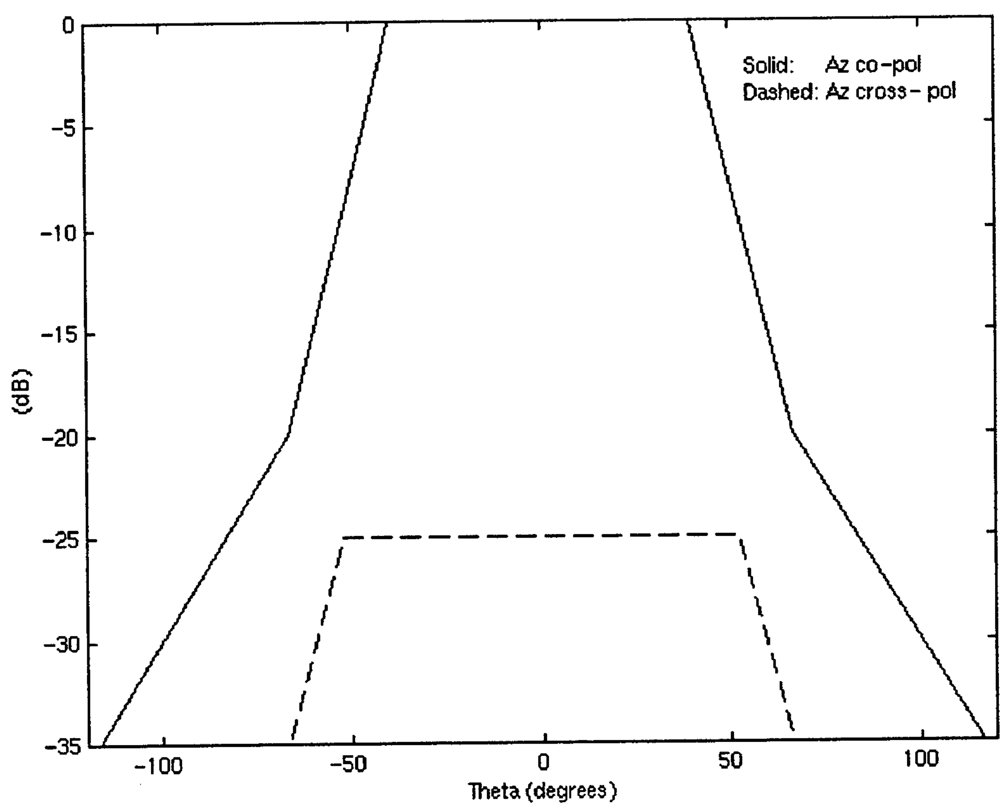

Fig. 6 Radiation pattern of the wide beam radio node antenna in the horizontal plane.

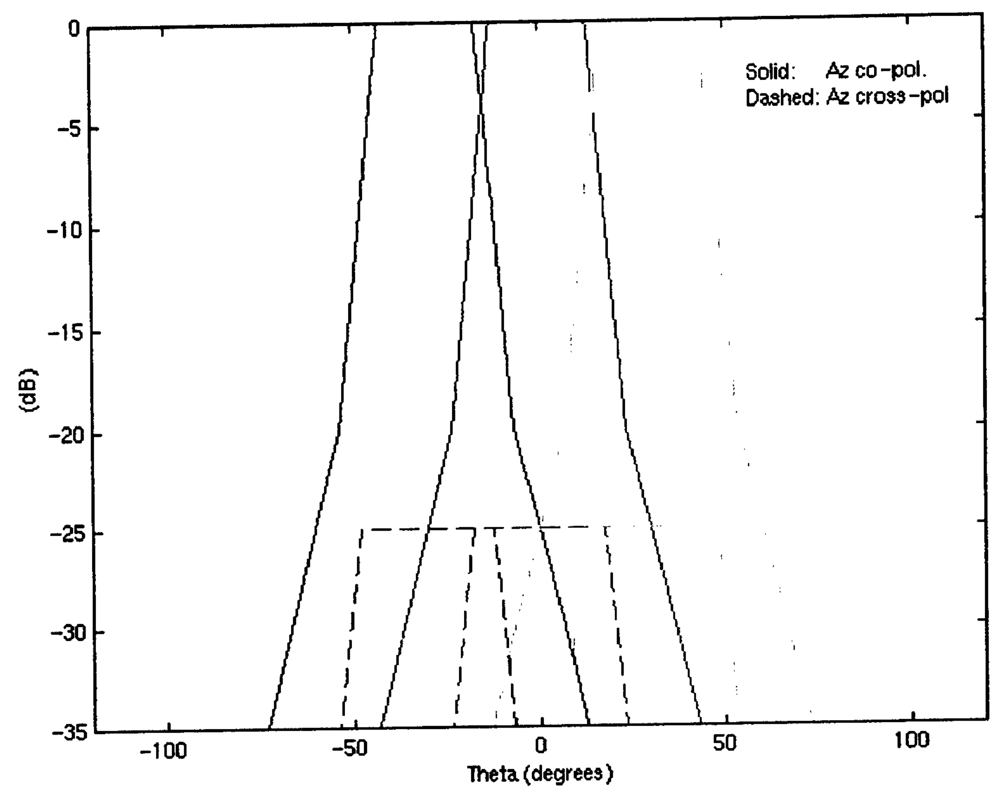

Fig. 7 Radiation pattern of the three-beam radio node antenna in the horizontal plane.

5. Number of beams

The C/I-ratio has been investigated when varying the number of radio node beams from one to four in every sector in a 3 by 5 hub network (Figure 5). A frequency plan of two is assumed in the simulations. The CDF is plotted in Figure 8 with the number of beams as a parameter. The C/I-ratio increases monotonically in the range of interest with increased number of beams. At a 5% fraction, the C/I-ratio increases from 21 dB to 27 dB, i.e., a potential increase of 6 dB when changing from one to three beams. At a 2% fraction, it increases from 18 dB to 23 dB, i.e., a potential increase of 5 dB. Further increasing the number of beams will only slightly improve the performance.

The fraction of ATs with bad C/I-ratio decreases with the increase in number of beams. At a C/I-ratio of 24 dB, the one-beam case has a bad fraction of 8% compared to less than 3% with the three-beam antennas. The improvements in C/I-ratio utilizing multi-beam radio node antennas have the potential to be exploited for higher modulation schemes, better quality of services, or a tighter frequency re-use plan.

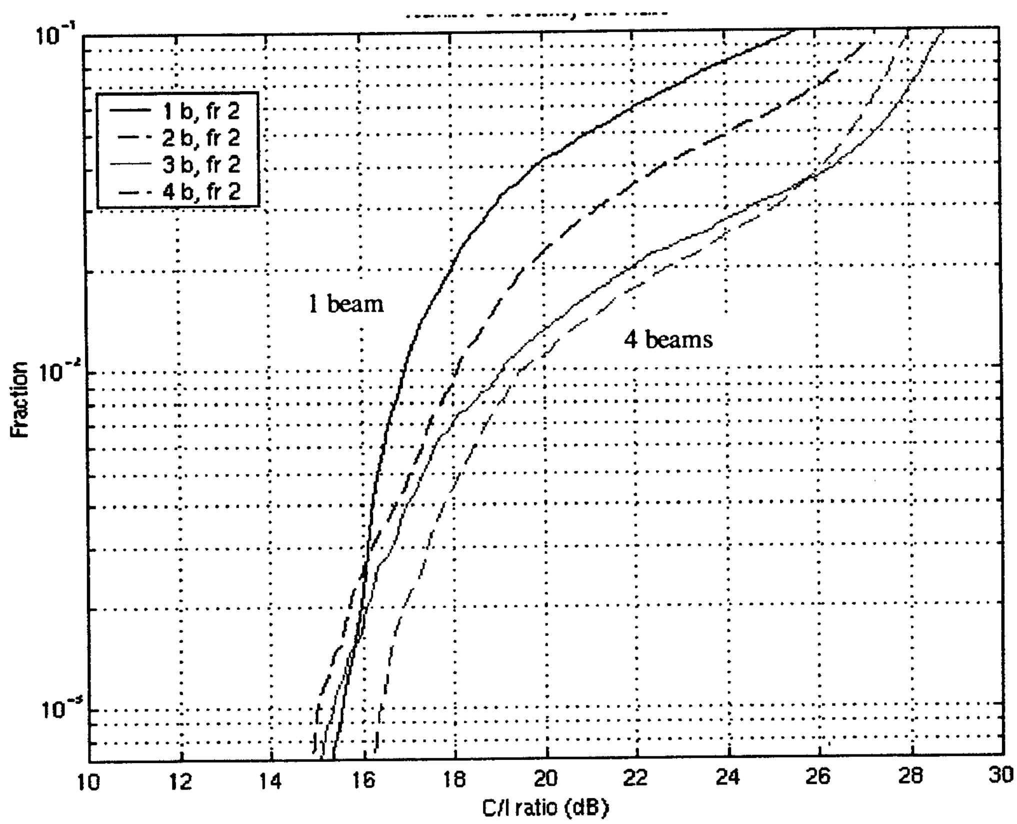

Fig. 8 Up-link CDF-curves for the C/I-ratio in a 3 by 5 radio hub network scenario with a frequency re-use plan of two. The number of beams is varied from one to four at all nodes.

6. Frequency re-use of one

In cases when there are few frequency bands available or when an operator requires only one type of radio, a frequency re-use plan of one is desirable. The same frequency is then used in all sectors with alternating polarization directions in adjacent sectors. Simulations of such a frequency re-use plan have been performed in order to assess the potential of multi-beam node antennas in a single frequency network. The same assumptions as before have been used except that the same frequency is now used in all sectors. The cell plan is laid out in Figure 9.

The interfering ATs come much closer in a network that uses a frequency re-use plan of one. The major co-channel interfering AT is now along the sector diagonal two sectors away. The interference level in up-link is–6.4 dB relative to the carrier for the four closest interfering ATs.

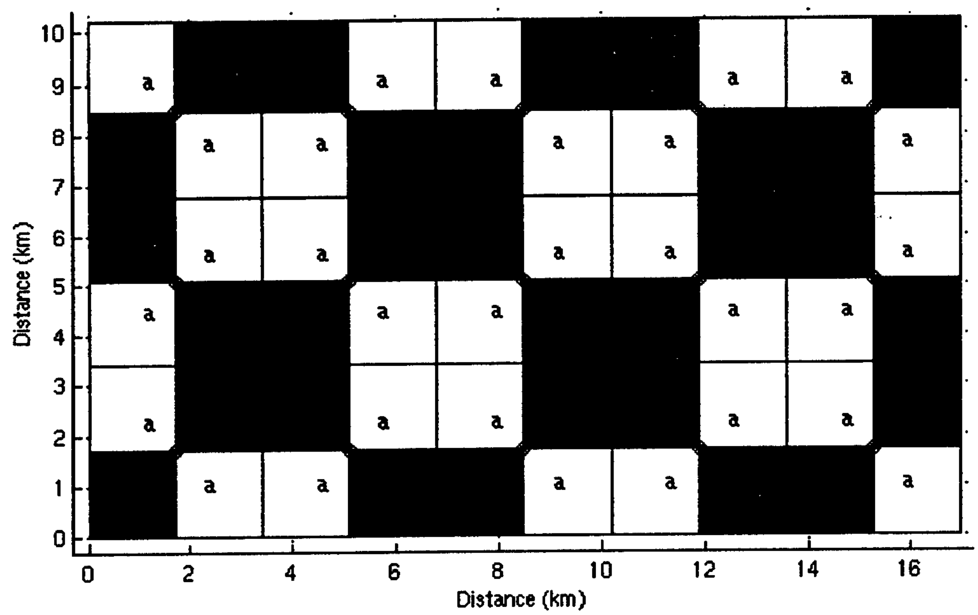

Fig. 9 A square cell plan with 3 by 5 radio hubs indicated with ⊗. Upper (dark) and lower (light) cases represent orthogonal polarization directions that use the same frequency.

Calculated CDF-curves are presented in Figure 10 for wide beam and three-beam radio node antennas in a 3 by 5 radio hub network utilizing a single frequency. Results are also plotted for a frequency re-use plan of two for comparison. The degradation in C/I-ratio at the 5% fraction level is in the order of 8 to 10 dB when changing from a frequency plan of two to one. Some of the degradation is recovered by replacing the wide beam sector antennas with three-beam antennas. A potential improvement of 4 dB in the single frequency plan using three-beam antennas gives an acceptable C/I-ratio of 17 dB at the 5% fraction level.

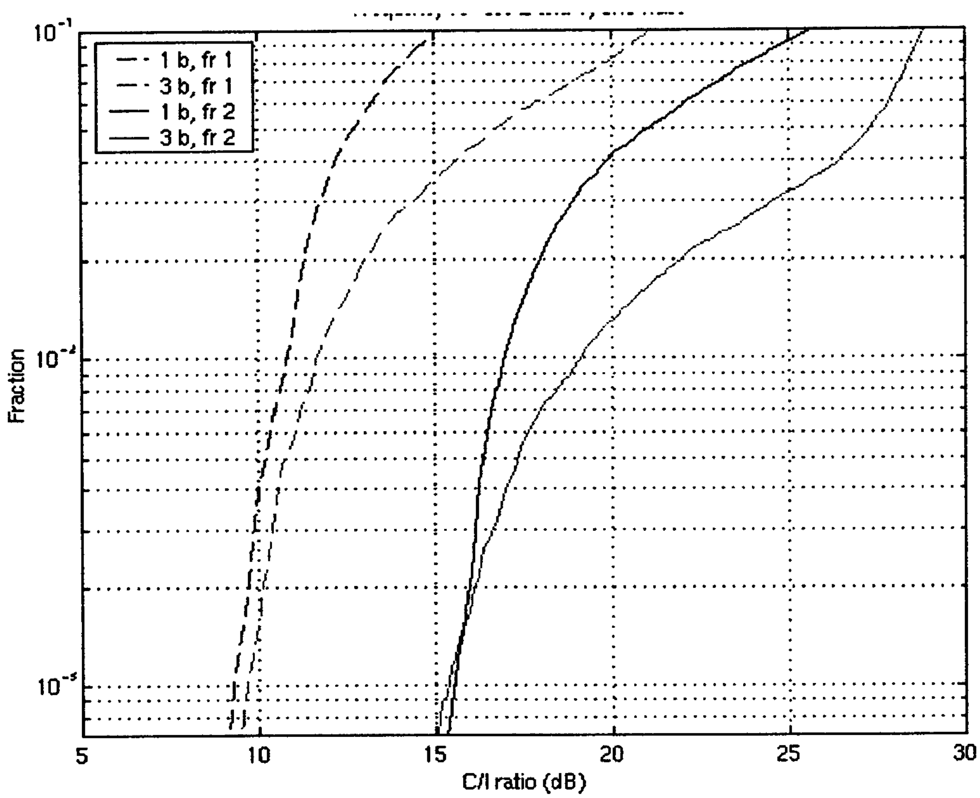

Fig. 10 Up-link CDF-curves for the C/I-ratio in a 3 by 5 radio hub network scenario with a frequency re-use plan of one and of two. The number of beams is either one or three at all nodes.

7. Conclusions

LMDS networks using wide beam radio node antennas have a capacity asymmetry in up-link/down-link due to up-link interference limitation. Simulations have shown that multi-beam antennas at the radio node can be used to reduce the interference level in up-link. Each of the beams may then cover only a single interfering sector, and not two or more as for the wide beam antennas.

The potential increase in C/I-ratio is on the order of 5 dB by utilizing three-beam radio node antennas instead of wide beam sector antennas. This is valid both for a network employing a frequency re-use plan of one and of two. The improvements in C/I can be used to implement higher modulation schemes or better communication quality.

AFFORDABLE ANTENNA ARRAY FOR MULTIPLE SATELLITE LINKS

Sarjit S Bharj — Princeton Microwave Technology
Alex Merzhevskiy
Paul Oleski — AFRL, Rome
Boris Tomasic — AFRL, Hanscom
S.Liu — Aerospace Corporation

ABSTRACT

The low cost manufacturing of Transmit/Receive (T/R) modules for the next generation of Phase Array Radar for the AIR Force Satellite Communications Network has been achieved. The T/R modules are a critical component of a multi-beam ground based phase array system, which will allow several tracking, communications and control systems to operate simultaneously from a common aperture. The T/R module, operating at Up-link and down-link frequencies of 1.8 GHz and 2.2 GHz, each consist of four five bit digital phase shifters based on MMIC devices, two power amplifiers, two low noise amplifiers, two limiters, four five bit digital attenuators, two 100 dB rejection transmit filters, two receiver filters, power dividers and quadrature couplers. The control of the T/R module is conducted via a single Field Programmable Gate array through a GPIB computer interface. The T/R module has been designed to cost to meet a $100.00 target figure for a typical system comprising of 44000 such elements. To this end the paper will detail the innovative methods used to focus towards the goal without compromising the performance.

1.0 Introduction

The purpose of the antenna array is to serve radar, electronic support measure and electronics, electronic warfare and communication functions. The phase array antenna considered in this presentation is specific for Air Force Satellite Communications Network. Implicit in the system function array is the need to operate the array in full duplex operation. Additionally the array should be capable of controlling fundamental radiation characteristics such as beamwidth, beam size, sidelobe levels and radiated power, in order to realize the different antenna characteristics required by the various systems. It is also intended to have a self-healing capability to retain a degree of usefulness in the event of component failures. The array aperture consists of a large number of radiating elements that are spaced approximately half a wavelength at the upper end of the operational frequency band. The frequency response and excitation of each element in the aperture can be independently controlled. This enables the antenna to reconfigure around damaged or failed areas or to vary the array illumination. The aperture can be fully or partially utilized either to direct energy over a large volume or intentionally directed in a certain direction. Satellite communications, Airborne radar, EW, and Communications systems differ significantly in their antenna requirements. Not only do the various systems differ in their primary functions, but also the many variations within one system will affect antenna requirements. Each of these radar systems has aperture requirements unique to its function. Additionally radar and communications require both transmission and reception of energy where as ESM and ECM systems require only reception of energy. The capability of the array to provide transmit and receive functions simultaneous and to rapidly alter the set of configurations is possible due to the active element control circuit.

The active control circuits allow the Phase Array Radar to control their radiation characteristics. The aperture can be uniformly illuminated to achieve maximum gain or tapered illuminated to achieve low sidelobes or shaped beam. The combination of the variable attenuator and phase shifter permits the array illumination to be modified and the antenna beam to be scanned in any direction.

The main goals for the development of the Transmit/Receive module was to develop

- Low cost microwave components
- High Isolation filters
- Low cost Manufacturing
- Demonstrate a fully functional antenna sub-array

The specifications of the Transmit Section are detailed in Table below.

Parameter	Specification
Frequency	**1.764 – 1.864 Ghz**
Gain	**20 dB**
Power Output per channel	**30 dBm**
Phase shift	**360 degrees**
Control	**Electronic**
Retrofit	**Change in hot condition**
Efficiency	**>40 %**
Spurious Levels	**<-85 dBc**
Attenuation control	**3 to 10 dB**

Receiver section

The receive section of the T/R module consists of dual channels. The input signals are routed through a low loss band-pass filter, limiters and low noise amplifiers. The output of the low noise amplifiers is fed through a 90-degree hybrid followed by gain stages and a power splitter. The output is then fed into dual phase and amplitude control circuits. Both the phase shifter and attenuators are 5 bit digital control circuits.

The specifications for the receive section are detailed below.

PARAMETER	**SPECIFICATIONS**
Frequency	**2.2-2.3 GHz**
Gain	**30 dB**
Noise Figure	**1.2 dB**
Phase Shift	**360 Degree**
Attenuation	**30 dB min**

1.1 Concept of Antenna

The basic concept of the antenna is based on [1] a hemispherical dome as shown in Figure 1, below.

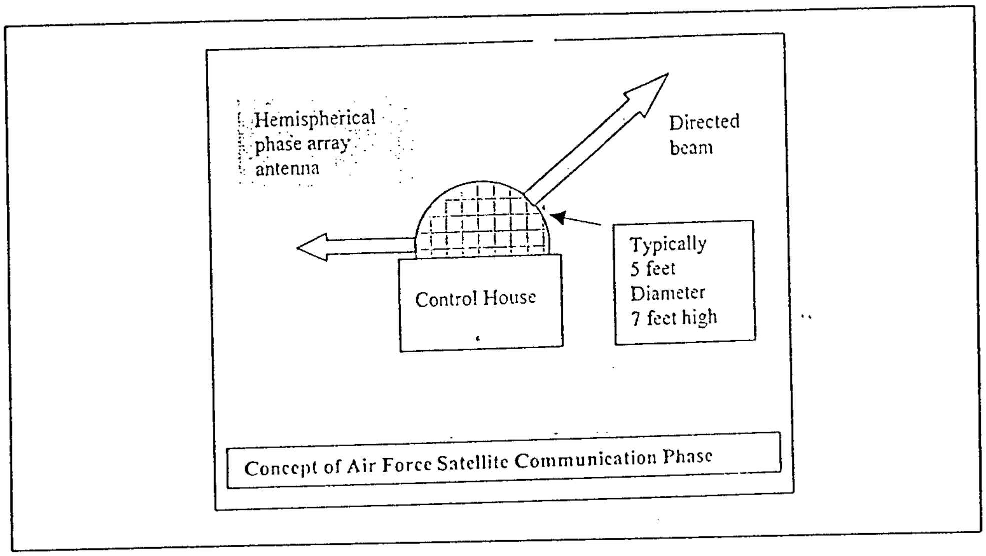

Concept of Air Force Satellite Communication Phase

1.2 Block Diagram of Transmit/Receive Module

The block diagram of the T/R module is detailed in Figure 2. The transmit section of the T/R module consists of two control circuits at the input, comprising of a phase shifter and an attenuator, which are combined in phase power combiner. The output of the combiner is amplified in a driver amplifier and fed into a 90- degree hybrid through a single pole double throw switch. The quadrature outputs of the hybrid are amplified in MMIC amplifiers to a power output of 30 dBm and transmit through high rejection ceramic filters.

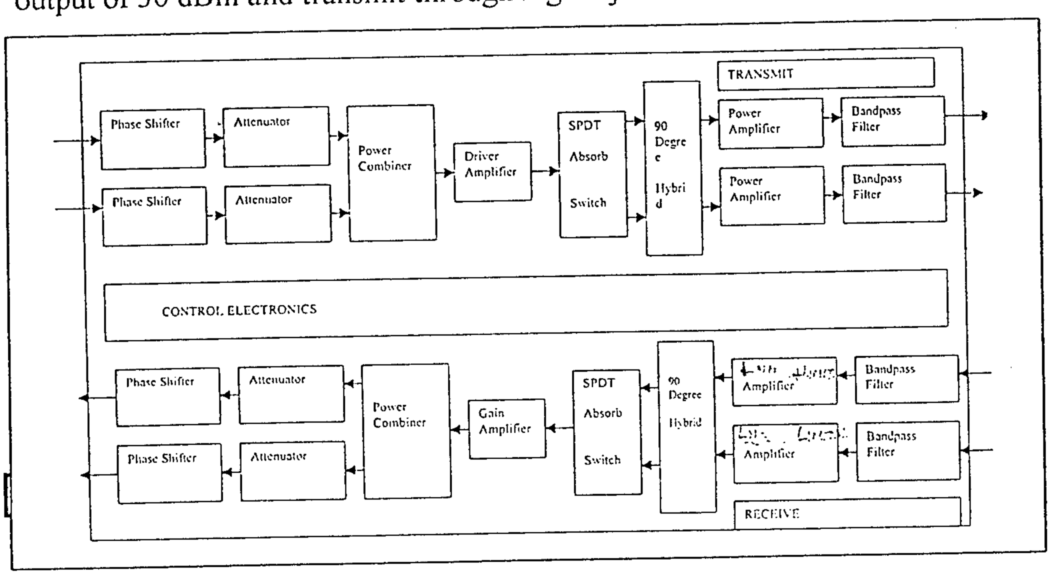

1.3 Components of the T/R Module

The main components of the Transmit/Receive module are:

- Transmit Filter with 100 dB rejection at receive frequency
- Receive filters with high rejection at transmit frequency
- Low noise MMIC amplifiers
- High Power MMIC driver and Power MMIC amplifiers
- Quadrature and in phase hybrids
- 5 Bit Transmit digital Phase shifter
- 5 Bit receive digital Phase Shifter
- 5 Bit digital control attenuators for transmit and receive channel
- Limiters for receive channel
- SPDT switch for RH and LD polarization.
- Xilinx digital controller

1.4 Performance of the individual Components

1.4.1 Transmit Filter

The transmit filters are made of ceramic resonator. It consists of six resonators in a coaxial structure. The main goal was to have high rejection of at least 100 dB at the receive frequency. The measured performance of the filter is detailed in Figure 3.

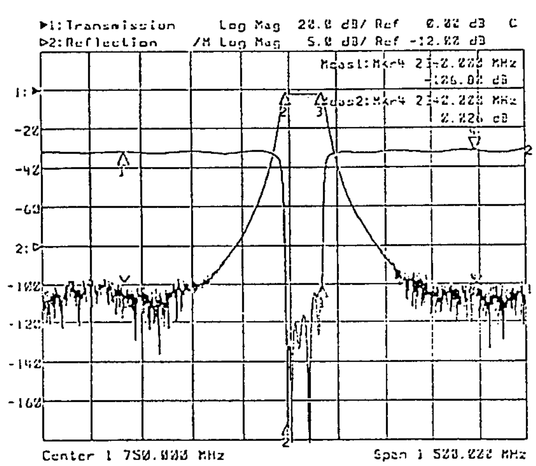

Figure 3: Measured performance of the Transmit Filter

failures. The array aperture consists of a large number of radiating elements that are spaced approximately half a wavelength at the upper end of the operational frequency band. The frequency response and excitation of each element in the aperture can be independently controlled. This enables the antenna to reconfigure around damaged or failed areas or to vary the array illumination. The aperture can be fully or partially utilized either to direct energy over a large volume or intentionally directed in a certain direction. Satellite communications, Airborne radar, EW, and Communications systems differ significantly in their antenna requirements. Not only do the various systems differ in their primary functions, but also the many variations within one system will affect antenna requirements. Each of these radar systems has aperture requirements unique to its function. Additionally radar and communications require both transmission and reception of energy where as ESM and ECM systems require only reception of energy. The capability of the array to provide transmit and receive functions simultaneous and to rapidly alter the set of configurations is possible due to the active element control circuit.

The active control circuits allow the Phase Array Radar to control their radiation characteristics. The aperture can be uniformly illuminated to achieve maximum gain or tapered illuminated to achieve low sidelobes or shaped beam. The combination of the variable attenuator and phase shifter permits the array illumination to be modified and the antenna beam to be scanned in any direction.

The main goals for the development of the Transmit/Receive module was to develop

- Low cost microwave components
- High Isolation filters
- Low cost Manufacturing
- Demonstrate a fully functional antenna sub-array

1.4.2 Receive Filters

The receive channel filters are made of ceramic resonators very similar to those of transmit filter. The measured performance of the filter is detailed in Figure 4. The receiver filters were designed for low loss and a rejection of at least 50 dB at the transmit frequencies.

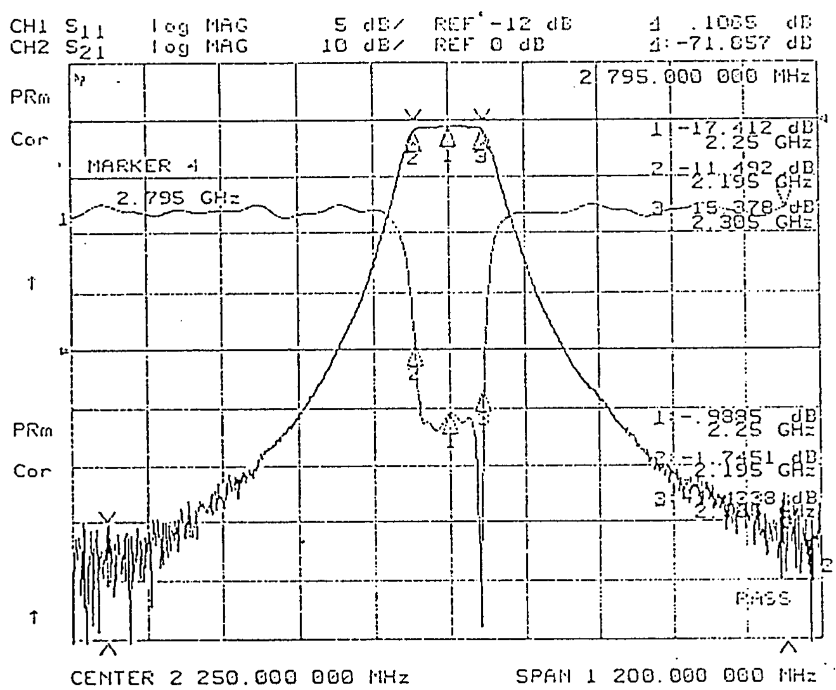

Figure 5: Measured Receive Channel Filter Performance.

1.4.3 **Low noise MMIC amplifier**

The low noise amplifier can either be designed or used as a MMIC amplifier. For a frequency of 2.2 to 2.3 GHz, Silicon Germanium devices such as BFP520, BFP 620 and Silicon Germanium MMIC amplifier MAX2641 were evaluated. The performance is detailed in Table below. For the T/R module, the MIC amplifier was selected due to the high volume and low cost application. New devices such as BFP 620 are presently being evaluated.

Parameter	BFP 520	MAX 2641
Frequency	2.2-2.3 GHz	2.2 – 2.3 GHz
Noise Figure	1.1 dB	1.23 dB
Gain	20 dB	14 dB
Voltage	2 Volts	3 Volts
IP3	25 dBm	10 dBm
Package	Surface mount	Sot -23

1.4.4 High Power MMIC amplifier

For the power amplifier, multitude of MMICs is available. One such MMIC evaluated and used for the Transmit channel, with a power output capability of 32 dBm is detailed below.

The data is for AP119 DCS MMIC

Frequency Range	1700-1900 MHz
Gain	20 dB
Power added efficiency	> 45%
VSR	10:1
Operation Voltage	3.5 V max drain voltage 10 V
Package	SSOP-16-enhanced Surface mount
Gain Control	30 dB
Control Voltage	-3 to-1 Volts
Phase change with control	10 degree maximum
Power output	32 dBm

The measured performance of the amplifier is shown in Figure 6.

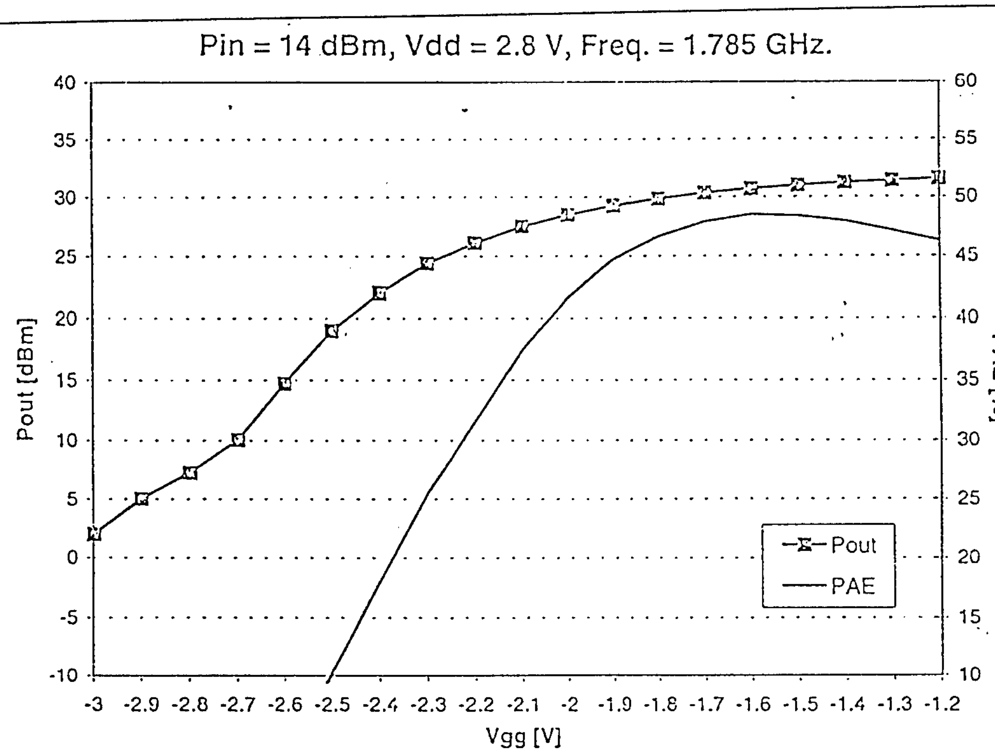

Figure 6: Measured performance of MMIC Power Amplifier

1.4.5 5 Bit Transmit and Receive Phase Shifters

The design of the Transmit and Receive channel phase shifters are based on delay line phase shifters. Appropriate MMICs, in the SPDT and dual SPDT were procured and used in the development of the phase shifter. The measured performance of the phase shifter is detailed in Figure 7 and Figure 8. The insertion loss of the phase shifter was measured at 8 dB with a total change in insertion loss of 0.4 dB in all phase states. The size of the phase shifter has been reduced to 1.5 inch by 0.8 inch and used commercial devices.

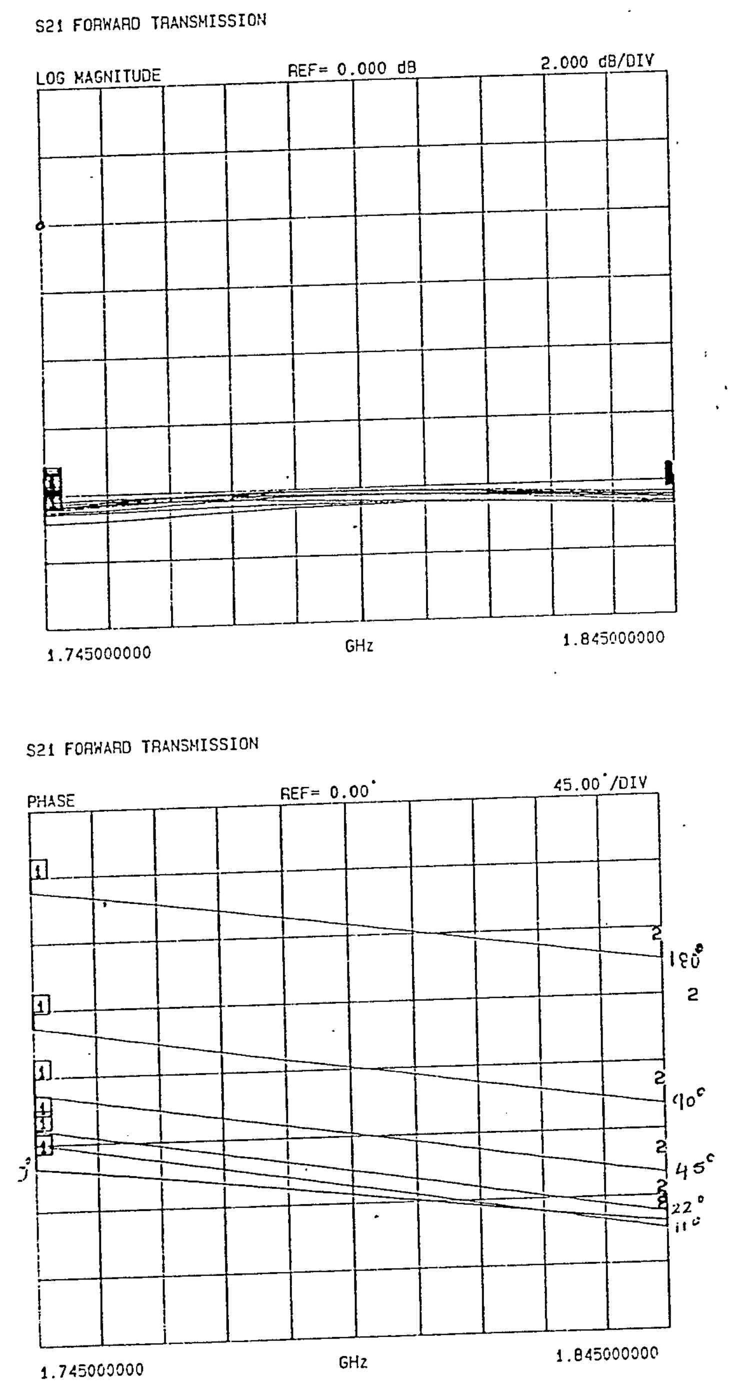

Figure 7: Measured performance of Transmit channel Phase shifter

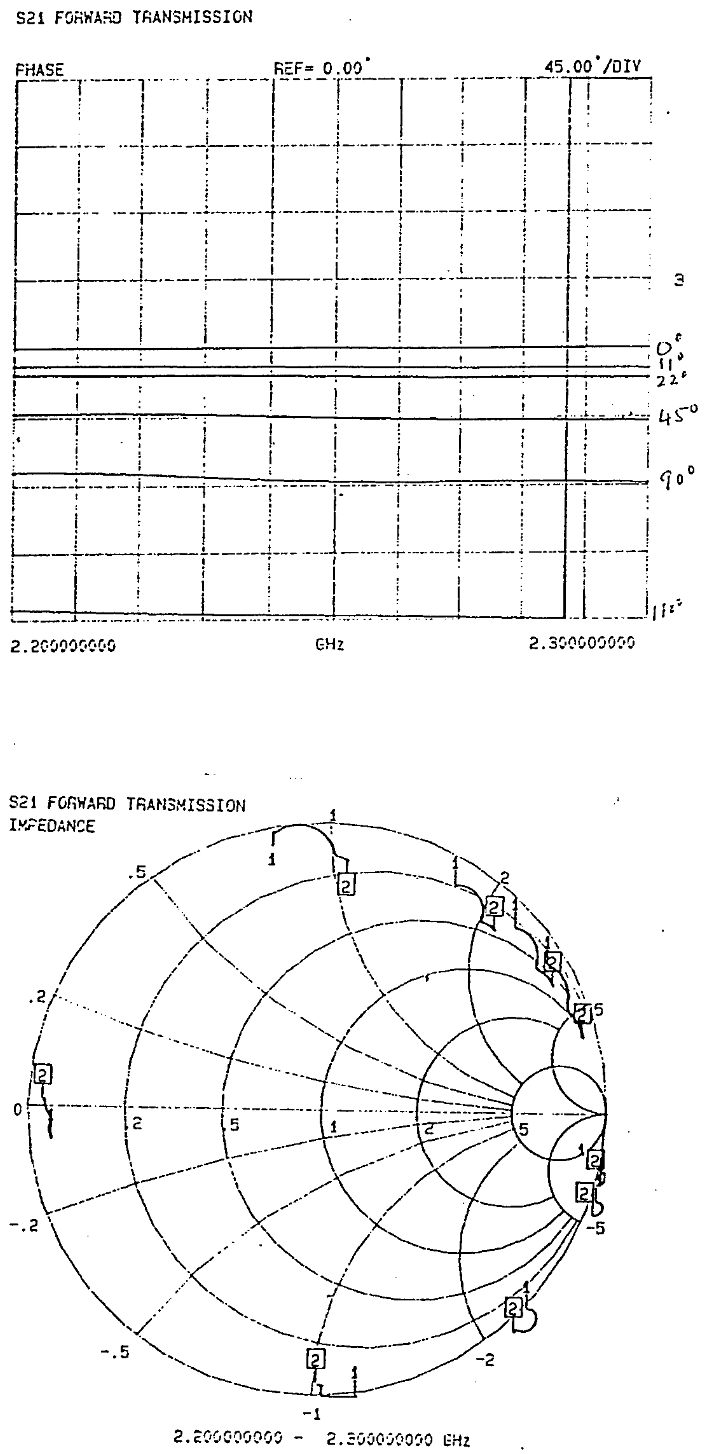

Figure 8: Measured performance of Receive Channel Phase Shifter.

1.46 MMIC Attenuator for Amplitude Control

An MMIC based 5 bit digital attenuator was implemented in the design. The measured performance is detailed below in Figure 9. Also detailed in figure 10 is the combined amplitude and phase performance of the phase shifter combined with the attenuator.

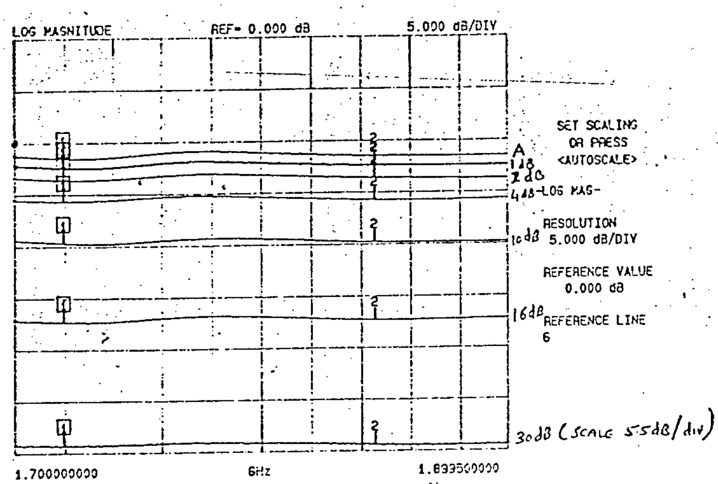

Figure 9: Measure performance of the digital attenuator.

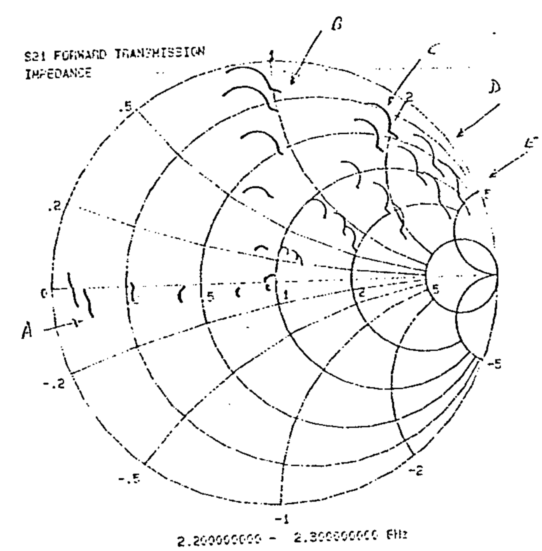

Figure 10: Measured Amplitude and phase control

1.4.6 Limiters for Receive channel protection

Surface mount limiters have been designed and performance measured. The active device in a narrow I region pin diodes with a dc return for current in the self-bias mode. The design of the T/R module is based on Coplanar WaveGuide with a ground. The diodes are therefore mounted directly across the 50-Ohm line. The insertion loss is 0.2 dB. The flat leakage is sufficient to protect the LNA.

1.4.7 Hybrid combiner and Splitters.

As detailed in the T/R module block diagram four in phase power dividers and four quadrature couplers are required. Using the normal coupler design, the size of the T/R module becomes large. Also the used of the procured 90-degree, surface mount hybrids was investigated and found to be very prohibitive in cost at large volume prices. To achieve the performance at low cost, novel couplers have been designed and implemented in the T/R modules. The performance of these will be presented.

1.4.8 Layout

The final layout of the T/R is presently being conducted. All the individual components of the T/R module have been developed. The performance of the module will be presented.

1.5 Design To Cost

The design of the T/R module has focused on the design to cost strategy. From onset, the cost associated with the components without any compromise in the performance has been the guiding rule. The availability of the active devices for the PCS market has really influenced the cost of amplifiers and phase shifters. Added with novel design and layout, the design to cost goal is near reality. The individual cost associated with the components is detailed below in tabular fashion. Some venues for further reduction in cost are being evaluated and will be presented.

The control of the entire T/R module is being done through a Xilinx FPGA. Full details of the circuit will be presented at the meeting.

ELEMENT	QUANTITY	VENDOR	QUANTITY	COST	COMMENT
Tx Filter	2	Comnav	100K	$20.00	
Rx Filter	2	Comnav	100K	$20.00	
Power Amp	2	Alpha	100K	$3.00	
LNA	2	Maxim	100K	$1.50	
Phase Shifter	4	Marconi	200K	$30.00	New circuit
Attenuator	4	Alpha	200K	$3.00	
Board+ Manufacture	1	Tachnoics	50K	$3.00	
Connectors	8	Various	300K	$8.00	Antenna
Shields	2	Various	100K	$2.00	
Electronics	FPGA	Xilinx	50K	$7.00	
Assembly	Lot	PmT	50K	$8.00	
Inspection	Each	PmT	50K	$5.00	
Test	Each	PmT	50K	$2.00	
Yield		TBD	TBD		
Total Cost				**$112.00**	**Target $100.00**

1.6 Conclusion

The individual components of the AFSCN Transmit/receive module have been developed and their results have bee presented. The design to cost study has shown that the target Cost of $100 is with in grasp. The major goal that are being addressed are those of interface with the control electronics and the antenna elements.

References:

[1] Communications with Dr. B. Tomasic, S. Liu, P.Oleski at SBIR meetings on the Air Force Contract No. F30602-98-C-0093.